Broadband Bow-Tie Antenna with Tapered Balun

Hussein Mohammed Jaafar

Submitted to the
Institute of Graduate Studies and Research
in partial fulfillment of the requirements for the Degree of

Master of Science
in
Electrical and Electronic Engineering

Eastern Mediterranean University
February 2014
Gazimağusa, North Cyprus

Approval of the Institute of Graduate Studies and Research

Prof. Dr. Elvan Yılmaz
Director

I certify that this thesis satisfies the requirements as a thesis for the degree of Master of Science in Electrical and Electronic Engineering.

Prof. Dr. Aykut Hocanın
Chair, Department of Electrical and Electronic Engineering

We certify that we have read this thesis and that in our opinion it is fully adequate in scope and quality as a thesis for the degree of Master of Science in Electrical and Electronic Engineering.

Supervisor
Assist. Prof. Dr. Rasime Uyguroğlu

Examining Committee

1. Prof. Dr. Hasan Amca
2. Assoc. Prof. Dr. Hasan Demirel
3. Asst. Prof. Dr. Rasime Uyguroğlu

ABSTRACT

In microwave applications spectrum Industrial, Scientific and Medical (ISM) band, especially in wireless communication systems applications such as GSM, 3G, Wi-Fi and Wi-MAX applications, high antenna characteristics such as high gain and wide bandwidth are required. In this thesis, a broadband Bow Tie Antenna (BTA) with high performance characteristics has been designed, to cover the wireless application requirements.

One of the fundamental problems of the transmission line in the antenna system is the power loss due to the radiation which occurs on the feed excitation. This kind of transmission lines is called Unbalance Transmissions Lines (UTL). To reduce the power radiation on transmissions lines, in other words, to modify transmission line from unbalance to balance (BTL), i.e. UTL-to-BTL transition, the "balun technique" can be used. In this study, for UTL bow tie antenna with Microstip Line (MSL) and coaxial cable feeds have been used. On the other hand for BTL bow tie antenna with Coplanar Strips line (CPS) feed has been used. Two kinds of taper impedance matching techniques have been applied to reduce reflection in the signal.

A broadband BTA antenna with dual bands has been designed and simulated having the bandwidth 1.89-3.25 GHz and 3.5-3.67 GHz for operating frequency 2.45 GHz. Maximum gain achieved at 2 GHz which is equal to 6.9 dB and the gain for 2.5 GHz, 3 GHz, and 3.5 GHz, are equal to 4.8 dB, 5.1 dB, and 3.8 dB respectively.

Keywords: Broadband Antenna, BTA, bow tie, Wireless Applications, UTL, BTL, Balun, taper, Microstrip line to Coupled Transitions.

ÖZ

Birçok mikrodalga uygulamasında (ISM band), özellikle 3G, Wi-LAN ve Wi-MAX kablosuz haberleşme alanlarında kullanılan antenlerde yüksek kazanç, geniş band gibi yüksek performans özellikleri aranmaktadır. Bu tez çalışmasında kablosuz haberleşme alanıda kullanılabilecek genişband ve yüksek kazanç özelliklerine sahip papyon anten tasarlanmıştır.

Anten sistemlerinde en temel sorunlardan biri, besleme mikroşerit hattaki radyasyondan kaynaklanan güç kayıbıdır. Bu tür iletim hatları dengesiz iletim hattı olarak adlandırılır (Unbalance Transmission Line, UTL). İletim hatlarındaki bu güç kayıbını önlemek için, diğer bir deyişle, iletim hattını dengesiz durumdan dengeli (Balanced Transmission Line, BTL) duruma çevirmek için (UTL-BTL) "balun tekniği" kullanılmaktadır. Bu çalışmada, UTL için mikroşerit ve ortak eksenli kablo beslemeli papyon anten, BTL için ise eş düzlemli şerit kablo beslemeli popyon anten kullanılmıştır. Ayrıca, iki tür konik empedance uyumlama tekniği uygulayarak yansıma sinyalinin azalması sağlanmıştır.

2.45 GHz frekası için, 1.89-3.25 GHz ve 3.5-3.67 GHz band genişlikleri olan çift band BTA tasarlanmıştır. En yüksek kazanç 2 GHz'te 6.9 dB olarak elde edilmiştir. Kazanç, 2.5 GHz, 3 GHz, ve 3.5 GHz frekanslarında ise sırası ile 4.8 dB, 5.1 dB, ve 3.8 dB'dir.

Anahtar Kelimeler: Genişband Anten, BTA, papyon, Kablosuz Uygulamalar, UTL, BTL, Balun, konik, Microstrip line to Coupled Transitions.

ACKNOWLEDGMENTS

Firstly, I would like to express my deep thanks to my supervisor Asst. Prof. Dr. Rasime Uyguroğlu for her unlimited help and support by helping me to overcome several obstacles in my study and thesis research.

Special thanks also go to all my faculty members staff especially vice Chairman Assoc. Prof. Dr. Hasan Demirel.

I also wish to thank and extend a full appreciation to my family who backed me up during my study. Without their supports in several sensitive matters, finalizing this work would be impossible.

Finally, I want to use this opportunity to sincerely appreciate all my friends in Eastern Mediterranean University and in my Country.

TABLE OF CONTENTS

LIST OF TABLES

LIST OF FIGURES

LIST OF SYMBOLS /ABBREVIATIONS

$A_{K11}^{(i)}$	Magnetic Vector Potential at Free Space
B	Discontinuity
C	Speed Light
D	Directivity
$Dmax$	Maximum Directivity
E	Electrical Field
$e_{K11}^{(i)}$	Fourier Sums
G	Gain
f_L	Lower frequency
$f_{m,n,l}$	Operation Frequency
f_r	Resonant Frequency
f_u	Upper Frequency
h	Substrate Thickness
$\bar{J}$	Current Density
L	Length of Taper
L_g	Length of Ground Plane
m	Mode Number
n	Mode Number
P_{in}	Input Power
P_r	Radiation Power
R_a	Antenna Resistance
R_L	Load Resistance
R_o	Characteristic Resistance

s	Microstrip Line Spacing
S_{11}	Scattering Parameter of Port 1
S_{21}	Scattering Parameter of Port 2
U	Radiation Intensity
U_{max}	Maximum Radiation Intensity
U_o	Isotropic Power Radiation Intensity
$W(Z_L)$	Width of Load Side
$W(Z_o)$	Width of Source Side
W_g	Ground Plane Width
X_a	Antenna Reactance
X_{eff}	Effective Side Length
x	Side Length
Y_{in}	Input Admittance
Z_{in}	Input Impedance
Z_1	Upper Line Impedance
Z_2	Lower Line Impedance
$Z_o(o)$	Odd Mode Impedance
z	Length of Taper
α	Bow Angle
β	Phase Constant
γ	Propagation Constant
ε	Absolute Permittivity
ε_r	Relative Permittivity
ε_o	Permittivity of Free Space
ε_{reff}	Effective Dielectric Permittivity

η_r	Radiation Antenna Efficiency
η_{cd}	Conductor Dielectric Antenna Efficiency
η_o	Total Antenna Efficiency
λ	Wavelength
λ_g	Guided Wavelength
λ_o	Wavelength at Free Space
μ	Permeability
μ_r	Relative Permeability
μ_o	Permeability of Free Space
π	PI
Γ	Reflection Coefficient
BBTA	Bow Tie Antenna with Balun
BTA	Bow-Tie Antenna
BTL	Balance Transition Line
B.W	Band Width
CPS	Coupled Stripline
DS-BTA	Double-Side Bow-Tie Antenna
EM	Electromagnetic
FDTD	Finite Difference Time Domain
FEM	Finite Element Method
FMM	Fast Multipole Method
FR4	Flame Retardant 4
GPS	Global Positioning System
GSM	Global System for Mobile
HFSS	High Frequency Structures Simulators

MOM	Method of Moment
MSL	Microstrip Line
MSL-to-CPS	Microstrip line to coupled Stripline
SL	Stripline
SWR	standing Wave Ratio
TL	Transition Line
UHF	Ultra High Frequency
UWB	Ultra Wide Band
VHF	Very High Frequency
VSWR	Voltage Standing Ratio
Wi-Fi	Wireless Fidelity
WLAN	Wireless Local Area Network

Chapter 1

INTRODUCTION

In high performance applications such as aircraft, satellite, and microwave especially in communication systems where the size of the antenna has to be electrically small, lightweight, aerodynamic antennas are required [1]. Presently, microstrip patch antennas are used to meet these requirements. Antennas are low profile, low cost and flexible to be used on the inflexible surfaces. However, limitation on the bandwidth and low gain are the major weaknesses of the microstrip patch antennas [2].

Recently, new antenna configurations known as printed Bow Tie Antenna (BTA) are proposed with broadband and high gain properties [3] [4] [5] [6]. The Bow-Tie Antenna is shaped from double side triangular sheet feed in the vertex. This kind of antenna is defined by the triangular flare angle only. In other words, the performance of this antenna type is not related to the frequency [**7**].

In this thesis, Bow Tie Antenna shapes and their feed excitations types have been studied. The radiation of the microstrip line is prevented and the mismatch between the feed line and the antenna was solved by balun technique which was suggested by Pozar [8]. The discontinuity in the power flow in the Balun was enhanced by using triangular and exponential taper instead of step width transformation on the transmission line.

1.1 Thesis Objective

- Analysis and design of Bow-Tie antenna shapes and their excitations.

- Reduction of power radiation which occurs in the transmission line (Balun).

- Reducing the signal reflection on the TL (taper technique).

1.2 Thesis Outline

The antenna overview is shown and the antenna concepts are described in chapter 2. Emphasis was made on some types of antennas and the antenna parameters.

The planar Bow-Tie Antenna design is given in terms of the antenna impedance, radiation power pattern, dimensions and Bow-Tie antenna feed excitations in chapter 3. Classification of the feed line in two types, balance and unbalance transmissions lines are also discussed. The simulation results of Bow Tie antenna with different kinds of feed excitations are illustrated too.

The details of the new Bow Tie Antenna with new balun feed line are given in chapter 4. Two taper techniques (exponential and triangular) are applied on the balun to reduce discontinuity in the power flow.

Conclusions and future work suggestions are presented in chapter 5.

Chapter 2

ANTENNA THEORY FUNDAMENTALS

2.1 Overview of Antennas

2.1.1 Antenna Definition

The first definition of the antennas was adapted from Webster's dictionary "a metallic device (rod or wire) used for radiating or receiving ratio waves" [1]. There are several other definitions for antenna depending on the IEEE standard for propagation (IEEE 145-1983), which is "a means for radiation or receiving ratio waves" [9]. In other words, antenna is a device used to send or receive electromagnetic waves to/from waveguide transmission line or voltage and current to/from transmission lines to launch an electromagnetic-wave into free space or any other media which is shown in Figure 2.1. It is worth to mention that the main aim of using an antenna system is to achieve an efficient radiation by minimizing the returning waves of the antenna system [1].

Some of the antenna parameters will be discussed in the next section.

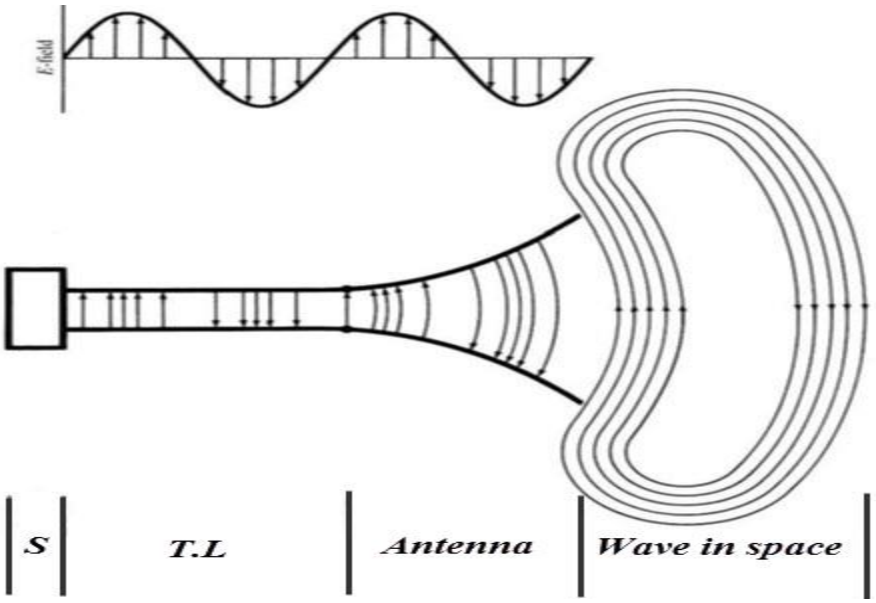

Figure 2.1: Transition modes for antenna **[**1**]**

2.2.2 Antenna Types

In this section, some classifications of antenna shapes will be discussed briefly.

2.2.2.1 Wire Antenna

One of the most popular antennas is the wire antenna and the simplest shape of it is dipole antenna. It consists of double wires put on the same axis. The other kind of wire antenna is known as the loop antenna and it consist of one or more turns, it does not necessarily have to be circular, they may be square, elliptic, rectangular or in any other shapes.

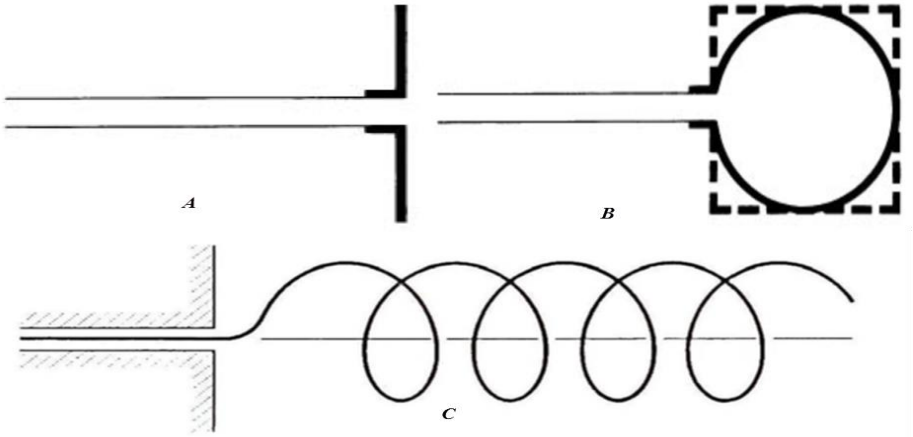

Figure 2.2: Wire antennas, (a) dipole, (b) loop, (c) helix [**1**]

2.2.2.2 Aperture Antenna

Aperture antennas are mostly used at microwave frequencies. There are numbers of forms of the aperture antennas with some popular shapes shown in Figure 2.3. The aperture in horn or waveguide can be designed as square, circular, elliptic, or may have any other configuration. The space applications that became more practical deals with aperture antennas, because of that we can put it on the body of moving objects such as spacecraft or aircrafts.

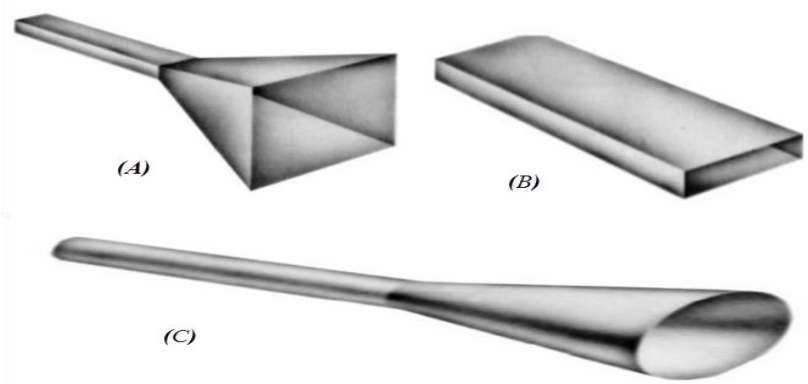

Figure 2.3: Aperture antennas, (a) pyramidal, (b) conical, and (c) rectangular [1]

2.2.2.3 Array Antenna

There are demands for antennas with specific characteristics that cannot be achieved by one element. For this reason the radiating elements with similar properties are arranged in certain geometry to form an array. Typical examples can be seen in Figure 2.4.

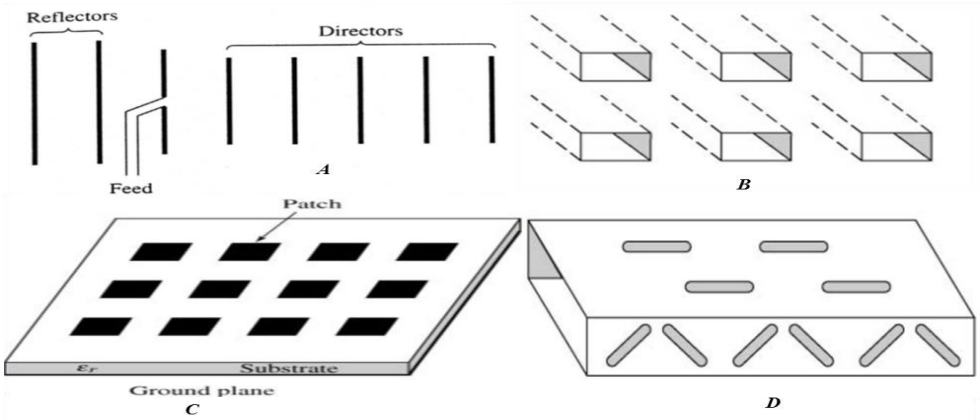

Figure 2.4: Antenna array, (a) Yagi-Udi, (b) Aperture, (c) Microstrip, and (d) Slotted **[**1**]**

2.2.2.4 Reflector Antenna

Reflector antennas are common antenna forms. There are many applications in the communication systems that need to make contact over large distance. Reflector forms of antennas are used to transmit and receive electromagnetic waves with high gain over lot of millions miles. There are many geometrical configurations to the reflectors such as curved, corner and planar reflectors as depicted in Figure 2.5.

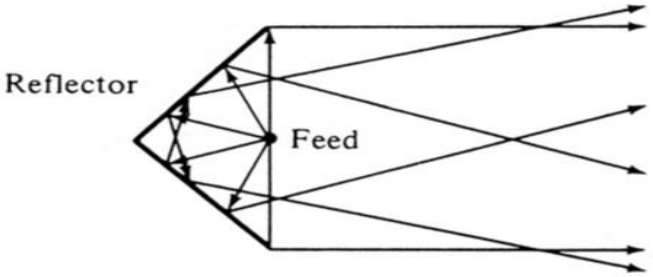

Figure 2.5: Reflector Antenna [1]

2.2.2.5 Microstrip Antenna

Since there are lots of applications requiring lightweight and flexible antennas such as aircraft, satellite, missile applications and mobile communication; microstrip antennas are used to satisfy these requirements. Such antennas have more advantages, e.g. low cost, fine profile, simple structure and easy to construct on the inflexible surfaces **[**1**]**. The major disadvantages of microstrip antennas are low polarization purity and limit in frequency bandwidth; this is a good reason for us to find solution to the problems.

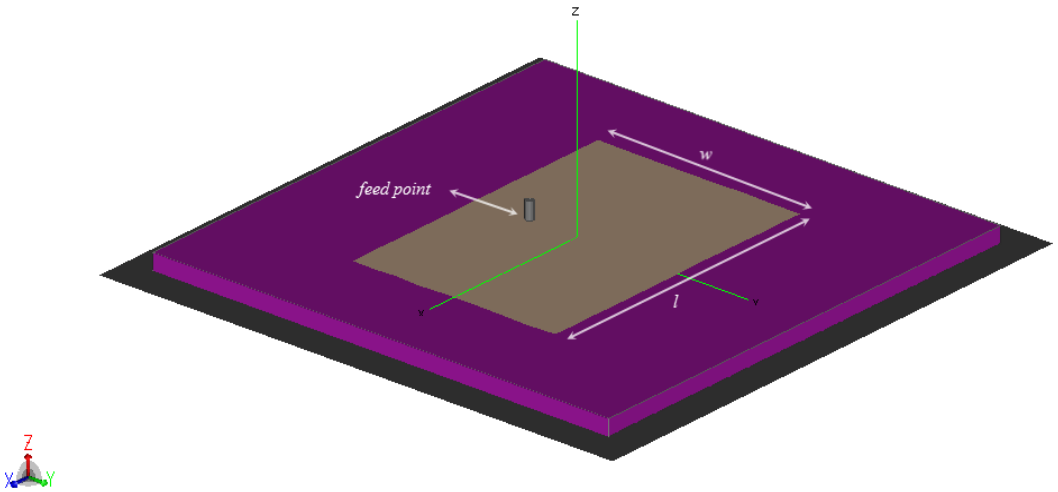

Figure 2.6: Microstrip Antenna (Rectangular Patch) [1]

2.2.3 Antenna Parameters

This section describes the performance of an antenna by considering all antenna parameters like gain, radiation power, polarization, efficiency and antenna impedance.

2.2.3.1 Radiation Pattern

Radiation pattern is a graphical description of the EM wave propagation in space or in any other medium. Radiation pattern plots are, in general, in 3-D spherical coordinates, but 2-D polar plots are also used to observe the field distribution in different planes.

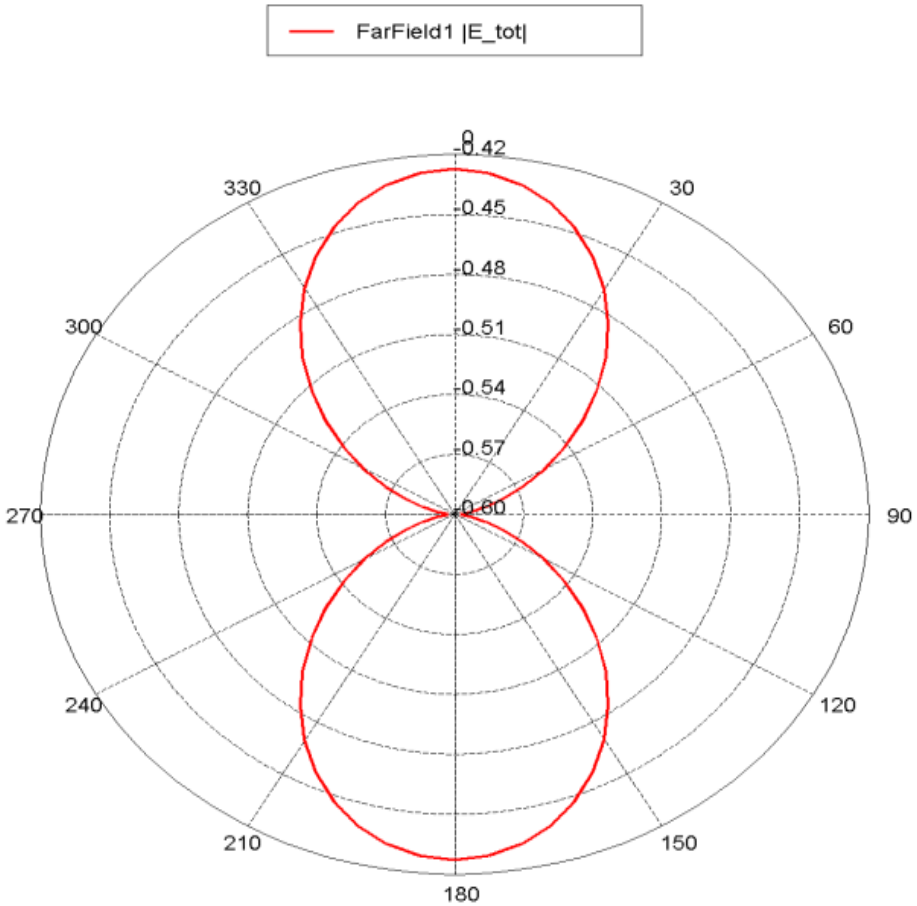

Figure 2.7: Polar Radiation Patterns FEKO

2.2.3.2 Directivity

The directivity demonstrates the comparison of power intensity in certain direction with the omnidirectional intensity.

$$D = \frac{U}{U_o} = \frac{4\pi U}{P_r} \tag{2.1}$$

The maximum directivity is calculated by Equation (2.2) [1]:

$$D_{\max} = \frac{4\pi * U_{\max}}{P_r} \tag{2.2}$$

where, D refers to the directivity, U is the radiation intensity, P_r is the radiation power, and U_o is the isotropic power intensity.

2.2.3.3 Gain

There is a close relationship between the gain and the antenna directivity. The gain is the ratio of power intensity to the lossless isotropic reference power (P_{in}) divided by (4π) and mathematical description can be shown in Equation (2.3).

$$G = \frac{4\pi * U(\phi, \theta)}{P_{in}} \tag{2.3}$$

2.2.3.4 Efficiency

The efficiency represents the measure of the ability to radiate the amount of power that is delivered to the antenna, and it can be calculated by using Equation (2.4).

$$\eta_{\circ} = (\eta_r * \eta_{cd}) * 100\% \tag{2.4}$$

where, η_o is the total efficiency, η_r is the reflection mismatch efficiency, and η_{cd} is the conductor dielectric efficiency.

2.2.3.5 Bandwidth

The antenna bandwidth is defined as the range of frequency which correspond the return loss of to less than 10 dB. Figure 2.8 shows the BTA bandwidth at operating frequency f_r approximately (0.5) GHz.

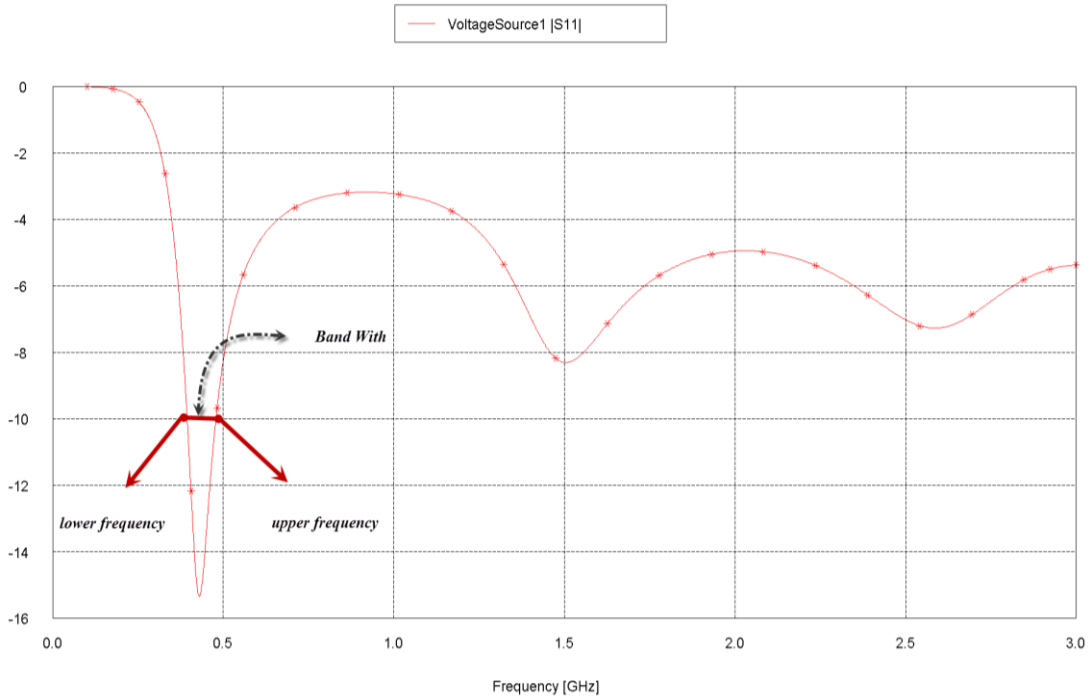

Figure 2.8: Antenna Bandwidth simulated by FEKO

The general equation to find antenna bandwidth is given by:

$$B.W = \frac{f_u - f_l}{f_r} * 100\% \tag{2.5}$$

Note that, f_u is the maximum frequency of the band, f_l is the minimum frequency and f_r is the resonant frequency.

2.2.3.6 Impedance

The impedance refers to the ratio of the appropriate component of the electric field over the magnetic field. The antenna impedance, in terms of the antenna resistance R_a and antenna reactance X_a is:

$$Z_a = R_a + jX_a \tag{2.6}$$

It is worth mentioning that X_a must be close to zero.

Chapter 3

BOW TIE ANTENNA

3.1 Introduction

A Bow Tie Antenna is made of a bi-triangular sheet of metal feed by a vertex [10]. In other words; Bow-Tie Antenna is the mixture of imaginary image for two triangular patches which are fabricated on a single substrate as shown in Figure 3.1. Because of the characteristics of Bow Tie Antenna such as matching impedance and broadband characteristics, BTA became one of the most common patch antennas in demand. The investigators of the triangular sheet antenna were Wood and Brown [11]. The International Telecommunications Conference of ITU in Atlantic City adopted "The wide band including 2.4 GHz band" [12] and then the broadband antennas which covers the spectrum from (2 GHZ to 3 GHZ) became extremely important. In fact a BTA has wireless applications such as GSM, WMAX, WLAN, and radio frequency applications that require specific characteristics such as, high gain, attractive radiation patterns and broad bandwidth antenna.

In this chapter, we will study the Bow-Tie antenna characteristics such as characteristic impedance, antenna radiation pattern and antenna dimensions.

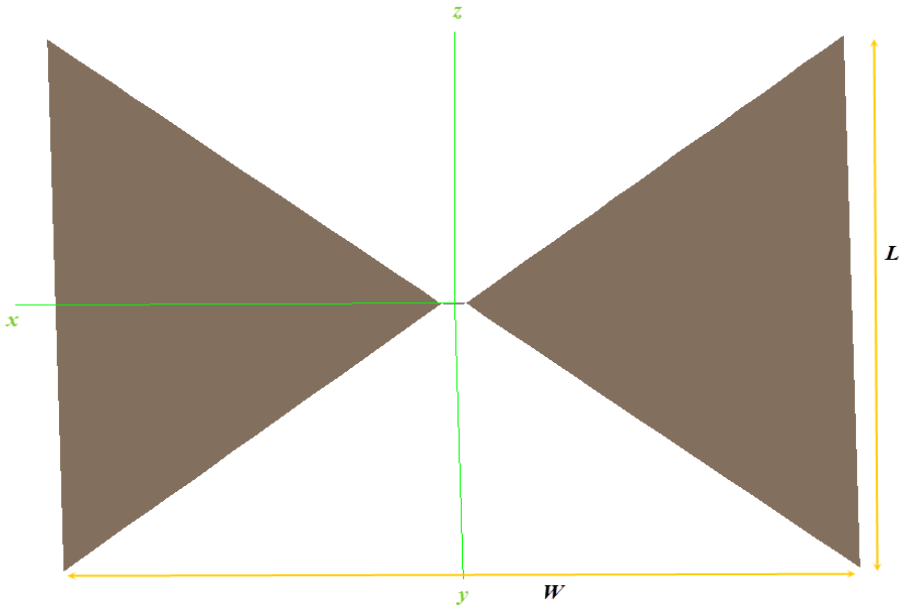

Figure 3.1: Simple Bow-Tie Antenna layout

3.2 Bow-Tie Antenna Design

3.2.1 Antenna Impedance Calculation

The impedance of the BTA is measured by considering the infinite length of BTA. In this way the impedance will be independent of the frequency. The transmission line theory can be used to accurately calculate the antenna impedance [7] which is given by the equations below.

$$Z = \sqrt{\frac{2 * \mu_{\circ}}{\varepsilon_{reff} + \varepsilon_{\circ}}} \cdot \frac{K(\mathrm{k}')}{K'(\mathrm{k})} \tag{3.1}$$

where $\mu_{\circ}$ is the free space permeability, ε_{reff} is the effective dielectric constant and $\varepsilon_{\circ}$ is the free space permittivity.

ε_{reff} is the effective relative to permittivity account for the fringing effects and the wave propagation in the transmission line.

$$K(\mathrm{k}') = \int_0^1 \frac{dx}{\sqrt{(1-\mathrm{x}^2)(1-\mathrm{k}^2\mathrm{x}^2)}} \tag{3.2}$$

$$K(\mathrm{k}') = K'(\mathrm{k}) \tag{3.3}$$

And

$$k' = \sqrt{1-k^2} \tag{3.4}$$

$$k = \tan^2(45^\circ - \frac{\alpha}{4}) \tag{3.5}$$

where k' and k are integration to the elliptical coordinate of the first kind and α is the Bow angle.

Figure 3.2 demonstrates the relationship between the antenna flare angle and the antenna impedance based on Equation (3.1).

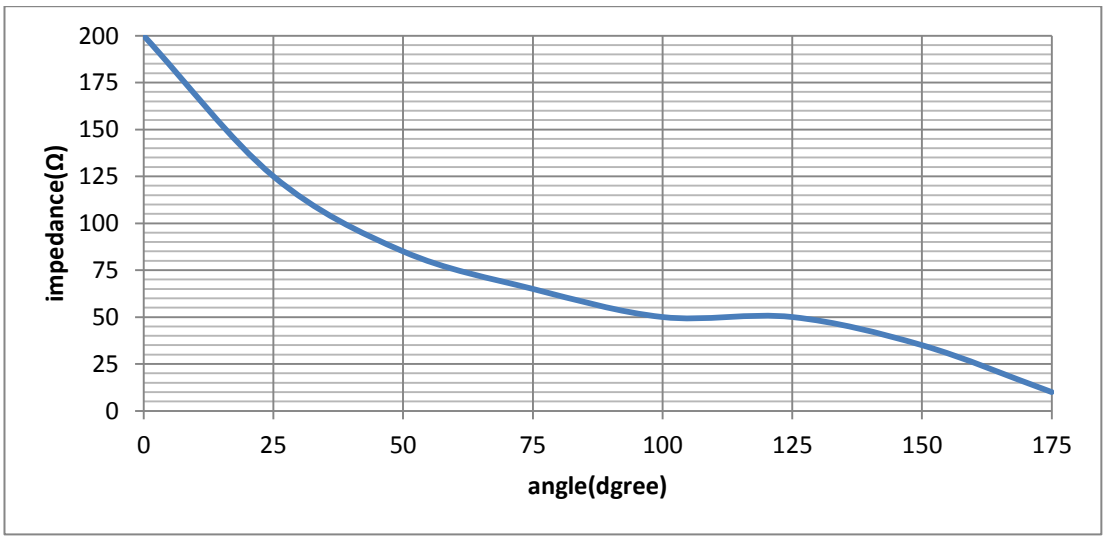

Figure3.2: Relationships between impedance and angle

3.2.2 Bow-Tie Antenna Radiation Pattern

There are many theoretical methods used to calculate the radiation pattern of the antennas such as FDTD, FEM and FMM. However, FEKO software full wave simulator uses Moment Method Solution (MoM) [13] to analyze Bow-Tie Antenna with finite length, and put on the infinite dielectric substrate, having the source at vertex. In cylindrical coordinates the feed current may be expressed as Equation (3.6):

$$\bar{J} = \frac{e^{\pm\frac{\gamma}{r}}}{\sqrt{\cos^2\phi - \cos^2\phi_\circ}}\hat{r} \tag{3.6}$$

The plus sign applies to the top half of the bow and the minus to the bottom half. The $e^{\pm\frac{\gamma}{r}}$ term describes an outward-travelling current wave.

The propagation constant γ may be written as an equation below where a first estimate for β will be provided by the quasistatic wave number. The real part of γ describes the decay of the current along the bow due to radiation

$$\gamma = \alpha + j\beta \tag{3.7}$$

3.2.3 Bow-Tie Antenna Dimensions

A number of methods are suggested to modify a triangular patch antenna dimensions that is close to the Bow Tie Antenna form. Some are proposed to replace the side length of the triangular part (x) and the dielectric constant of the substrate (ε_r) by the effective side length of the bow tie (x_{eff}) and the effective dielectric constant

(ε_{reff}) respectively [14]. Other ideas proposed to set the relative permittivity as a constant and replace only the side length (x) by the effective side length (x_{eff}) [10]. The formulas below explain how to find the dimensions as related with the frequency.

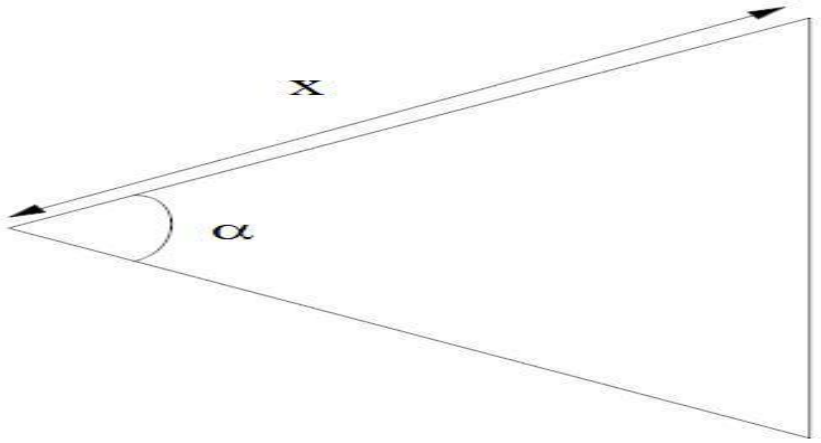

Figure3.3: Triangular shape patch antenna

The resonant frequency can be calculated as:

$$f_r = \frac{2c}{3x\sqrt{\varepsilon_r}}(m^2 + mn + n^2)^{\frac{1}{2}} \tag{3.8}$$

The above equation is valid when the triangular resonator is surrounded by a perfect magnetic wall. The effect of an imperfect magnetic wall on the resonant frequency can be included in an empirical fashion for easy calculation. This equation must satisfy the condition (m+n+l=0) where, m, n are mode numbers and they must be positive integer numbers.

$$x = \frac{2c}{3f_r\sqrt{\varepsilon_r}} \tag{3.9}$$

The side length x will be replaced by the effective side length (x_{eff}):

$$x_{eff} = x + \frac{h}{\varepsilon_r} \tag{3.10}$$

Here, h and ε_r are the thickness of the substrate and the dielectric constant, receptivity.

The effective dielectric constant will be calculated by Equation (3.11)

$$\varepsilon_{reff} = \frac{\varepsilon_r + 1}{2} + \frac{\varepsilon_r - 1}{2}\left(1 + \frac{12h}{x}\right)^{\frac{-1}{2}} \tag{3.11}$$

3.2.4 Feed Excitations to Bow-Tie Antenna

It is mentioned before that the Bow-Tie antenna is a brunch of MSA. So that, all feed excitations which are used with the MSA can be applied on the BTA. Two common kinds of feed excitations are used with BTA which are the unbalance transmission line UTL such as Microstrip line, coaxial cable, proximity coupled, aperture coupling transmission line and the balance transmission line BTL for instance, coplanar Microstrip line CPS.

3.2.4.1 Microstrip Line Feed

MSL feed is one of the most popular UTL configurations. It is also named by a single ended transmission line. Figure 3.4 displays the signal plane (conductor) placed on the upper layer of the dielectric and the reference plane (ground plane) fixed under the dielectric substrate. The dimensions of the ground plane and the microstip line can be calculated by equations below [1].

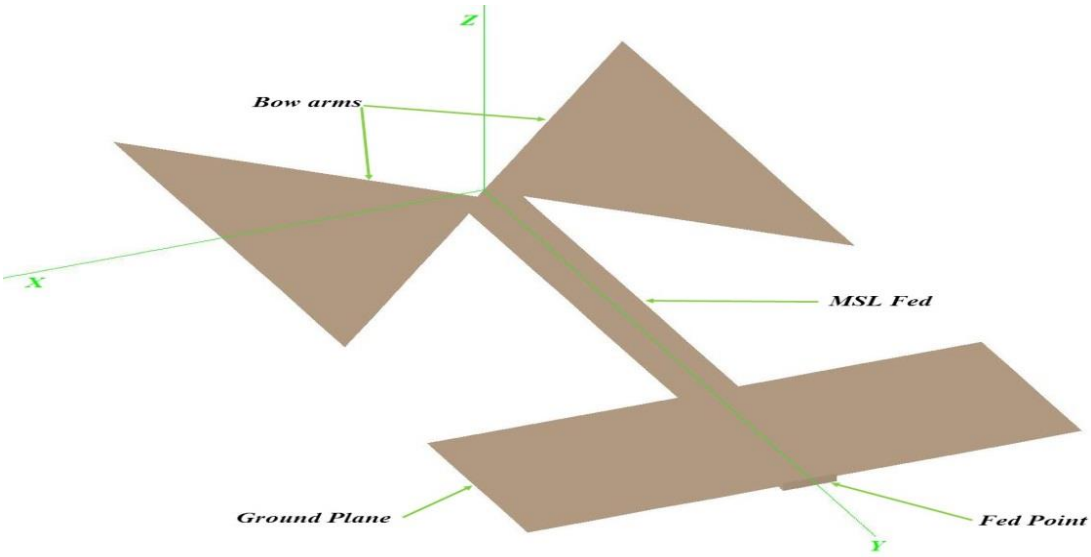

Figure 3.4: BTA fed by MSL simulated by FEKO

For the microstrip line the width/thickness ratio can be calculated by the following approximations:

$$\begin{cases} \dfrac{w}{h} = \dfrac{8e^{A}}{e^{eA}-2} & For\ \dfrac{w}{h} \le 2 \\ \dfrac{w}{h} = \dfrac{2}{\pi}[B-1-\ln(2B-1)+\dfrac{\varepsilon_r-1}{2\varepsilon_r}(\ln(B-1)+0.39-\dfrac{0.62}{\varepsilon_r})] & For\ \dfrac{w}{h} \ge 2 \end{cases} \quad (2.12$$

)

where:

$$A = \frac{Z_\circ}{60}\sqrt{\frac{\varepsilon_r+1}{2}} + \frac{\varepsilon_r-1}{\varepsilon_r+1}(0.23+\frac{0.11}{\varepsilon_r}) \quad (3.13)$$

$$B = \frac{377\pi}{2Z_\circ\sqrt{\varepsilon_r}} \quad (3.14)$$

And the effective dielectric constant is:

$$\varepsilon_{reff} = \frac{\varepsilon_r + 1}{2} + \frac{\varepsilon_r - 1}{2(1+12\frac{h}{w})^{\frac{1}{2}}} \tag{3.15}$$

The minimum size to the reference plane the length, l_g and width, w_g can be calculated by equations that are presented below [1].

$$w_g = w + 6h \tag{3.16}$$

$$l_g = l + 6h \tag{3.17}$$

3.2.4.2 Coaxial Cable Feed

Coaxial cable feed as shown in Figure 3.5, is composed of two major components, the inner conductor feed and outer conductor (shielded). It is UTL because of the radiation produced from skin effect problem. When the coaxial cable is used as a transmission line to the Bow-Tie antenna, the inner conductor will be connected to the BTA and the shielded part will be connected to the ground plane. There are other methods used to excite the BTA such as, aperture and proximity coupled techniques. These methods have some disadvantages such as complication in fabrication, narrow bandwidth and also too much amounts of surface waves [1]. So, these are not good for coupling.

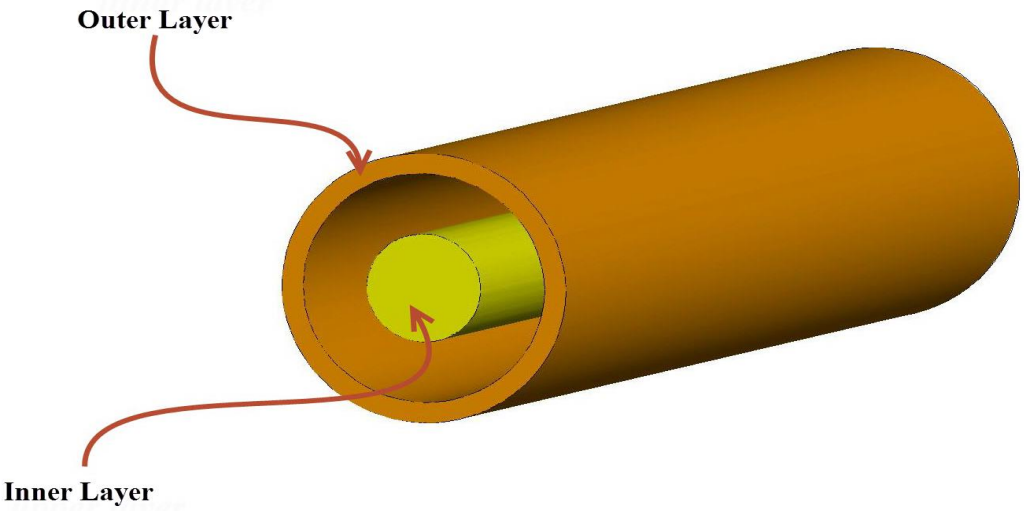

Figure 3.5: Coaxial cable configurations

3.2.4.3 Coupled Transmission Lines

Coupled transmission lines are defined as a Balance TL and also named by differential TL [15]. The coupled transmission lines consist of double signal conductors placed on the substrate and the ground plane placed below the substrate. If the conductors are on the substrate without the ground plane they are named as coplanar strips conductors (CPS). The main advantages of the Balance Transmission Lines are that they provide noise protection and prevent power radiation on the transmission line and this is achieved by reduction fringing waves.

To compute the characteristics impedance of the coplanar TL the following equations can be used [15].

$$Z_{\circ,\square}(\mathrm{o}) = \frac{Z_{\circ}(\mathrm{o})\sqrt{\dfrac{\varepsilon_{reff}(\mathrm{o})}{\varepsilon_{reff,\circ}(\mathrm{o})}}}{1-\dfrac{Z_{\circ}(\mathrm{o})}{\eta_{\circ}}\sqrt{\varepsilon_{reff}(\mathrm{o})Q_{10}}} \tag{3.18}$$

where $Z_{\circ}(\mathrm{o})$ is calculated from Equation (3.12) and $\varepsilon_{reff}(\mathrm{o})$ is given by Equation (3.15):

$$\varepsilon_{reff,\circ}(\mathrm{o}) = [0.5(\varepsilon_r + 1) + \mathrm{a}_{\circ}(\mathrm{u}, \varepsilon_r) - \varepsilon_{reff}(\mathrm{o})]\mathrm{e}^{-cg^d} + \varepsilon_{reff}(\mathrm{o}) \tag{3.19}$$

$$a_{\circ}(\mathrm{u}, \varepsilon_r) = 0.7287[\varepsilon_{reff}(\mathrm{o}) - 0.5(\varepsilon_r + 1)](1 - \mathrm{e}^{-0.179u}) \tag{3.20}$$

$$c = b_{\circ}(\varepsilon_r) - [\mathrm{b}_{\circ}(\varepsilon_r) - 0.207]\mathrm{e}^{-404u} \tag{3.21}$$

$$b_{\circ}(\varepsilon_r) = \frac{0.747\varepsilon_r}{0.15 + \varepsilon_r} \tag{3.22}$$

$$d = 0.593 + 0.694e^{-0.652u} \tag{3.23}$$

$$u = \frac{w}{h} \tag{3.24}$$

We can find Q_{10} from Equation (3.25):

$$Q_{10} = \frac{1}{Q_2}(Q_2 Q_4 - Q_5\, \mathrm{e}^{(\ln(\mathrm{u})Q6\mathrm{u}^{-Q_9})}) \tag{3.25}$$

$$Q_1 = 0.869u^{0.194} \tag{3.26}$$

To find Q_2 and substitute in Equation (3.25):

$$Q_2 = 1 + 0.7519g + 0.186g^{2.31} \tag{3.27}$$

$$Q_3 = 0.1975 + [16.6 + (\frac{8.4}{g})^6]^{-0.387} + \frac{1}{241}\ln[\frac{g^{10}}{1+(\frac{g}{3.4})^{10}}] \tag{3.28}$$

$$Q_4 = \frac{2Q_1}{Q2(\mathrm{e}^{-g}\mathrm{u}^{Q3} + (2-\mathrm{e}^{-g})\,\mathrm{u}^{-Q_3})} \tag{3.29}$$

$$Q_5 = 1.797 + 1.14\ln(1 + \frac{0.638}{g + 0.5g^{2.4}}) \tag{3.30}$$

$$Q_6 = 0.231 + \frac{1}{280}\ln(\frac{g^{10}}{1+(\frac{g}{5.8})^{10}}) + 0.2\ln(1 + 0.6\,\mathrm{g}^{1.15}) \tag{3.31}$$

$$Q_7 = \frac{10 + 190g^2}{1 + 82g^3} \tag{3.32}$$

$$Q_8 = e^{(-6.5 - 0.95\ln(g) - (\frac{g}{0.15})^5)} \tag{3.33}$$

$$Q_9 = \ln(Q_7)(Q_8 + \frac{1}{16.5}) \tag{3.34}$$

$$g = \frac{s}{h} \tag{3.35}$$

s , represent to the spacing between two Microstrips line.

3.3 Simulation of Bow Tie Antenna

3.3.1 Modified Dipole Bow Tie Antenna for 2.45GHz by Coaxial Cable Feed Excitation

A Dipole Bow-Tie Antenna (D-BTA) is introduced by Figure 3.6 with length *L*=10cm, flare angle α=90°, and feed in the vertex (edge port feed) with 1cm width. The simulation results are achieved by using FEKO software simulator. Figure 3.7 display 16 dB return loss at operating frequency 400 MHz

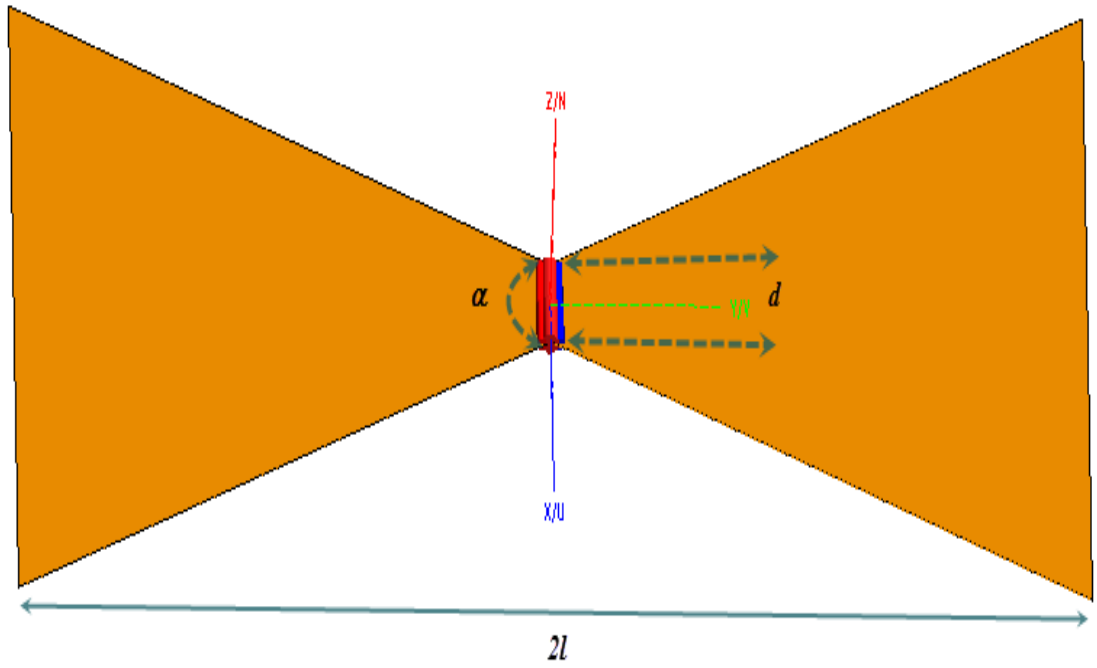

Figure3.6: Antenna configurations (FEKO)

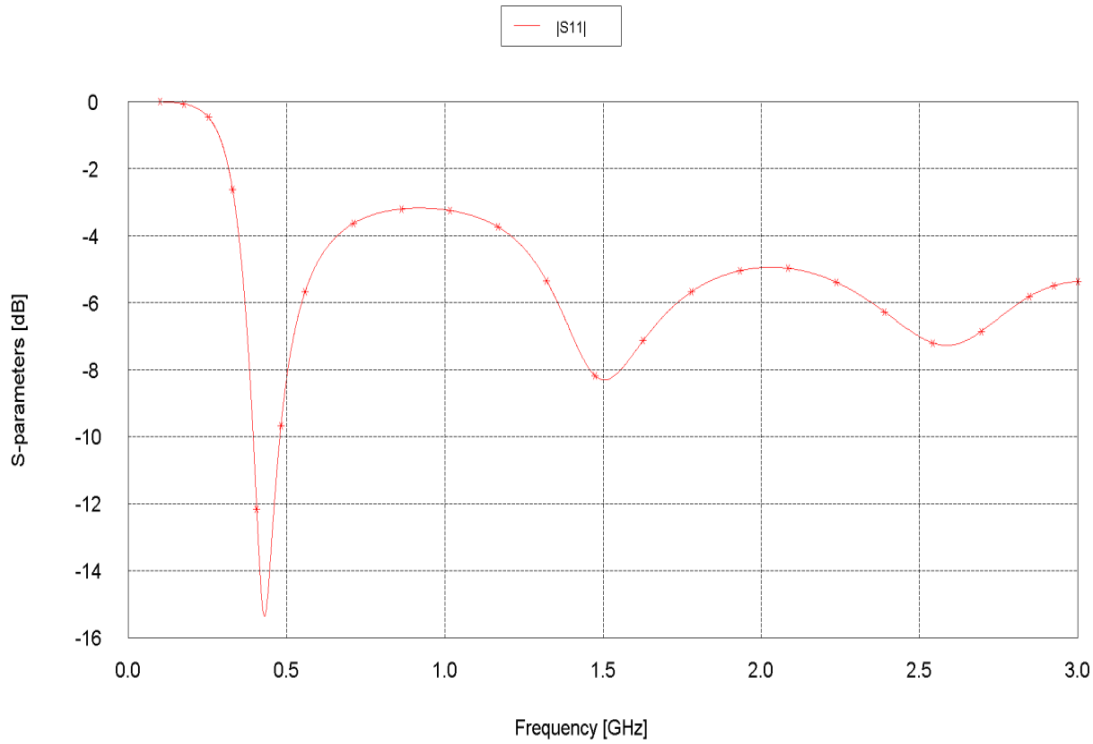

Figure 3.7: Reflection coefficients to BTA (FEKO)

So as to get resonance frequency at 2.45 GHz, we will optimize the antenna dimensions to be L=20.98 mm, d=2.83 mm and α=46.8^{o}. In Figure 3.8, it is clear that the real part of input impedance of D- BTA at 2.45 GHz is 50Ω and the imaginary part is approximately equal to zero which shows a good agreement with Figure 3.9.

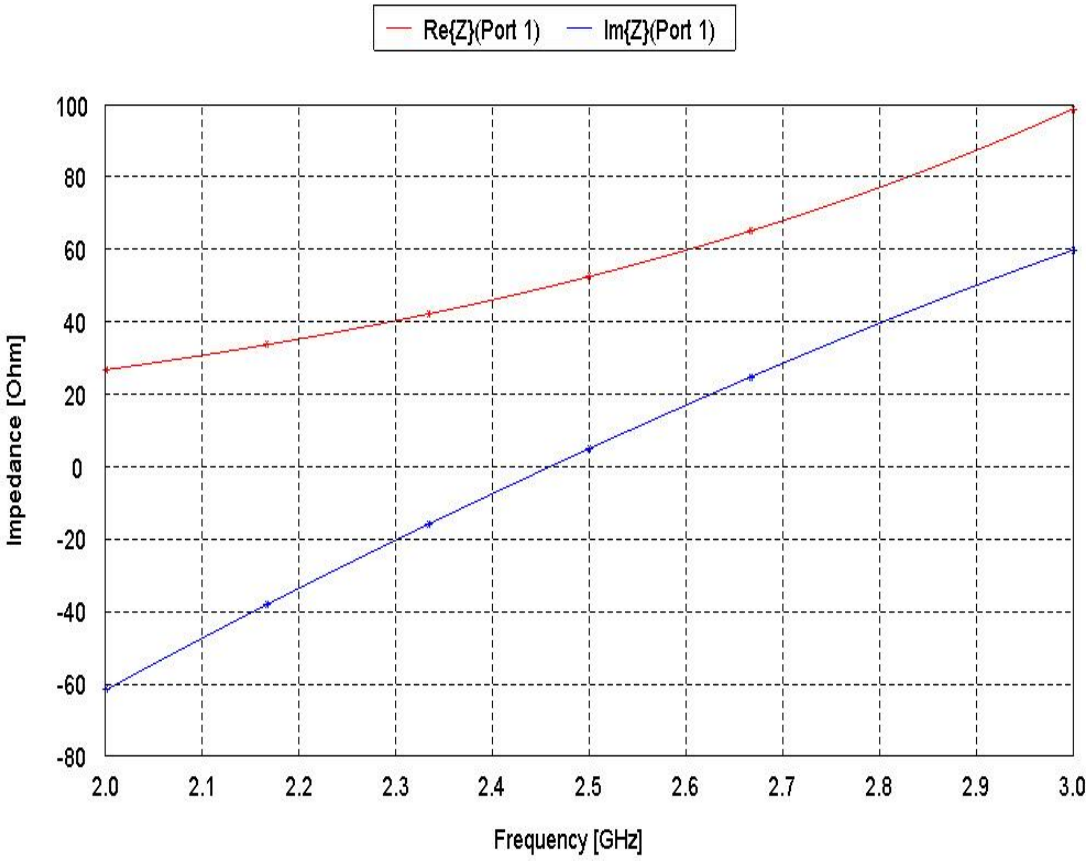

Figure 3.8: Input impedance dipole BTA

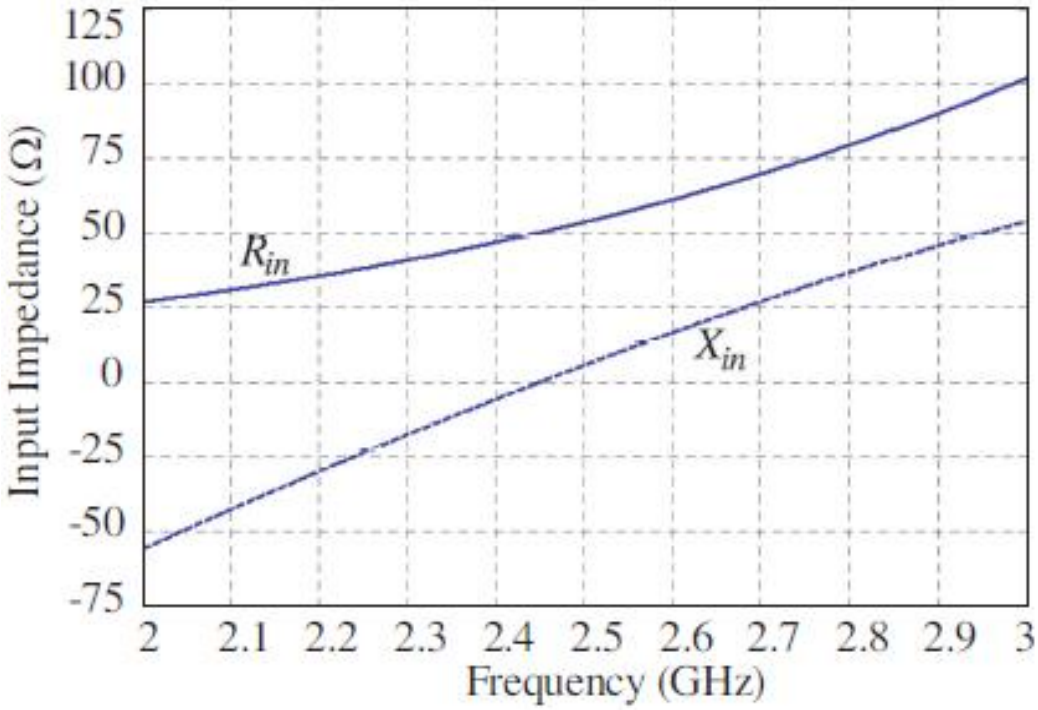

Figure 3.9: Input impedance D-BTA [16]

Broadband antenna with bandwidth 2.25GHz-2.7GHz under 10dB return loss is discussed in Figure 3.10. The radiation pattern of the antenna has omnidirectional radiation characteristics with gain around 1.7 dB along x-z plane as referred in Figure 3.13. Note that all simulation results are compared with previous work for validation [16].

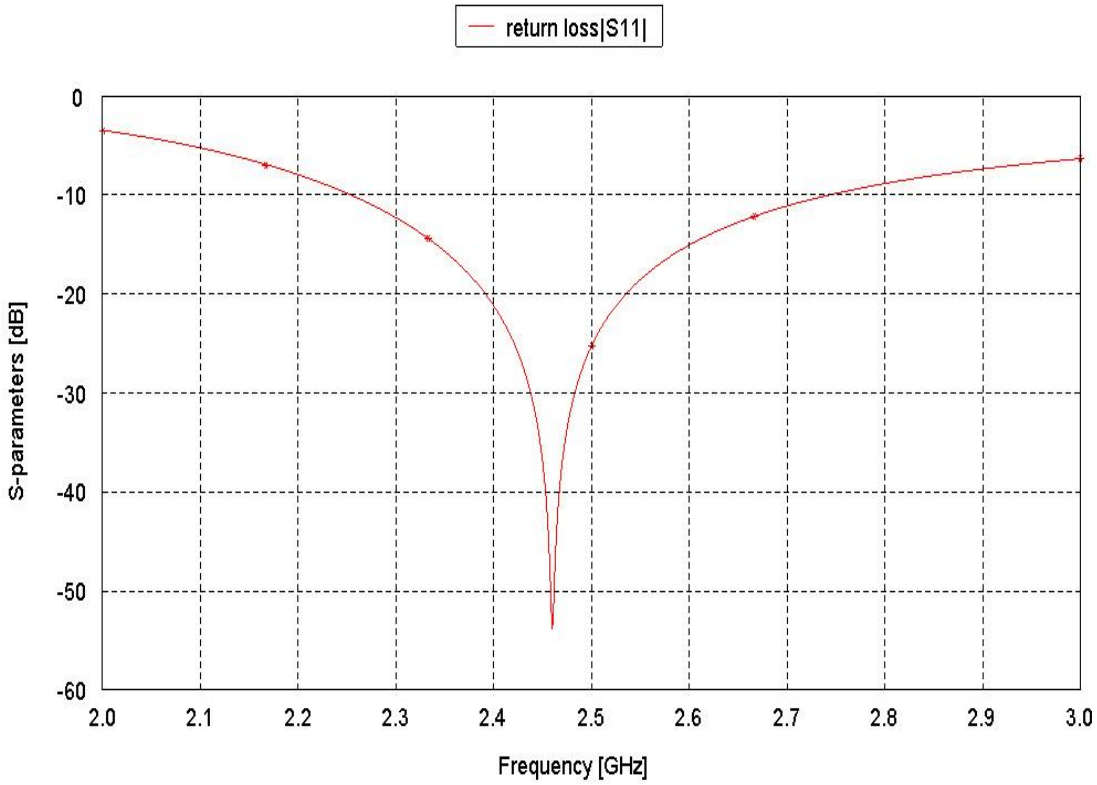

Figure 3.10: Return loss of diploe BTA

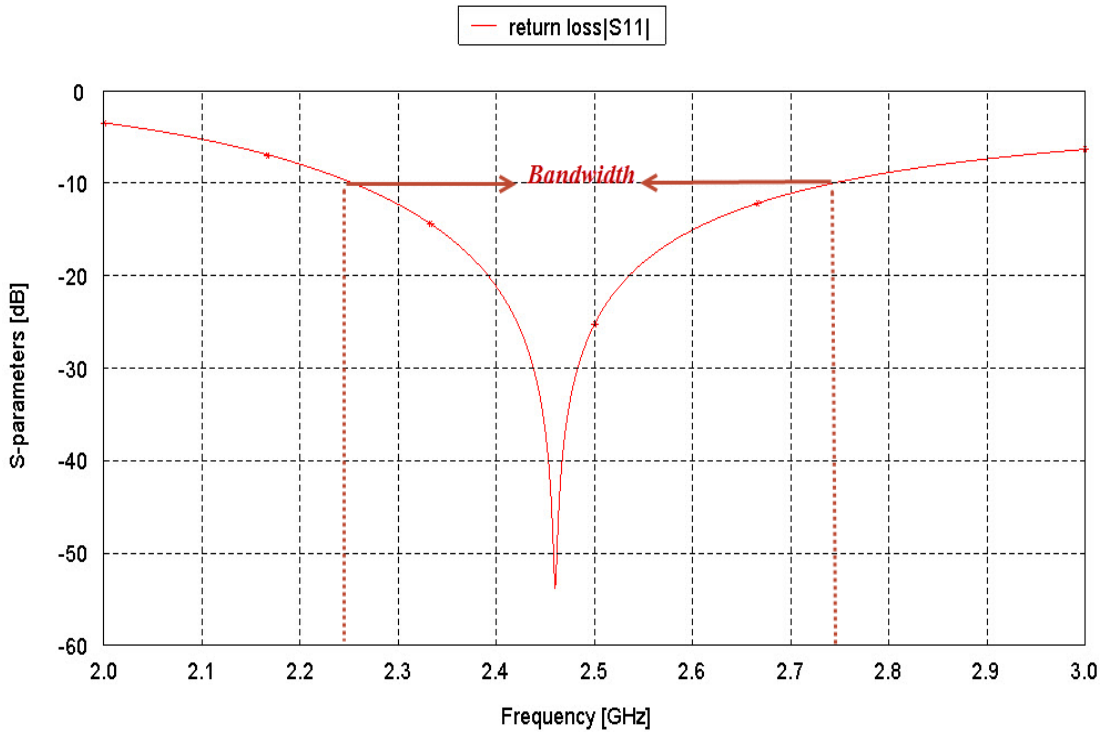

Figure 3.11: Antenna bandwidth (2.25-2.75) GHz

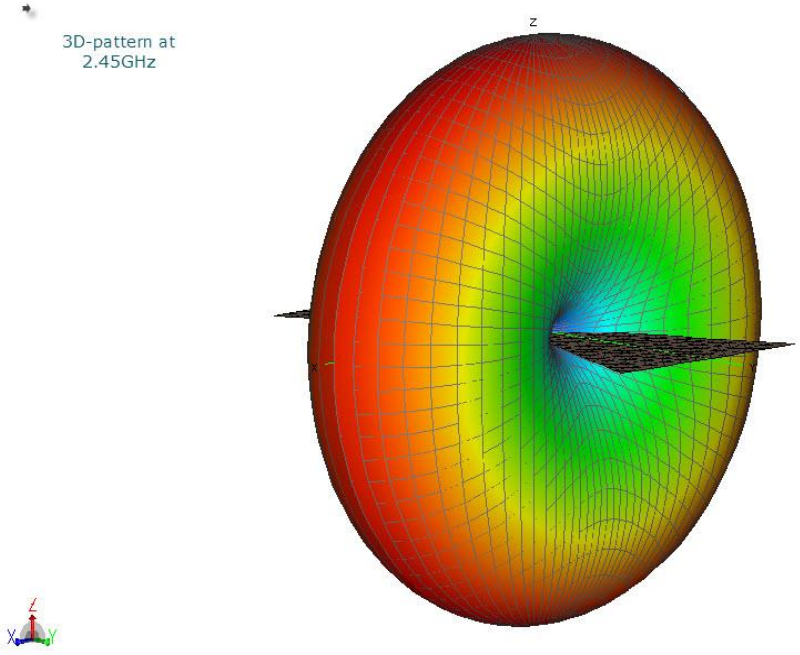

Figure3.12: 3-D radiation pattern for an optimize dipole BTA

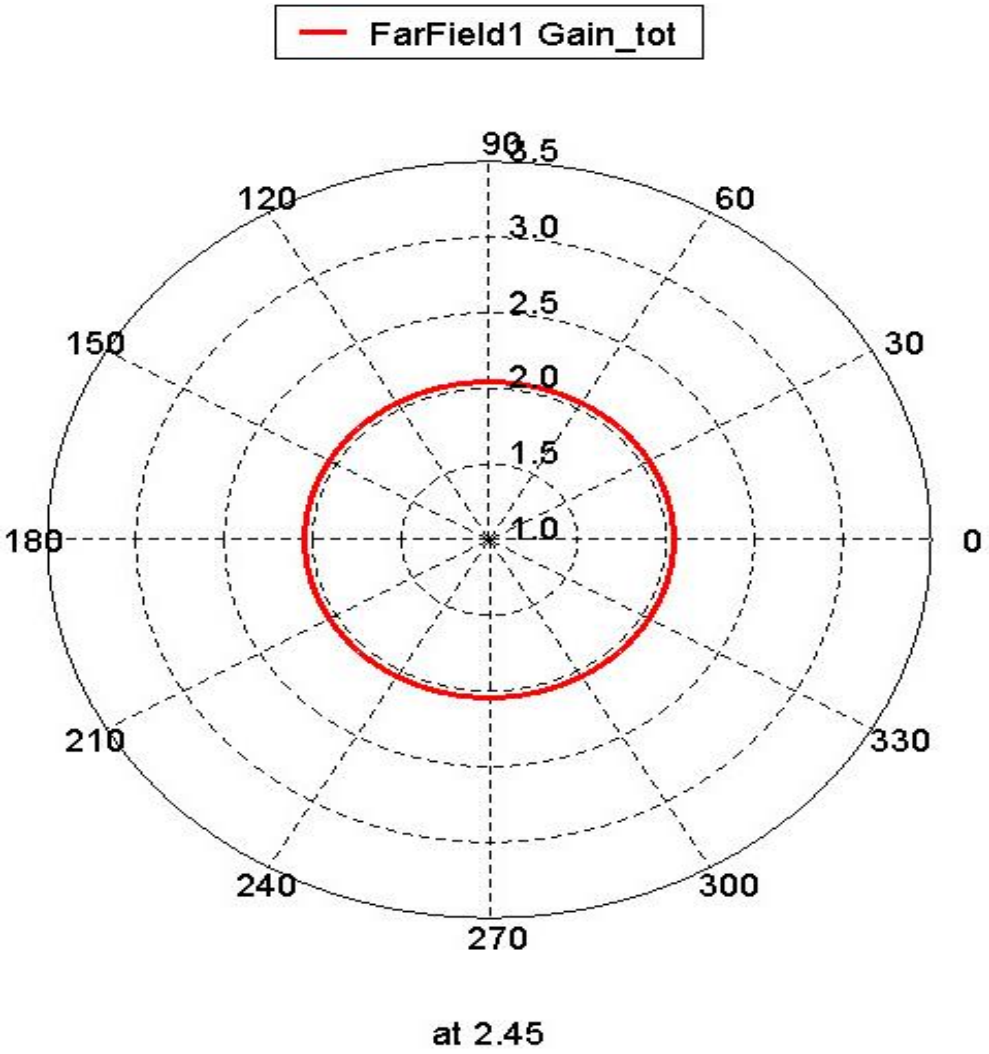

Figure3.13: Gain radiation pattern to dipole BTA along x-z plane

3.3.2 Simulation of Broadband BTA with Broad-Side Feed for S-Band

A double side printed Bow Tie Antenna with broadside coupled Microstrip feeding line has been simulated for UHF band [17]. As shown in Figure 3.14, the upper and lower layers are tinged by yellow and blue color respectively. Figure 3.15 indicates the side view of antenna system configuration. A metal reflector with dimensions 80mm*80mm and 0.03mm thickness was used to enhance the antenna gain as presented by Figure 2.16. FR4 dielectric substrate layer with ε_r=4 and thickness of 1.5mm was used to separate the patch arms. Both antennas (with and without

reflector) are simulated by FEKO 5.5 software simulator. All antenna dimensions are listed in Table 3.2.

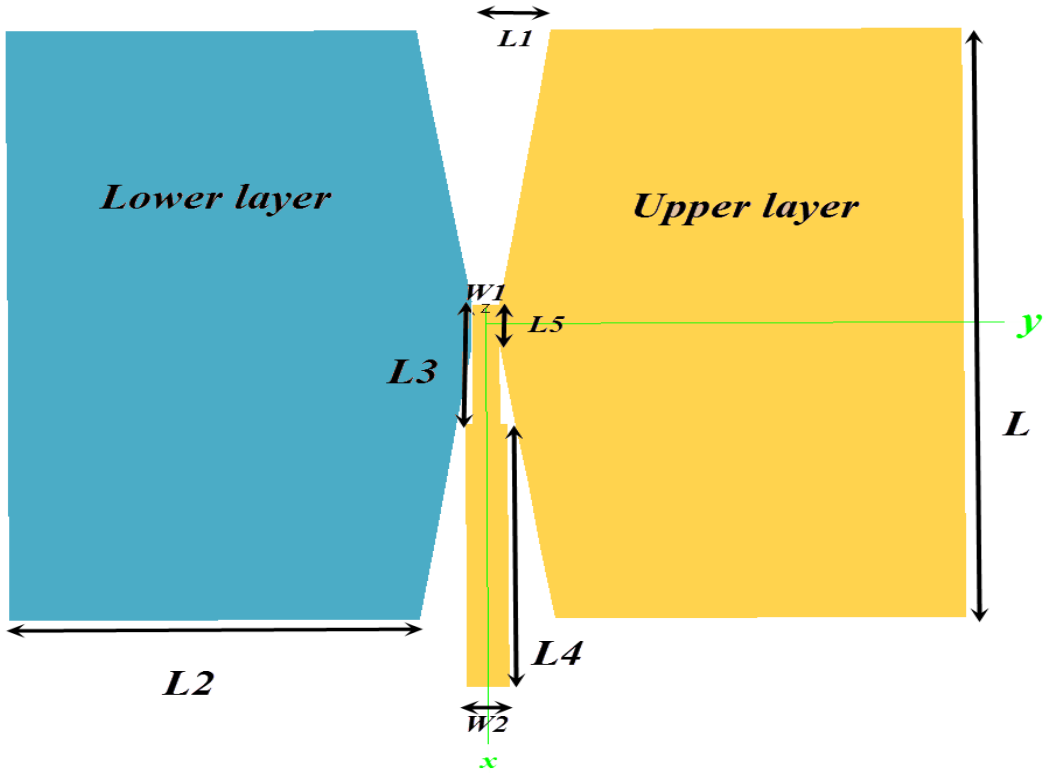

Figure3.14: Top view double side antenna geometry (FEKO)

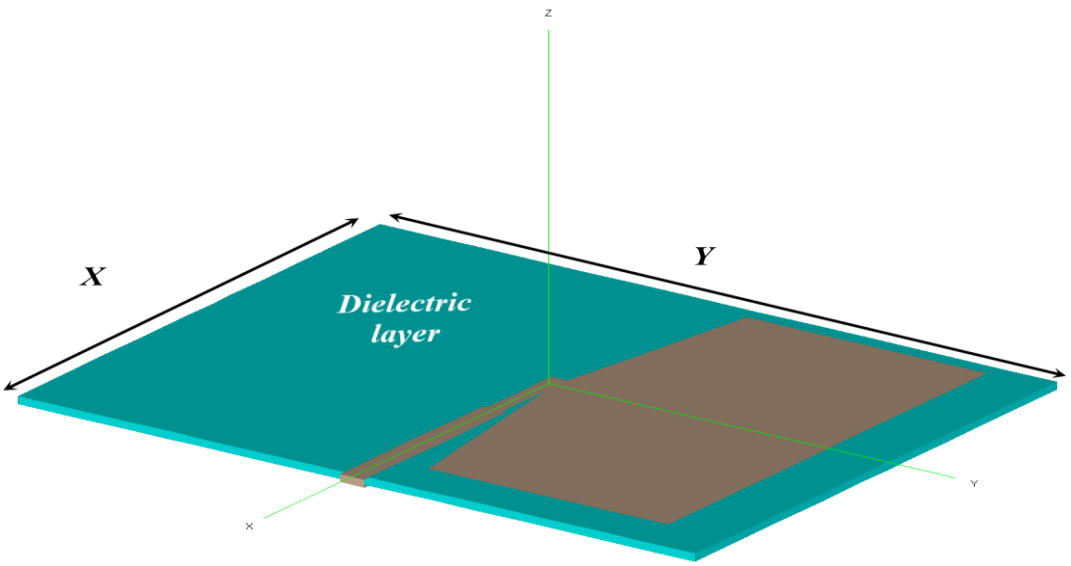

Figure3.15: FEKO simulation for side view antenna shape

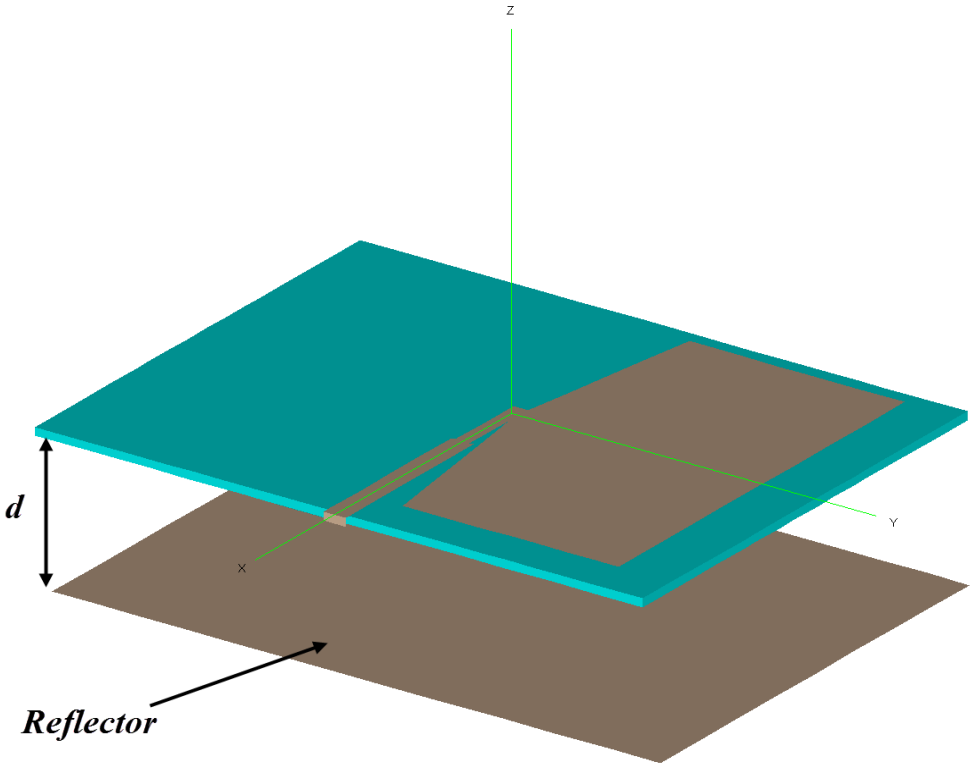

Figure 3.16: Bow-Tie Antenna with backing reflector

Table 3.1: Antenna dimensions in mm [17]

L	L1	L2	L3	L4	L5	W1	W2	X	Y	D
74	7.7	39	15	32	5	2.6	4	110	84	60

Figure 3.17 demonstrates the reflection coefficient at 1.5 GHz resonant frequency which is -35 dB and shows a good agreement with HFSS softnet as can be seen in Figure 3.18. The bandwidth characteristic of this antenna is broadband, with the rang of frequency from 1 GHz to 2.6GHz and the voltage standing wave ratio (VSWR) is less than 2 as can be seen by Figure 3.19.

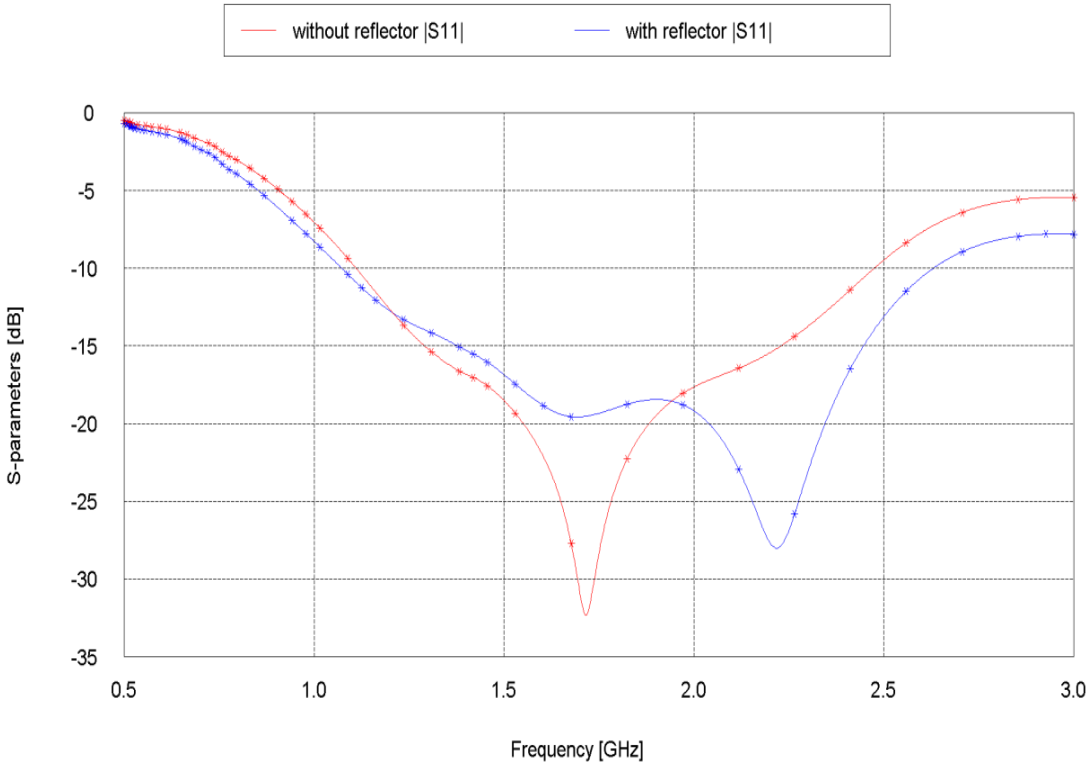

Figure 3.17: Comparisons return loss of antenna without reflector and with reflector

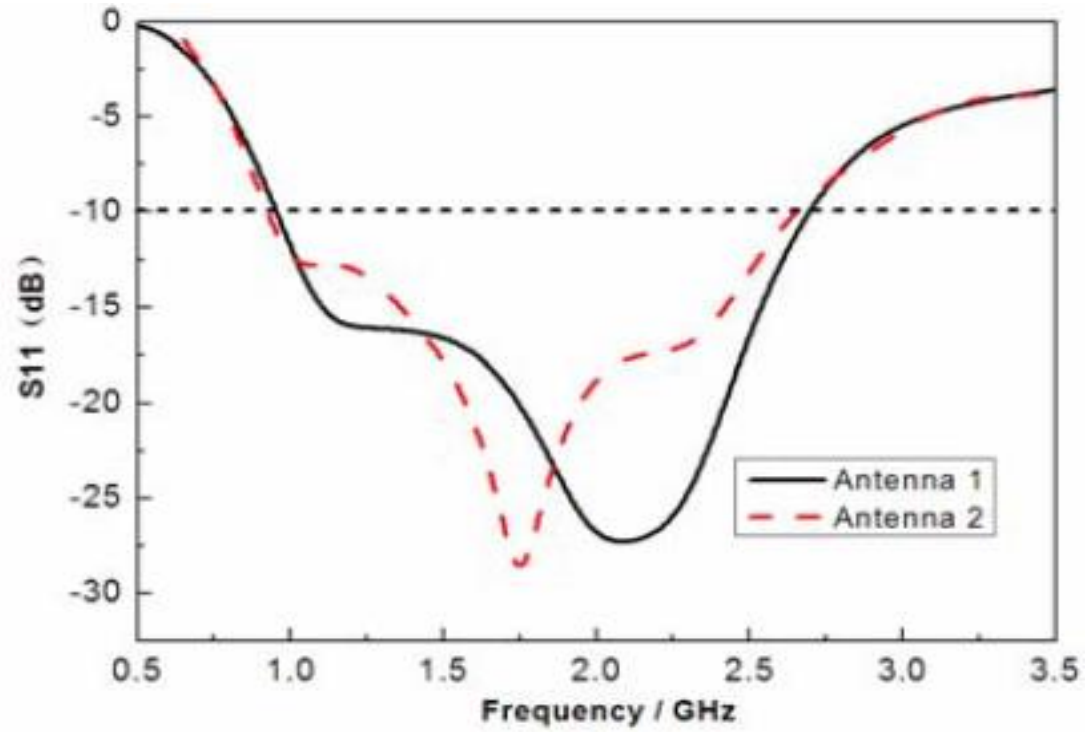

Figure 3.18: Comparisons return loss of antenna without reflector and with reflector [17]

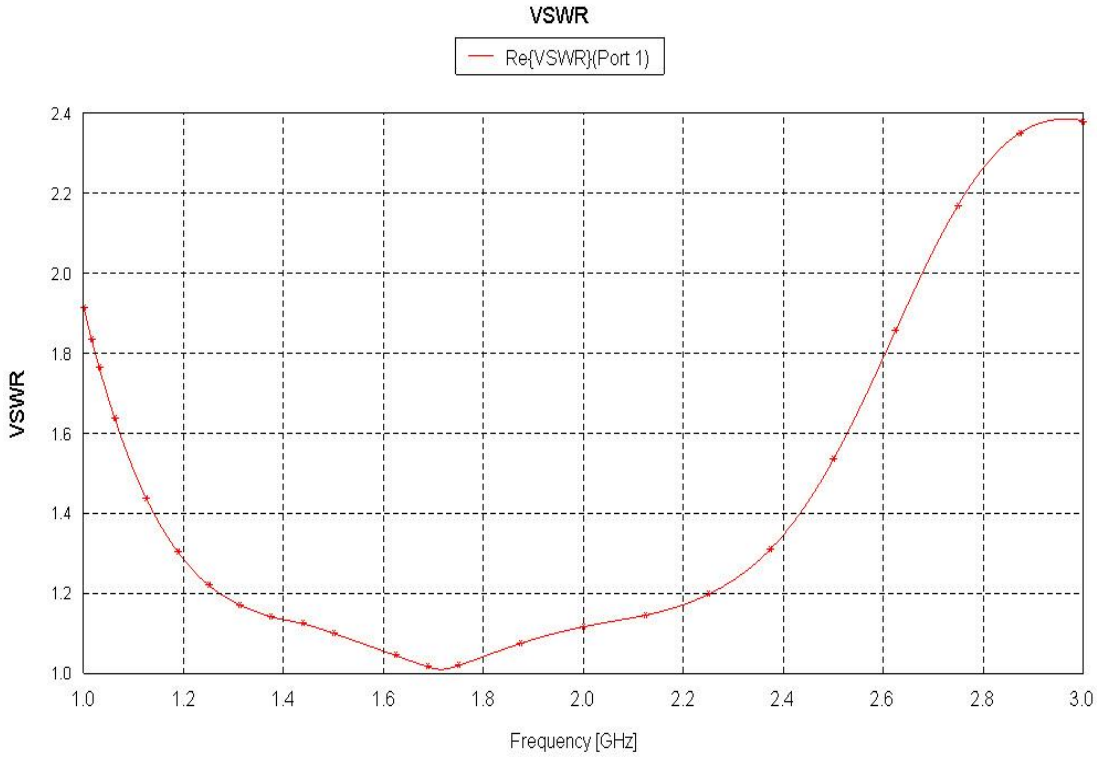

Figure 3.19: VSWR double-side BTA

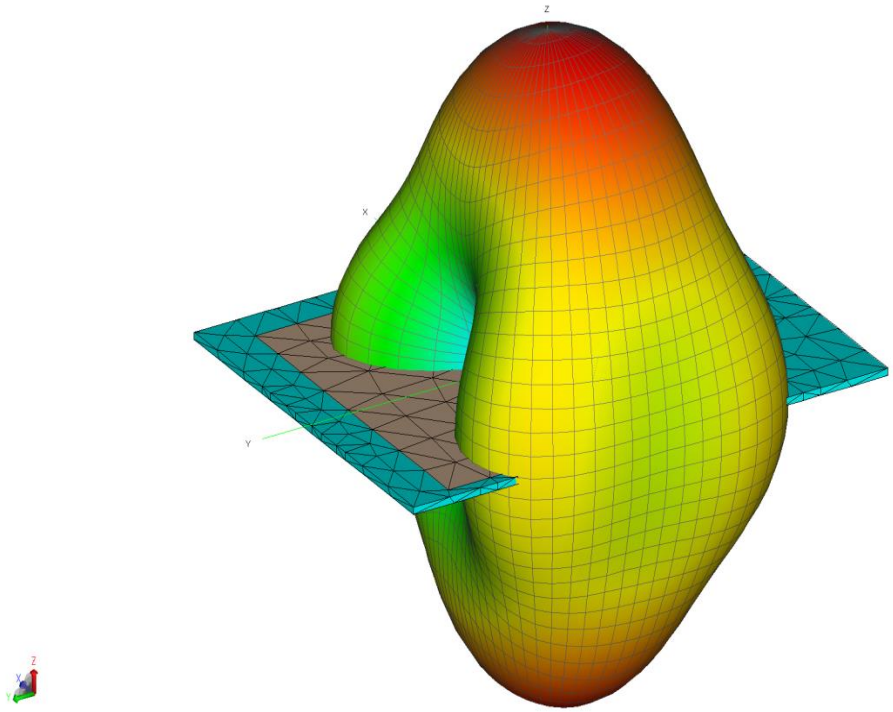

Figure 3.20: 3-D radiation pattern of BTA without reflector

When a reflector was added to the antenna, the return loss became 30 dB and the resonant frequency was shifted to 2.3 GHz. The radiation pattern and gain at 1, 1.5, 2 and 2.5 GHz for both antennas are presented in Figures 3.21 and 3.22. All the results are associated with previous work for justification [17].

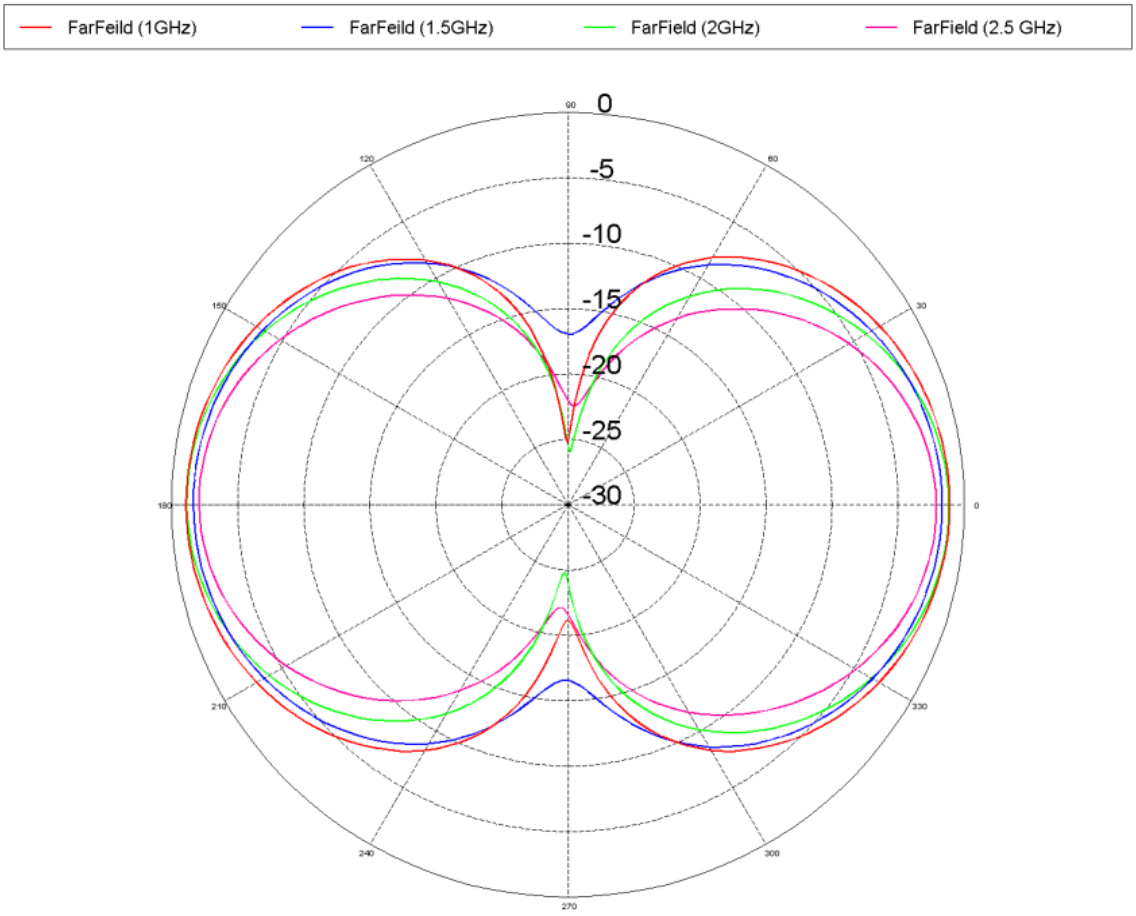

Figure3.21: Compact radiation patterns

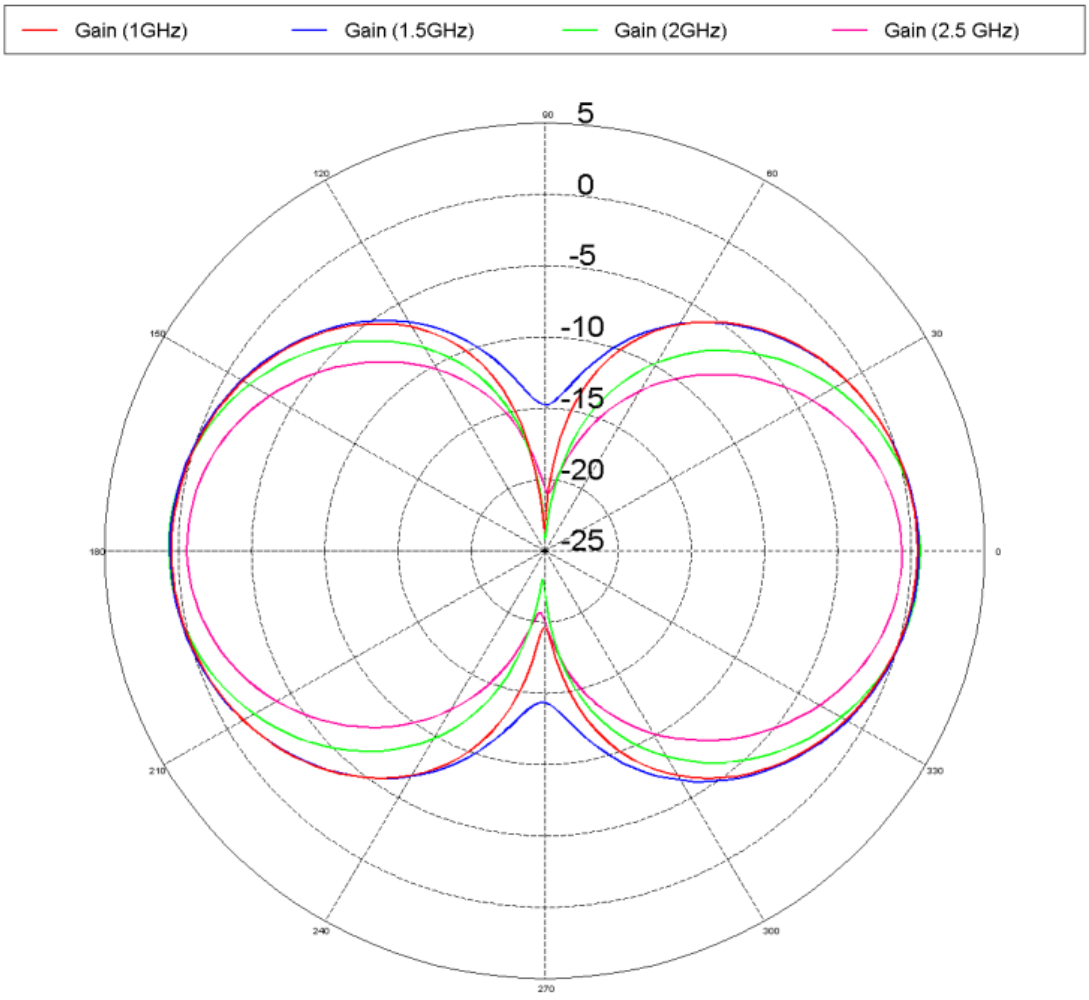

Figure 3.22: Compact antenna gain (dB)

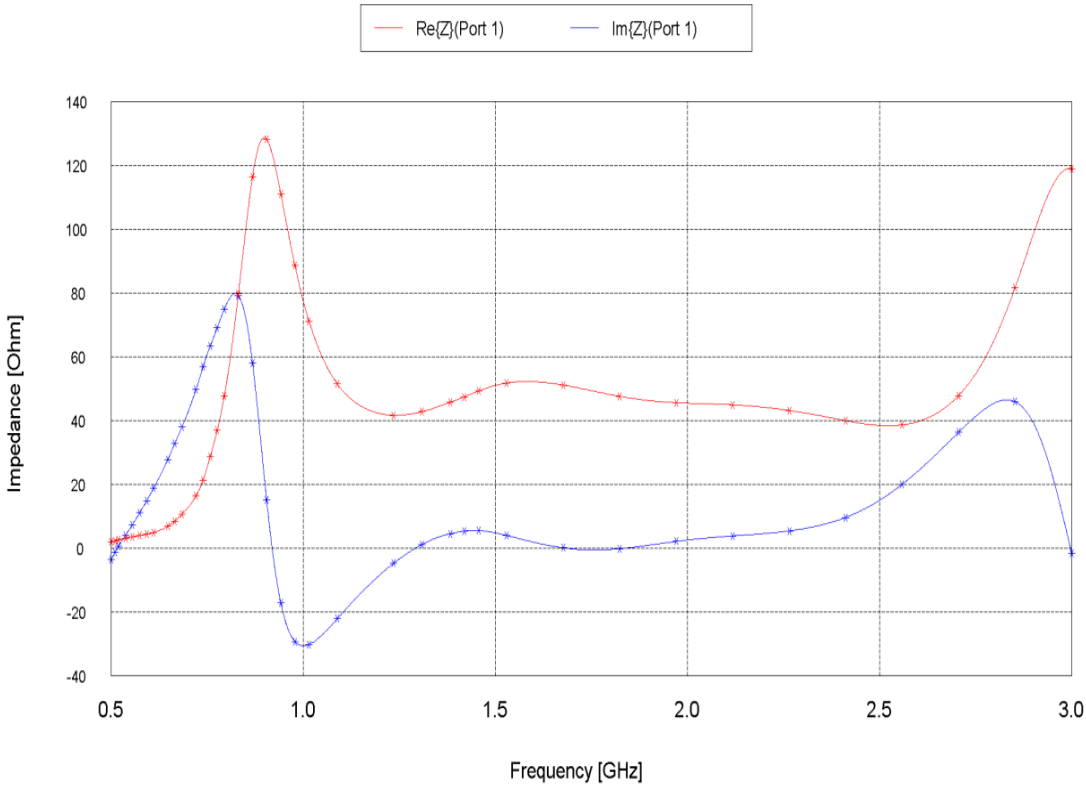

Figure 3.23: Double side BTA impedance without reflector

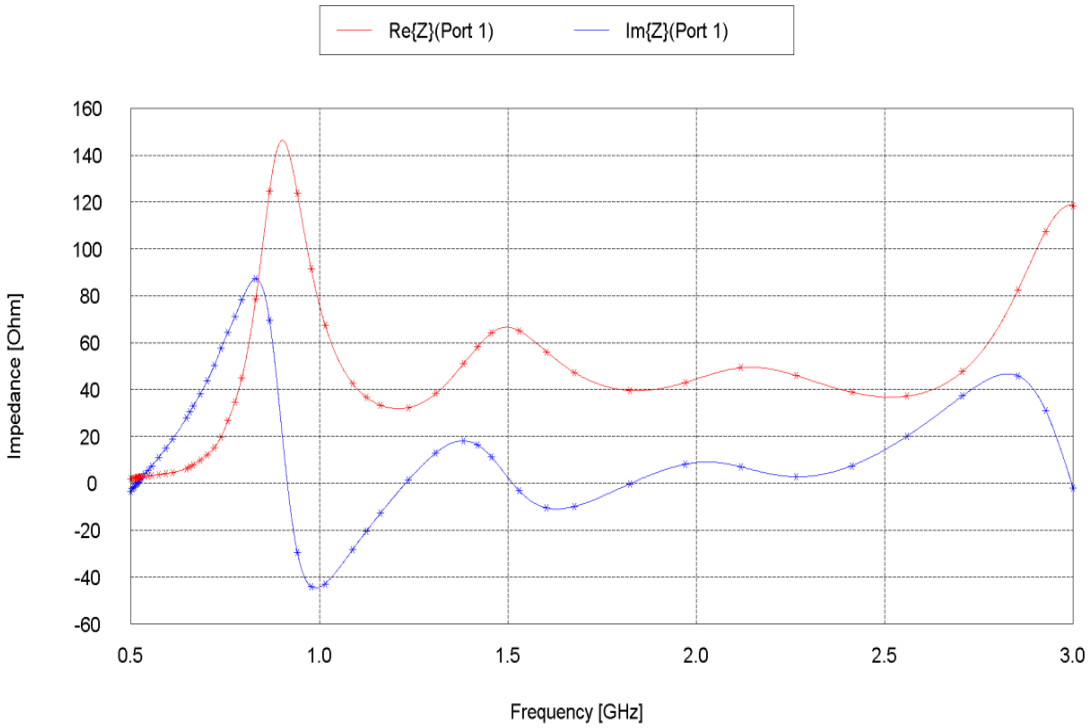

Figure 3.24: Double side BTA impedance without reflector

3.3.3 Multiband Bow Tie Antenna with MSL Feed

In this section, we will investigate the Double Side Bow-Tie Antenna with Microstrip Line Feed (DS-BTA-MSLF) for 5 GHz resonant frequency. Figure 3.25 shows that the antenna geometry consists of seven parts lying on the upper and lower RO3006 dielectric layer 50mm*50mm, with relative permittivity of 6.15 and a thickness of 1.27 mm; parts 1 and 5 represent the upper layer and parts 6 and 7 represent the lower layer, while parts 2, 3, and 4 lie on the sides of the dielectric substrate. Microstrip line designed to provide 50 Ω characteristics impedance as shown in Figure 3.29 to get a good agreement with feed port. All antenna and transmission line dimensions are listed in Table 3.3.

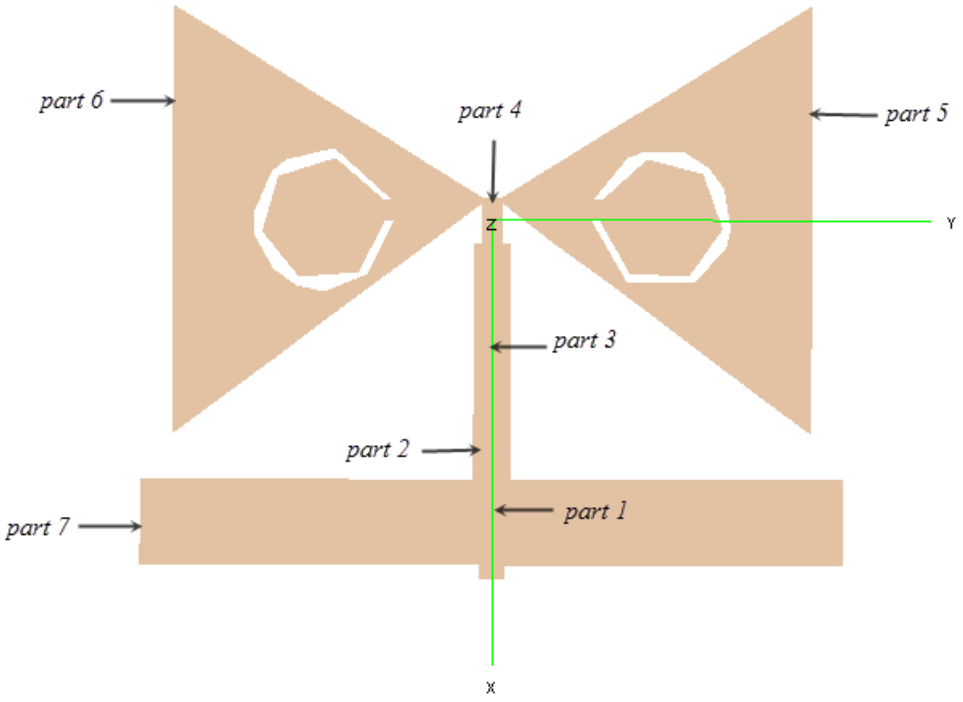

Figure 3.25: Antenna geometry modified by FEKO

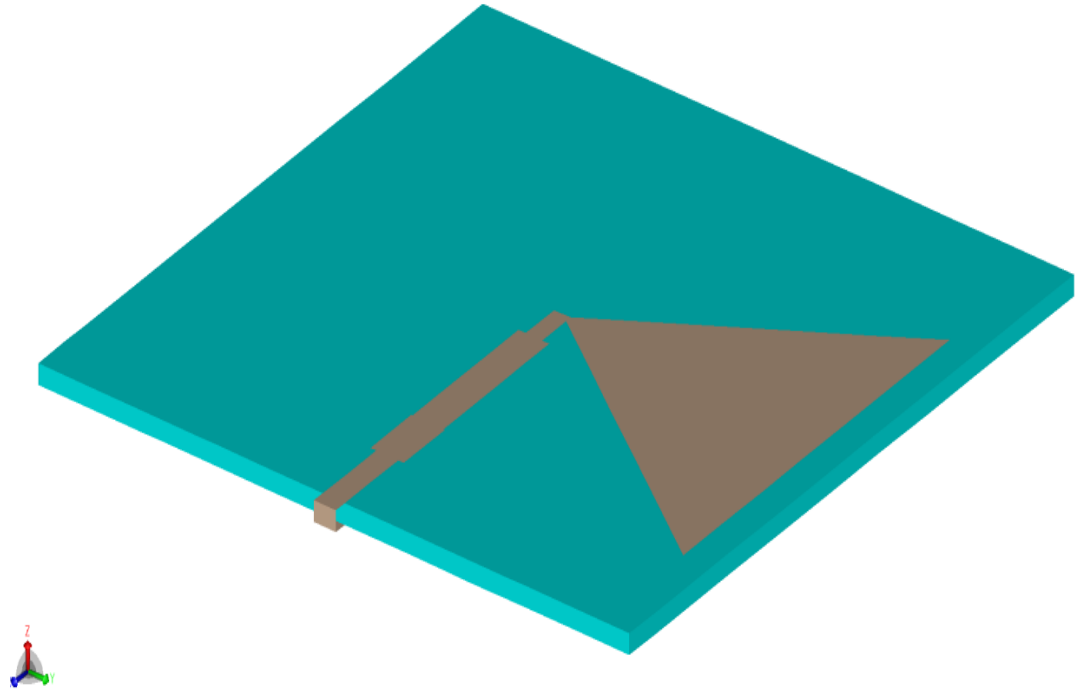

Figure 3.26: Upper layer antenna side view

Table 3.2: Dimensions of antenna and feeding network [18]

Part	Width (mm)	Length(mm)
1	1.87	6
2	2.8	4.6
3	2.6	11.9
4	1.4	3.2
5	22	30
6	22	30
7	50	6

In the simulation results, Figure 3.27 shows that corresponding return loss at resonant frequency is approximately 36 dB. Figure 3.28 shows the return loss to the antenna with HFSS software simulator and gave close result comparing with FEKO software simulation. In Figure 2.29, it clear that the characteristic impedance to the antenna system is around 50 Ω which is indicated to good matching between the antenna and MSL.

Table 3.3: Gain measured by FEKO

Resonance Frequency (GHz)	Gain (dB)
2.4	1.8
3.5	1.5
5.3	4.5

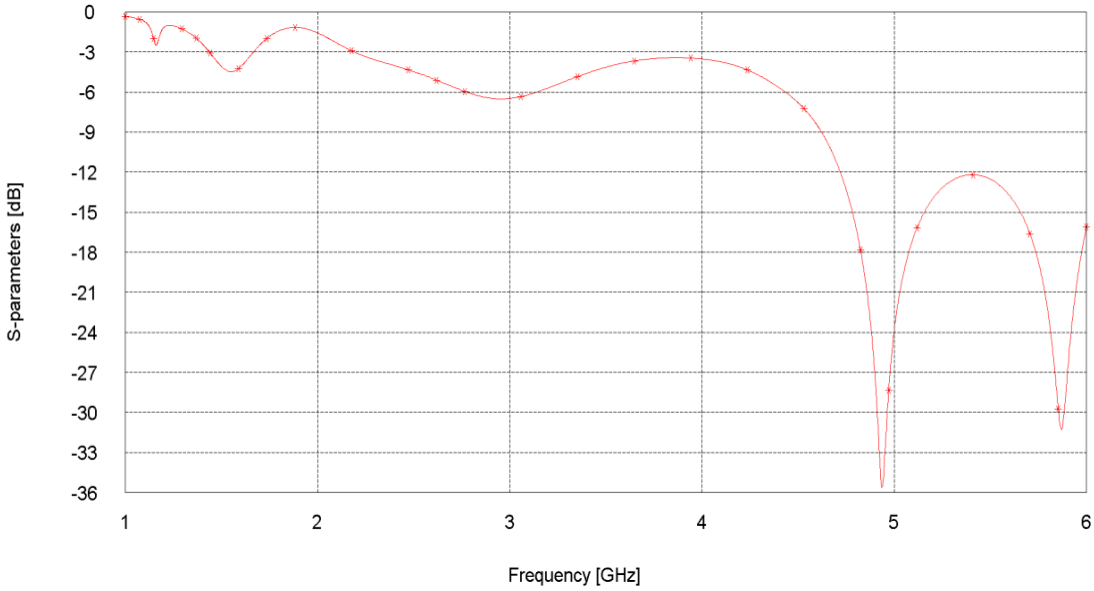

Figure3.27: FEKO result return losses for DS-BTA-MSLF

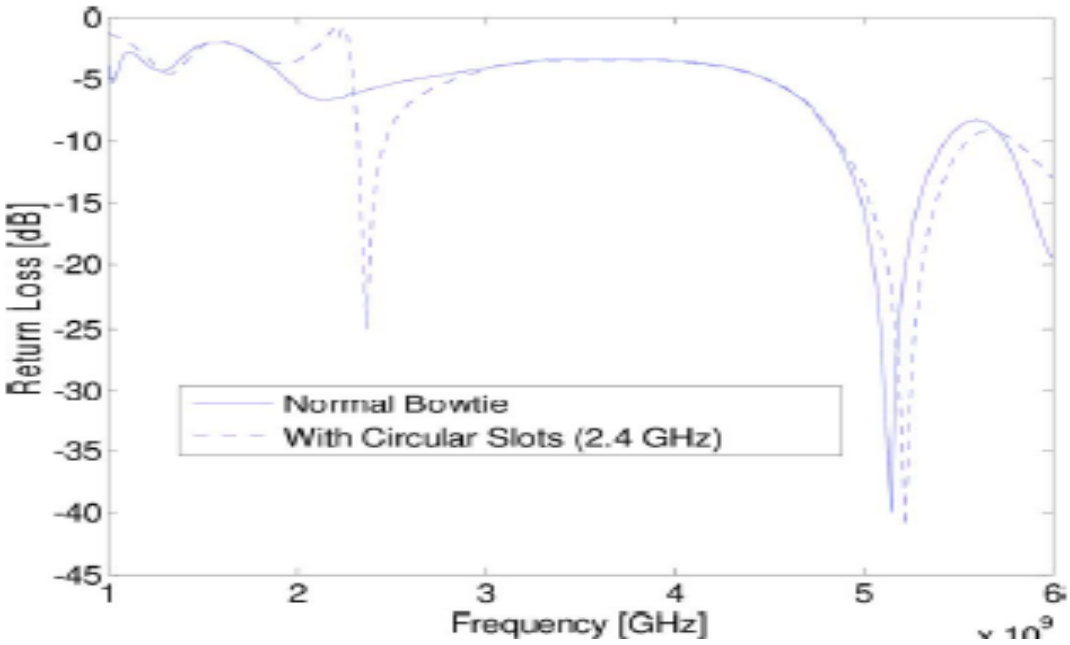

Figure 3.28: HFSS result return losses for DS-BTA-MSLF [18]

VSWR to the antenna system is less than 2 which is depicted in Figure 2.30. The gain for each resonant frequency is shown in Table 3.4. The antenna radiation pattern in Figure 3.31 and 3.32 has shown decent omnidirectional antenna characteristics. FEKO 5.5 full wave simulation was used to finish this work and also compared with Ansoft HFSS v 10.1 results in [18]

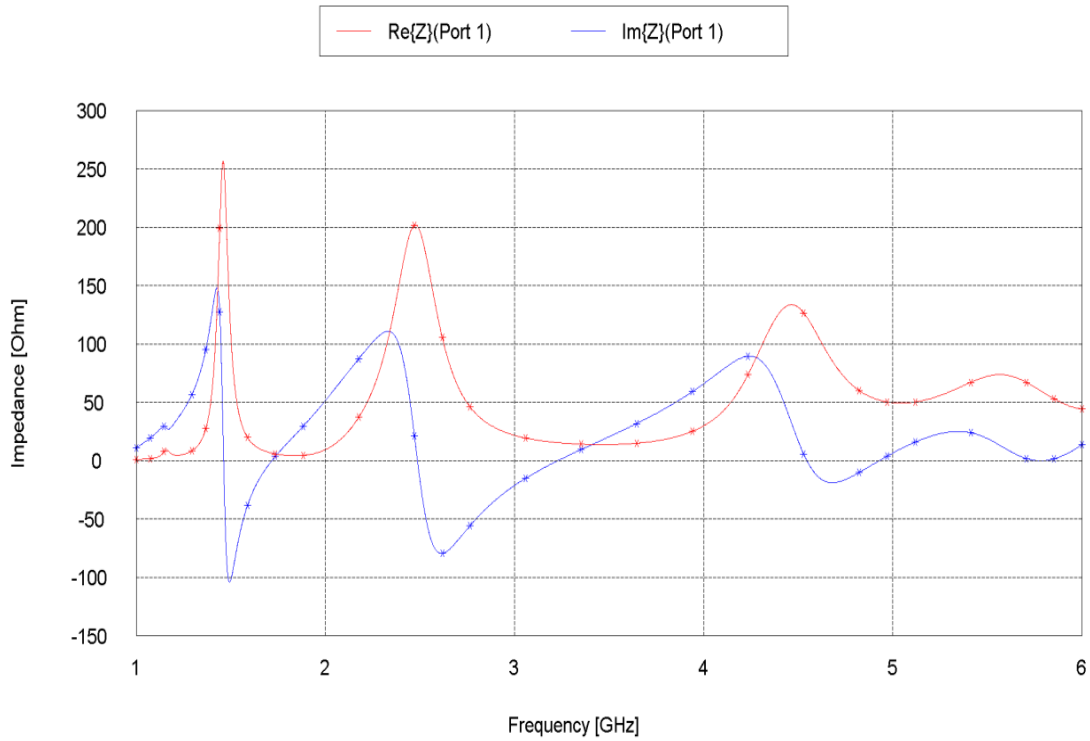

Figure 3.29: Input impedance to the DS-BTA-MSLF

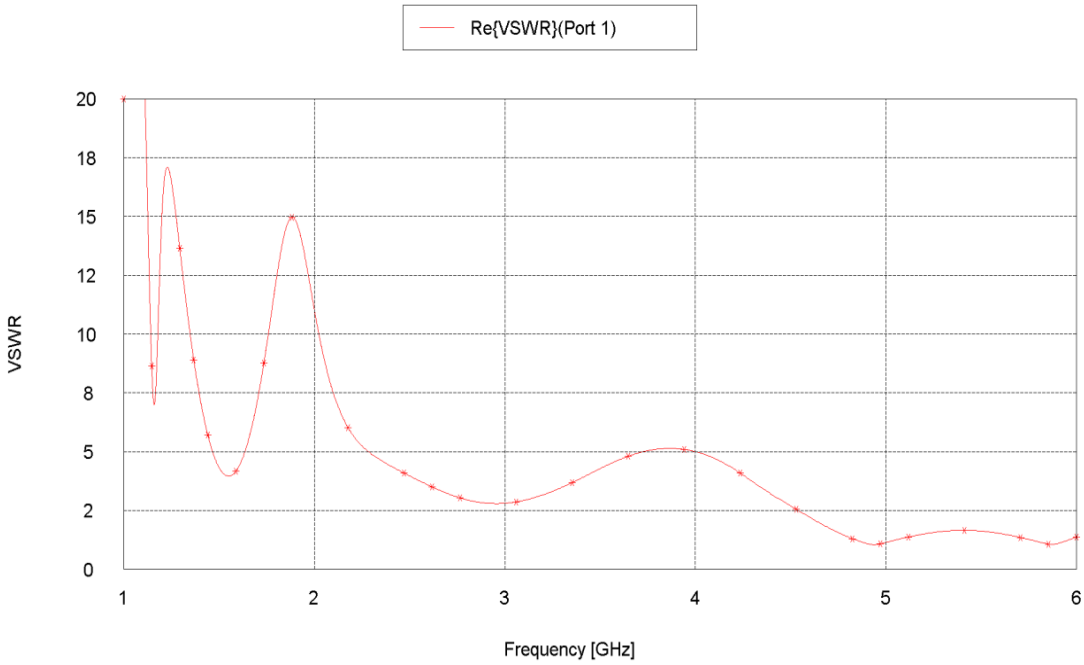

Figure 3.30: VSWR to the bow-tie antenna with MSL fed

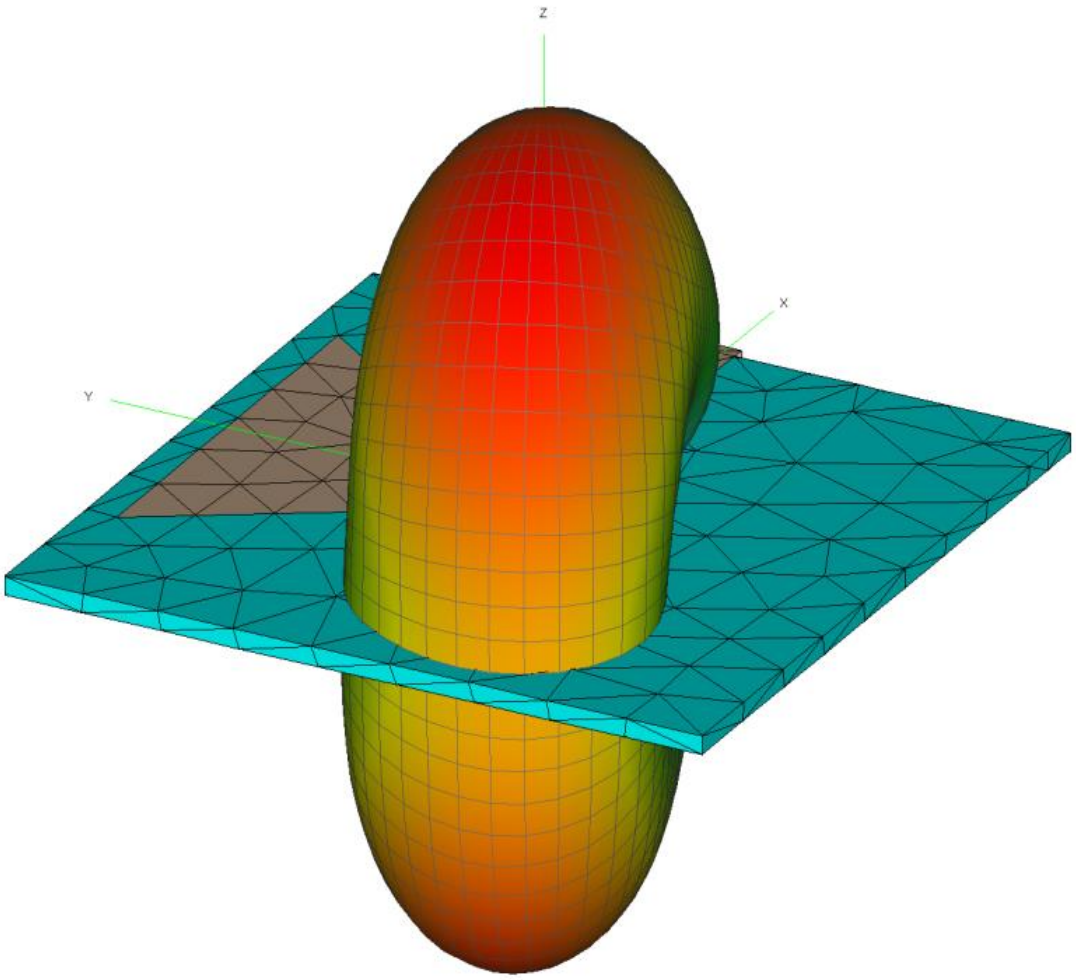

Figure3.31: Antenna 3-D radiations pattern at 5 GHz

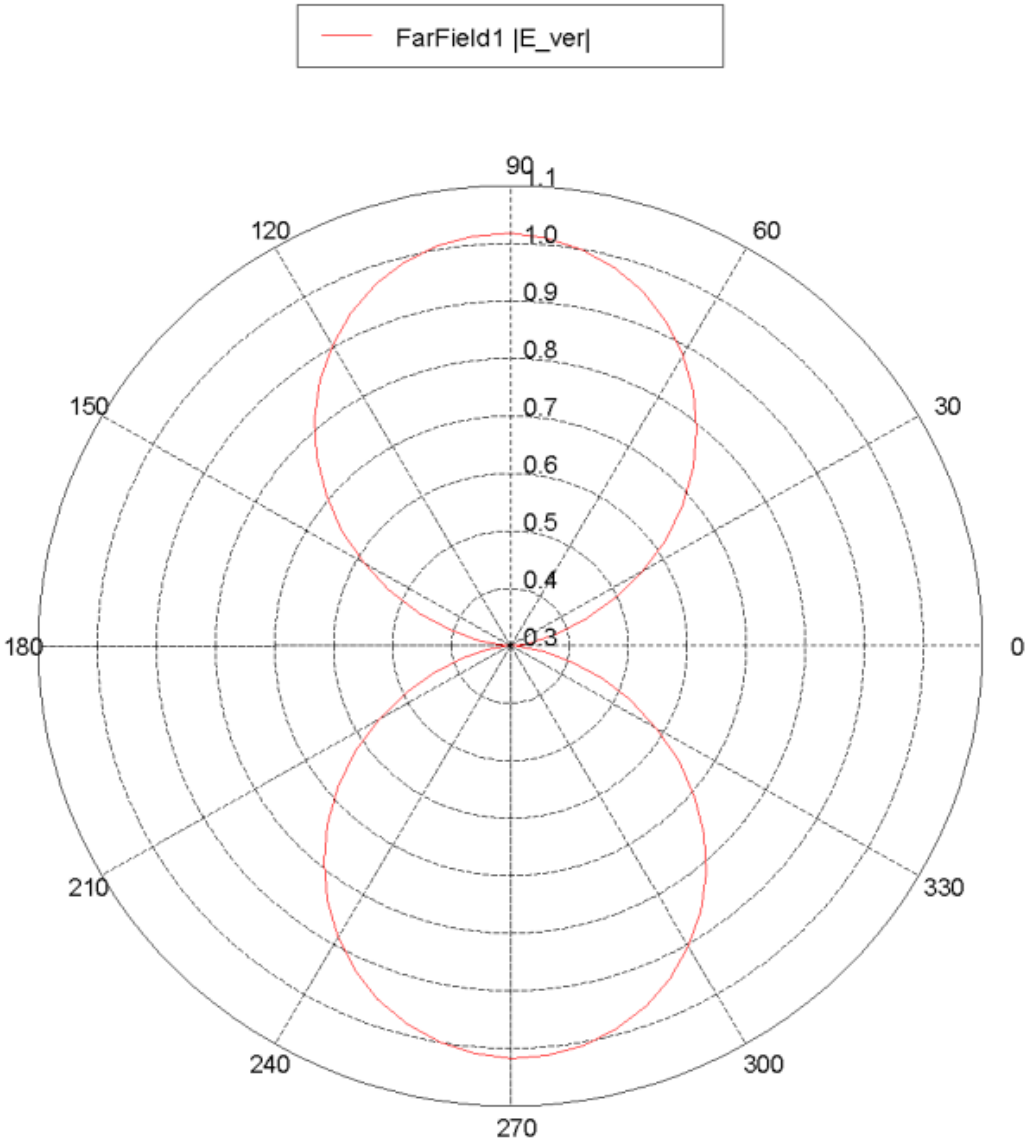

Figure3.32: 2-D antenna radiation pattern at $\theta=0^{o}$ and $\phi=90^{o}$

In the previous sections of this chapter, we modified different kinds of BTA with Unbalanced transmission line feed and show their performances.

The next section discusses how to change the transmission line from unbalanced to balance and then connect to BTA to verify antenna performance and compare with BTA which is connected to the UTL.

3.4 Unbalanced to Balanced Transitions

3.4.1 Basic Conceptions

First of all, the meaning of the balanced and unbalanced TL can be considered. This idea comes from TL considerations and has little to do with the antenna performance. It will be discussed with a simple example of Double-Microstrip Lines placed parallel as presented in Figure 3.33 so as to understand the balance.

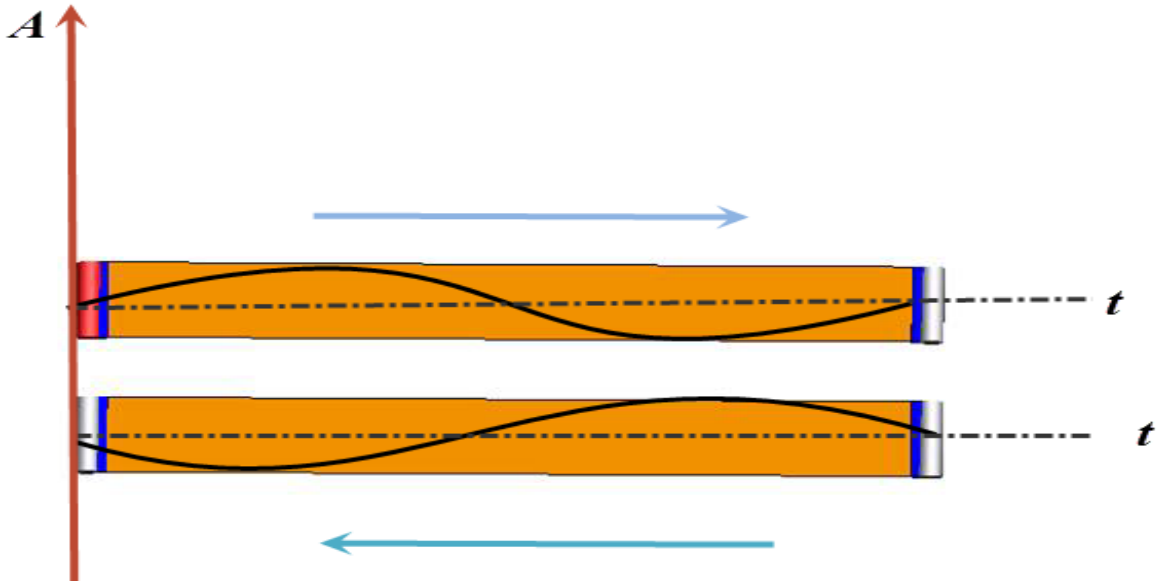

Figure 3.33: Signals traveling in transmission line

In an ideal case, the current distributions in the parallel Microstrip lines are equal in magnitudes and opposite in the directions to each conductor. So, in this case, the fields sum up to give the total effect, which is zero since its positive on one conductor and negative on the other [19]. It should be noted that to get perfect cancellation, two conductors must be in the same position which is impossible. In practice, the distance between two conductors must be as close as possible in terms of the wave length.

In the case of parallel TL, when the current on the conductors are not equal, the electrical field surrounded in both conductors will be different and it will not be canceled, so the radiation will occur on TL and it will lose part of the power that was delivered to the load. In other words, the power provided from the source is not equal to the power delivered to the antenna. This case is known as unbalanced TL [19].

3.4.2 MSL-to-CPS Transition (Balun)

In order to minimize the feed radiation, the balun will be used. There are many balun configurations that can be used for the transition of MSL to CPS. In this section, MSL-to-CPS T-junction balun transition will be presented, as can be seen in Figure 3-34. [20].

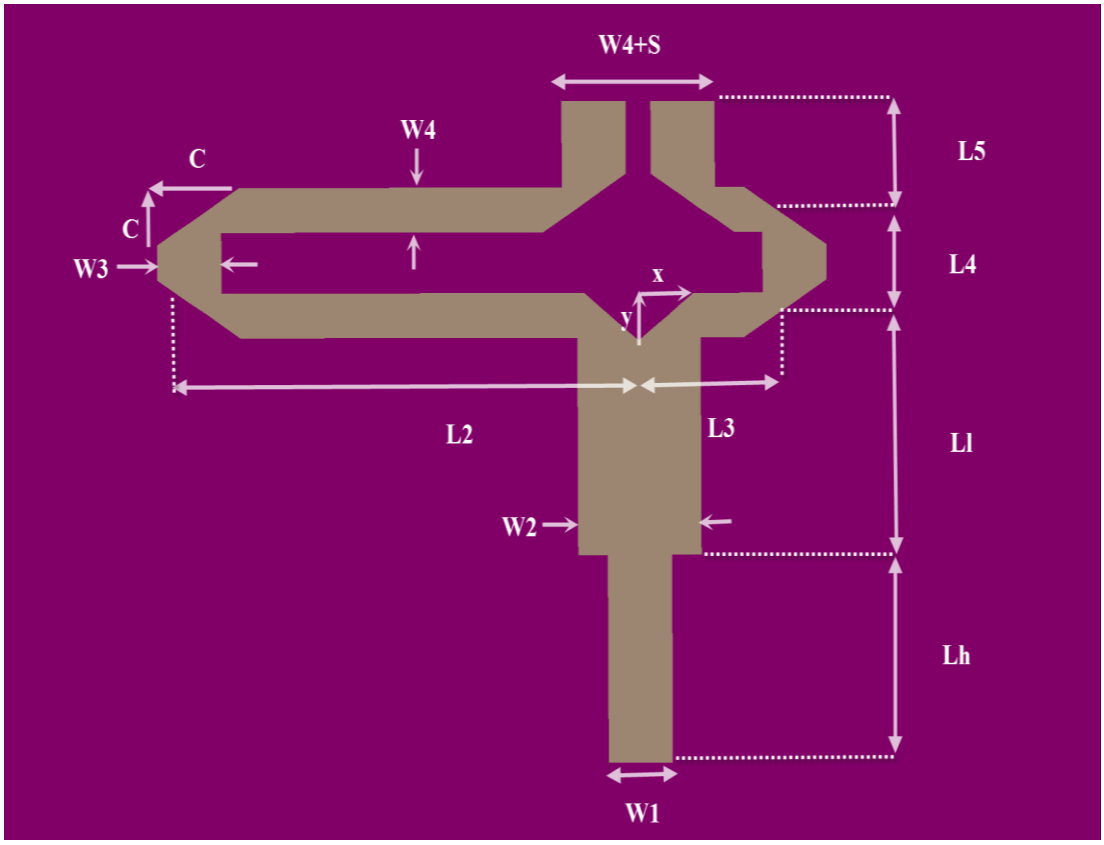

Figure 3.34: Tee-junction balun shape

3.4.2.1 Tee-Junction Balun Transition [20]

For this Tee-junction balun, the double ends to the CPS parts, as well as the end of MSL connected to the source are all assumed to be 50 Ω characteristics impedance. Quarter wavelength 35.5Ω impedance transition is employed for matching between MSL feed and T-junction (divided / combination) TL. 90^o miters bends are used to achieve λ/2 transmission line length.

Figure 3.35 shows the Tee-Junction equivalent circuit [**21**]. At this kind of junctions, discontinuities will occur in the power flow that will be processed in the next chapter by using taper technique and it can be accounted by lumped susceptance, B. Equation (3.36) is used for designing a divider, matched to the impedance Z_o.

i.e.

$$\frac{1}{Z_o} = \frac{1}{Z_1} + \frac{1}{Z_2} + jB \tag{3.36}$$

Where Z_o is the characteristic impedance to the common line, Z_1 is the characteristic impedance to upper line, and Z_2 represents to the characteristic impedance to the lower line.

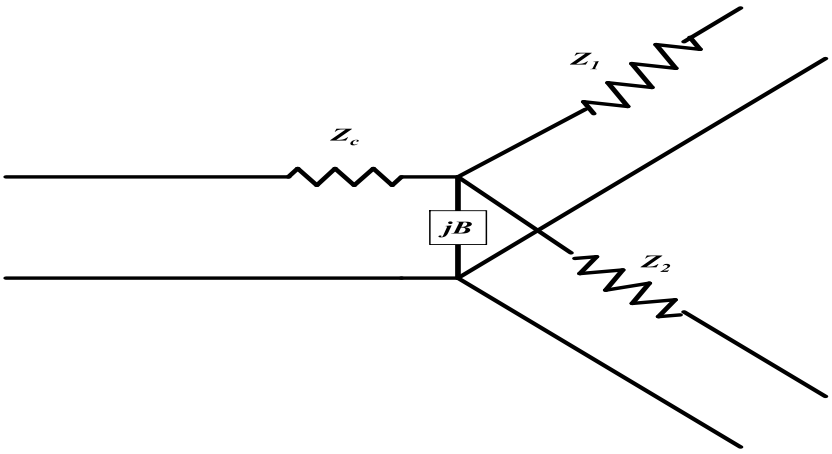

Figure3.35: Tee-junction divider/combination model

For the lossless transmission line, *B*=0 which makes the imaginary part zero. In that case, the characteristic impedance will be purely real.

$$\frac{1}{Z_{\circ}} = \frac{1}{Z_1} + \frac{1}{Z_2} \tag{3.37}$$

We can see from Equation (3.36) that if the input impedance of the Tee-Junction is 50Ω characteristics impedances, the output will be 100Ω, which is not acceptable i.e. 50Ω is required. This can be achieved by the quarter wavelength transformer which is used to produce 25 Ω at the terminal combining the input and output TL as in Figure3.35. The input impedance (Z_{in}) calculated by Equation (3.38).

$$Z_{in} = Z_1 \frac{Z_l + jZ_1 \tan \beta l}{Z_1 + jZ_l \tan \beta l} \tag{3.38}$$

Where $\beta = \frac{2\pi}{\lambda}$ So, $\beta l = \frac{2\pi}{\lambda}.\frac{\lambda}{4} \Rightarrow \beta l = \frac{\pi}{2}$

Which result to:

$$Z_{in} = \frac{Z_1^{\ 2}}{Z_l} \tag{3.39}$$

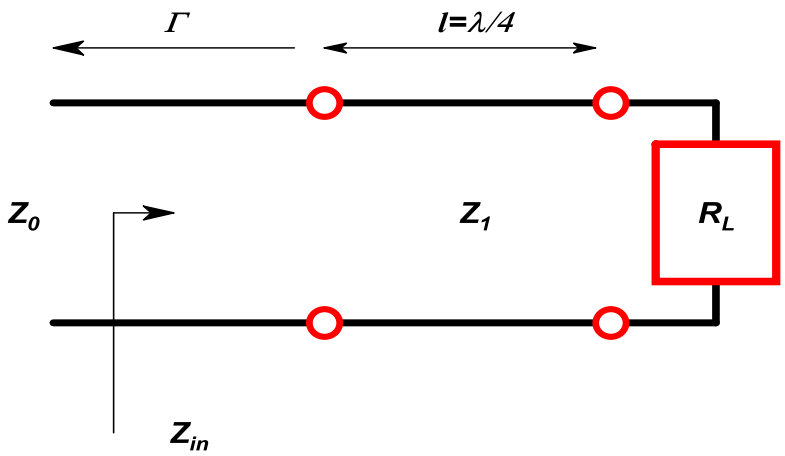

Figure3.36: Equivalent circuit with quarter wavelength added between input and output port

After the matching, 180^o phase shift delay was produced to achieve balance phase between two branches in CPS. This was achieved by adjusting their lengths so that l_2-l_3=λ_g/4. Where, λ_g is guided wave length, l_2 is the left side length, and l_3 is the right side length as indicated in Figure 3-35.

3.4.3 Simulation Results of Balun

MSL-to-CPS transition balun is designed by using the equations which were mentioned before to achieve 2.45 GHZ resonant frequency and modified by FEKO V.5.5 software simulator. The balun is placed on the RT-Duroid 6010 substrate layer

with relative permittivity of 10.2 and thickness of substrate of 2.5mm. All the dimensions of balun are listed in Table 3.5. At CPS side two kinds of excitation are used, even and odd excitations. When we connect the two ends of CPS with ground plane, it is known as even excitation mode, while the odd mode is that which connect the couple ports with each other. The current will be distributed by 180^{o}phase shift between them as shown in Figure 3.37.

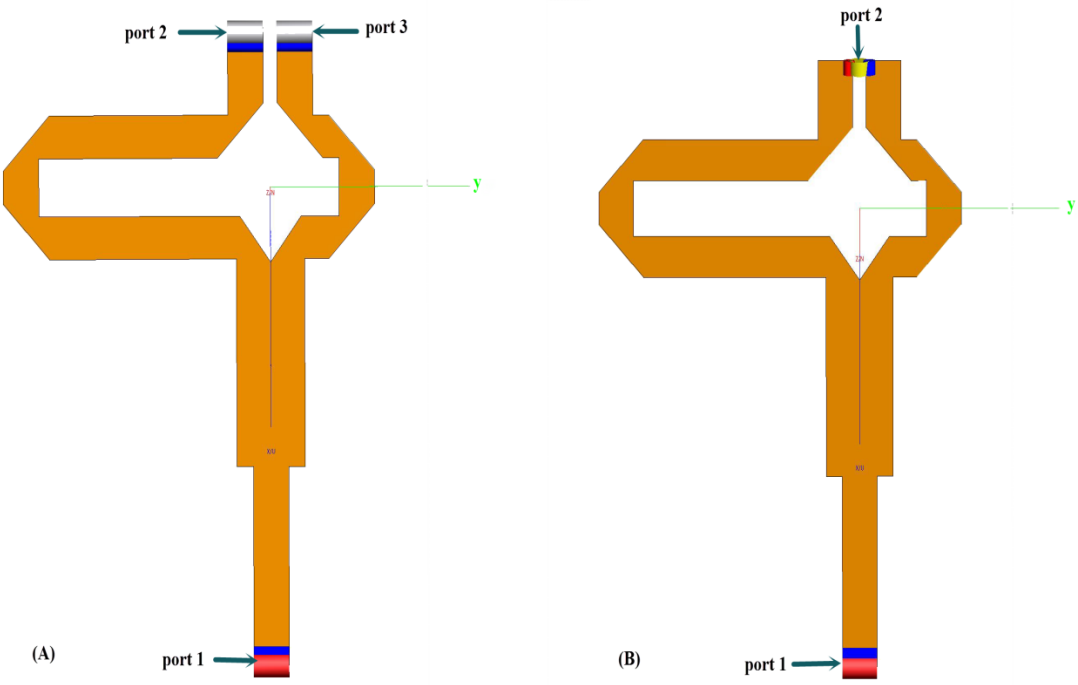

Figure 3.37: (A) Even mode balun geometry, (B) Odd mode balun applied by FEKO

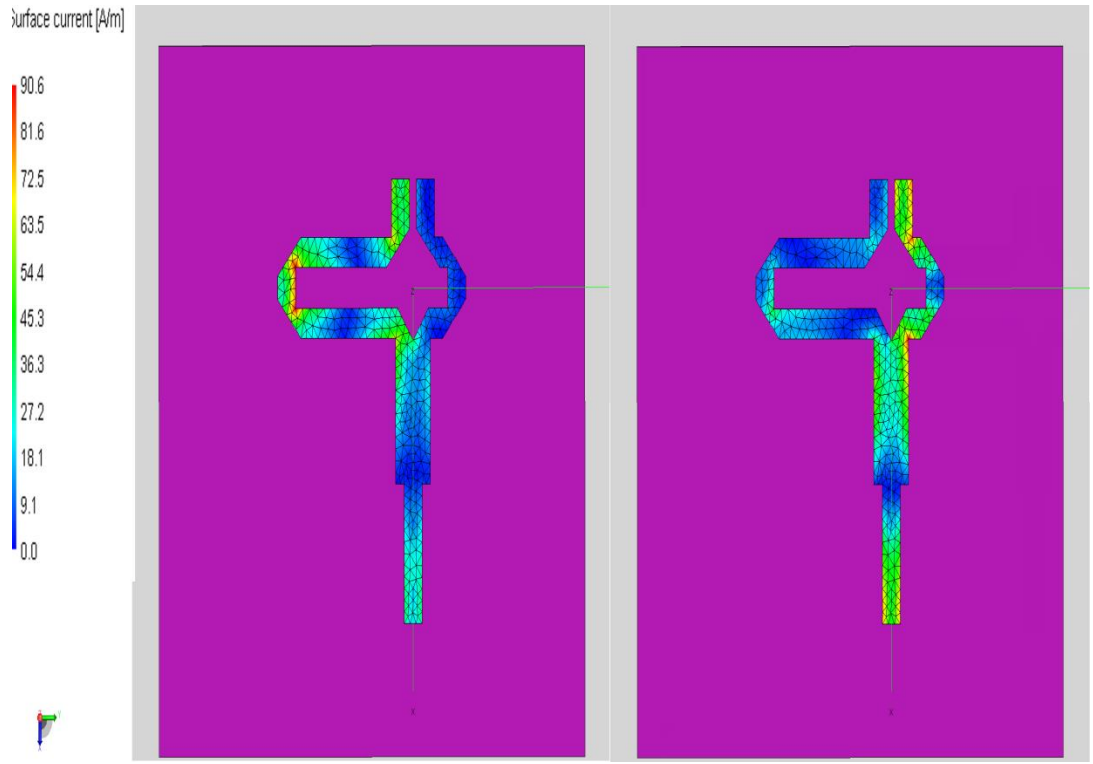

Figure 3.38: Phase current distribution between couple strip line in CPS

Figure 3.45 shows that MSL impedance is matched with CPS transmission line impedance. Figure 3.39 shows the reflection coefficient of the balun S_{11} which is referred to as the even mode (red line) and insertion losses (S_{21}) which is represented to odd mode (blue line). VSWR is less than 2 with broadband 1GHz-3GHz as displayed in Figure 3.41. Note that all the results were compared with Ansoft HFSS 11.2 software full wave simulator in [20].

Table 3.4: Dimensions for the MSL-to-CPS transition (balun)

Balun Element	**W1**	**L1**	**W2**	**L2**	**L3**	**W3**	**L_h**	**L5**	**S**	**X**	**Y**
Dimensions (mm)	2.33	11.3	4.48	5.66	16.32	2.33	10.8	5.66	0.9	2	2.5

Figure 3.39: Input impedance of the balun at port one

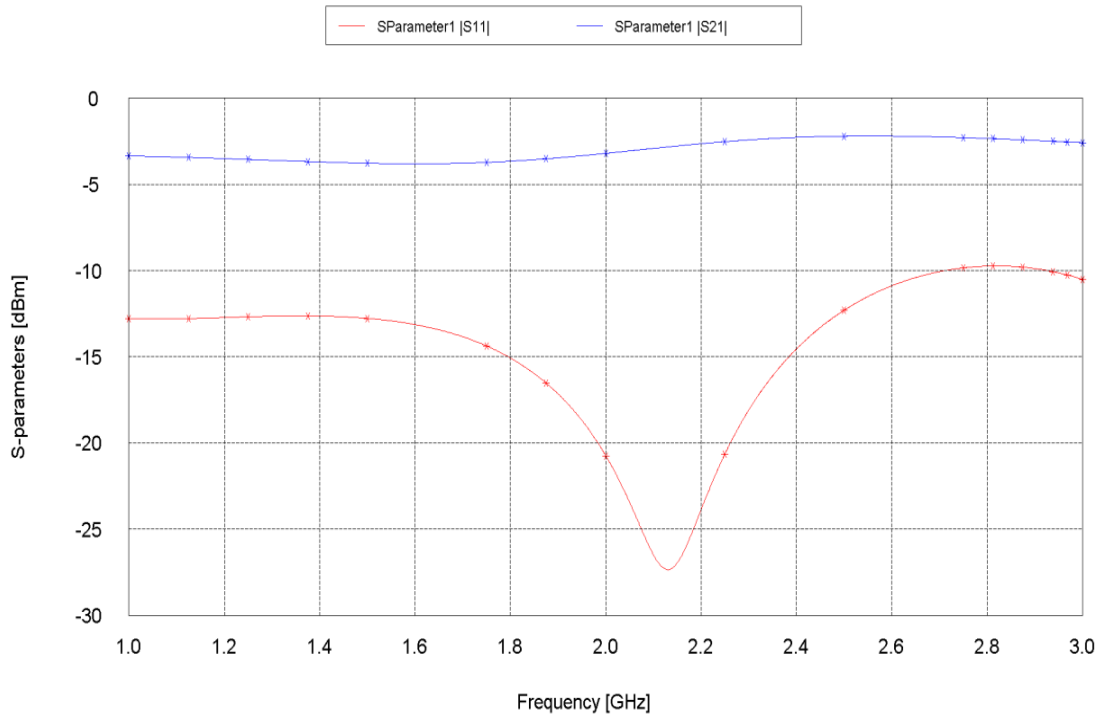

Figure 3.40: MSL-to-CPS balun return losses

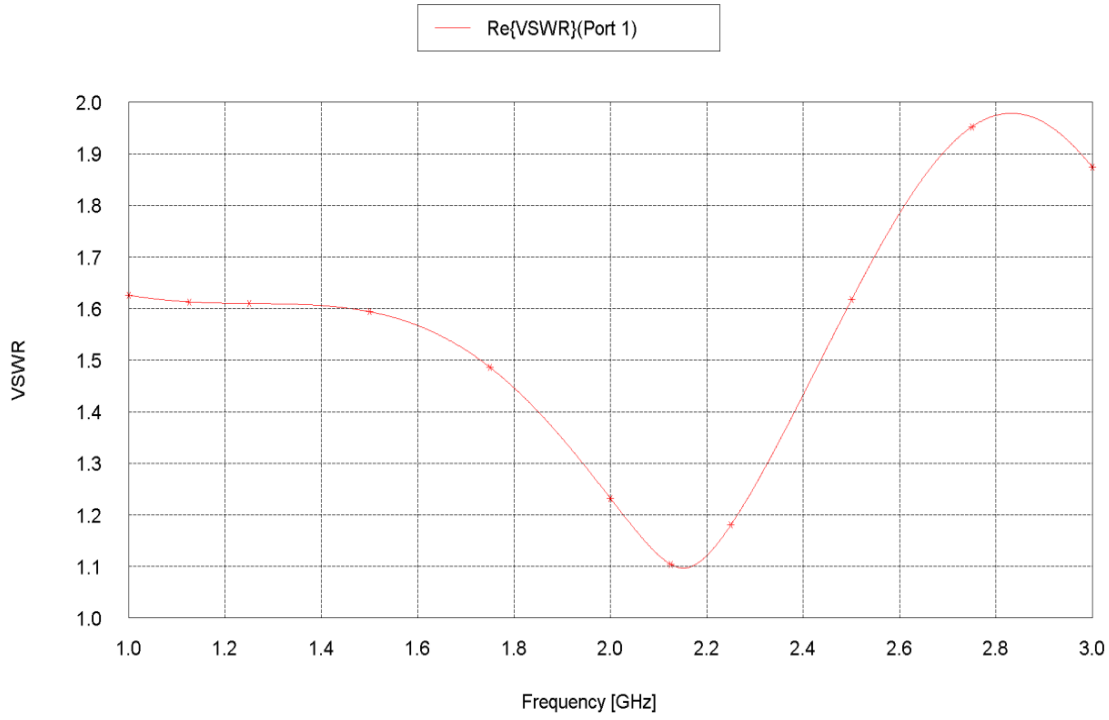

Figure 3.41: VSWR to the transition applied by FEKO

3.4.4 Design and Simulation Result to BTA as a Load to Balun

In this section, new Bow-Tie Antenna design with balance transmission line feed (balun) is suggested as shown in Figure 3.42. The antenna and balun are on the substrate layer with ε_r=10.2 and height 2.5mm. Below them there are truncated ground plane which was employed as a reflector to the antenna. The dimensions of proposed antenna are shown in Table 3.6. FEKO software 5.5 was used to simulate antenna system to see the performance.

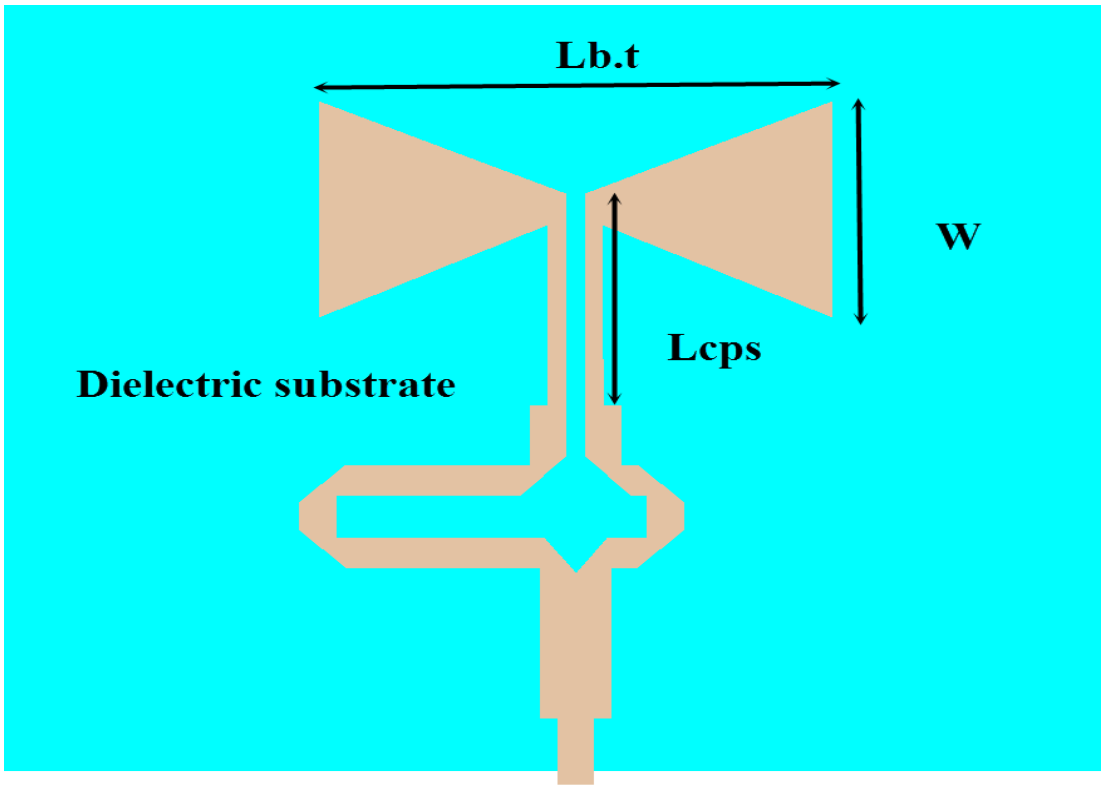

Figure 3.42: Antenna and balun configurations (FEKO)

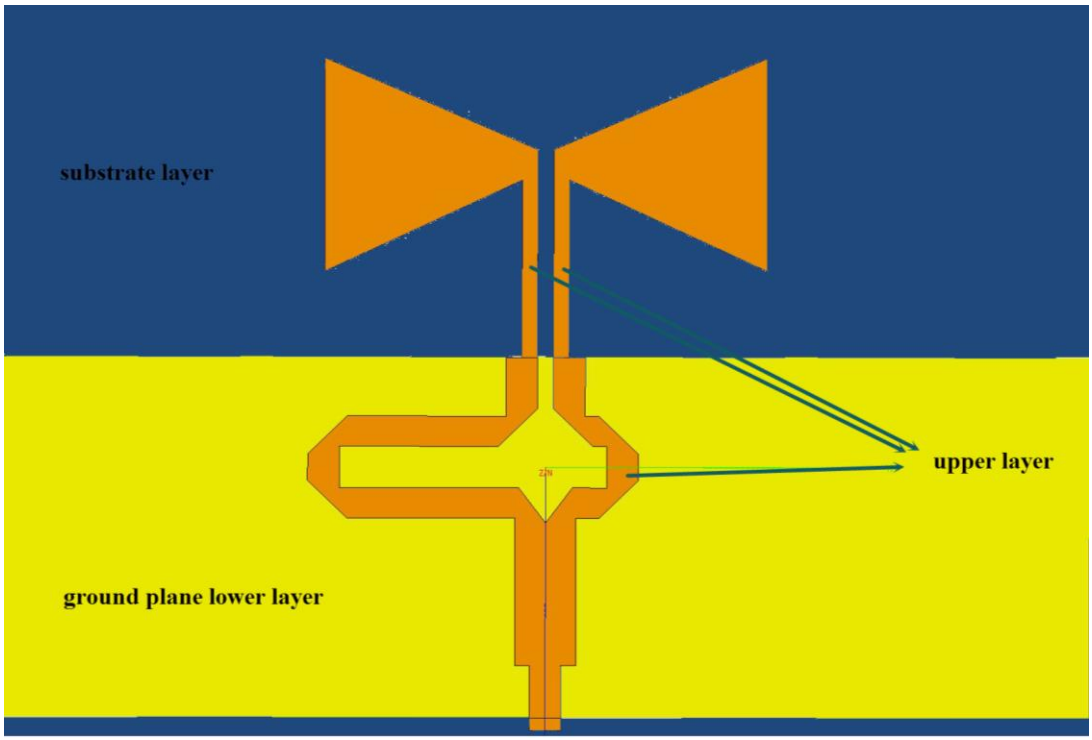

Figure 3.43: Top view describe truncated ground plane

Table 3.5: Antenna and balun dimensions

Antenna Balun Element	**W1**	**L1**	**W2**	**L2**	**L3**	**W3**	**L_h**
Dimensions (mm)	2.33	11.3	4.48	5.66	16.32	2.33	10.8
Antenna Balun Element	L5	S	X	Y	L_{cps}	L_{bt}	W
Dimensions (mm)	5.66	0.9	2	2.5	15.92	23.5	19.3

Figure 3.45 illustrates the return loss of the antenna system which is less than 10 dB and the insertion loss is less than 3 dB. VSWR is less than 2 to the bandwidth (1.95GHz-2.6GHz) as shown in Figure 3.46. The antenna gain at 90^o is equal to 3 dB as in Figure 3.48 and the radiation pattern is demonstrated in Figure 3.48.

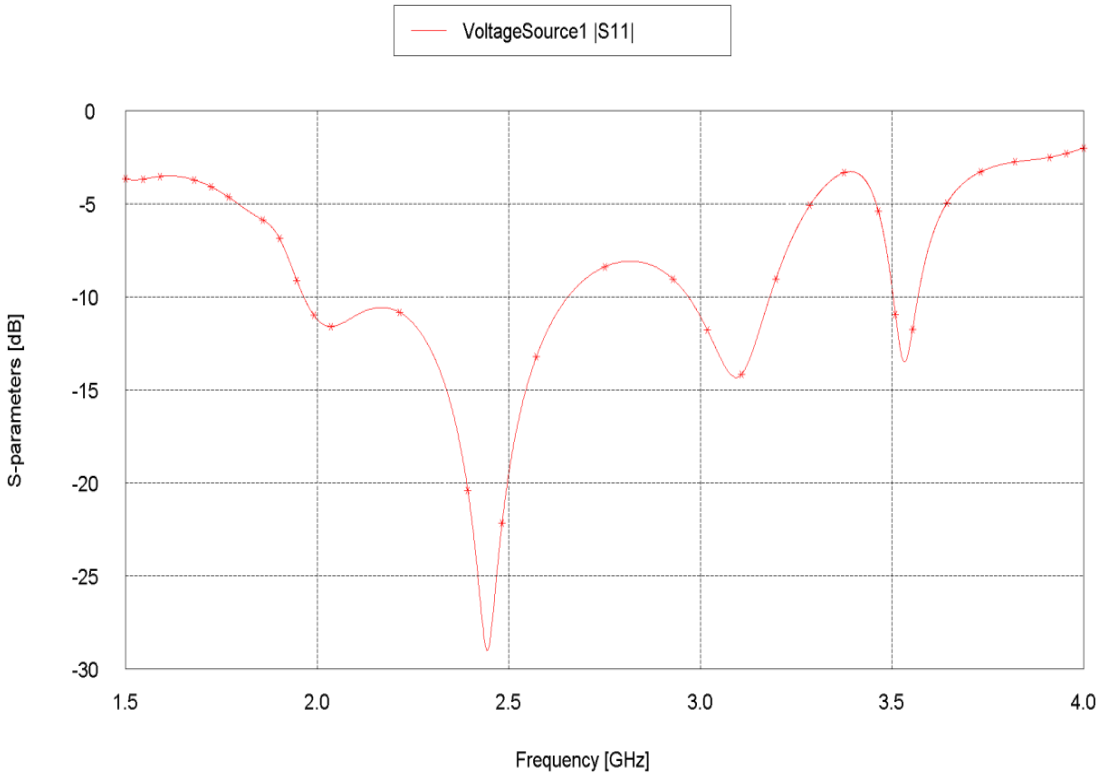

Figure 3.44: Reflection coefficient of BBTA

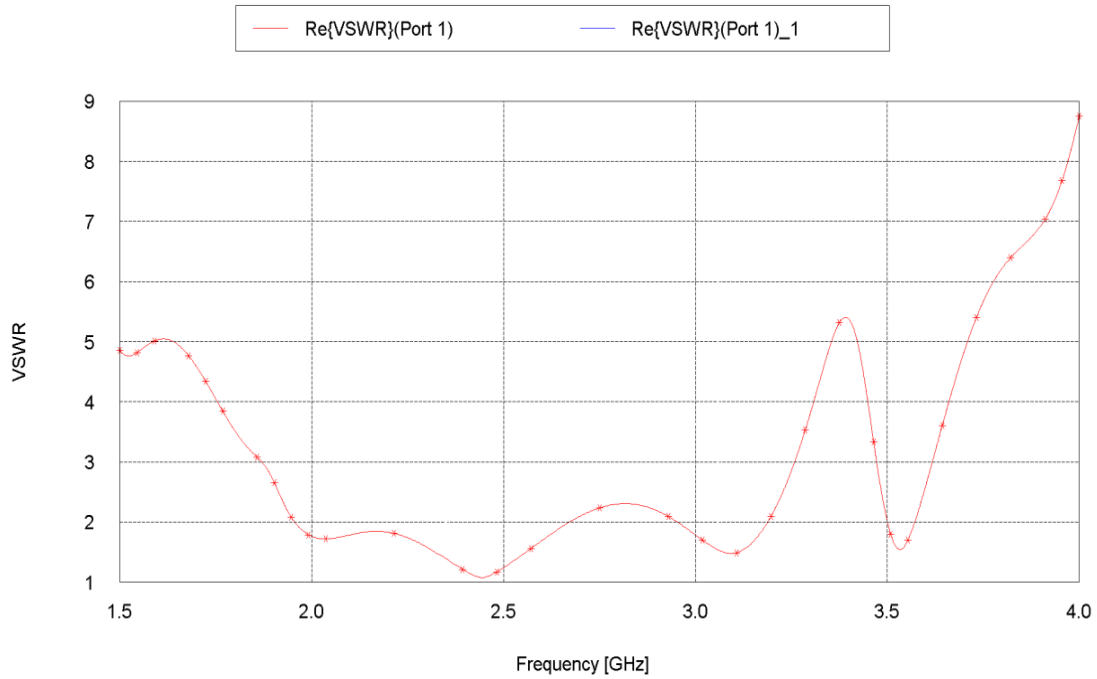

Figure 3.45: VSWR of BBTA

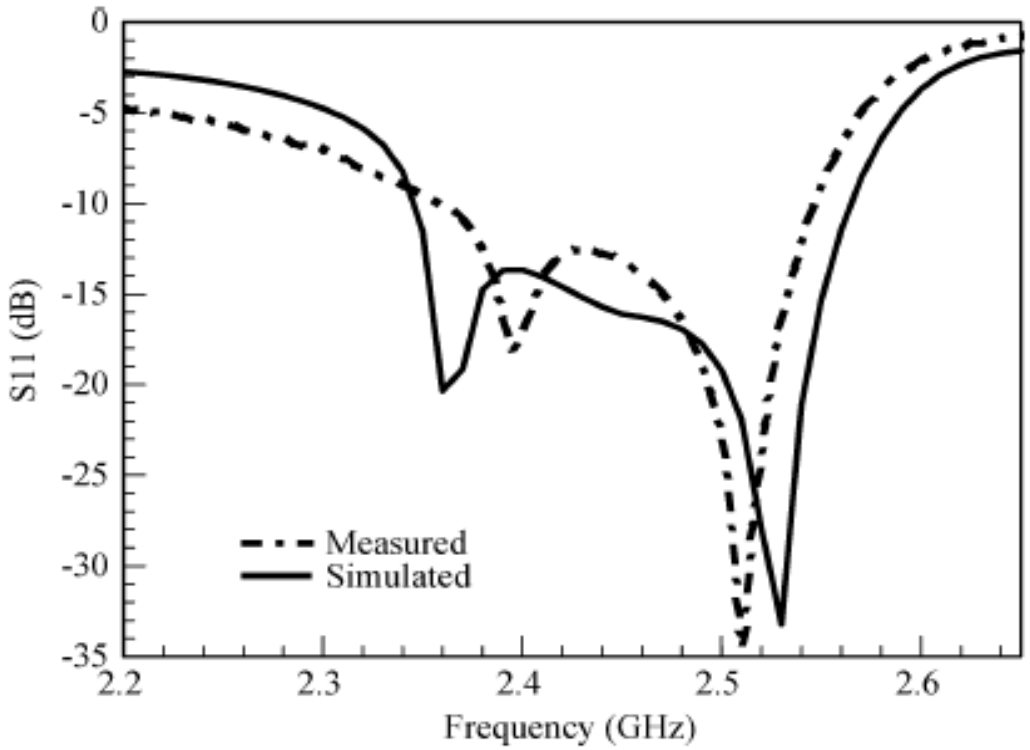

Figure 3.46: Return loss of antenna system in [20]

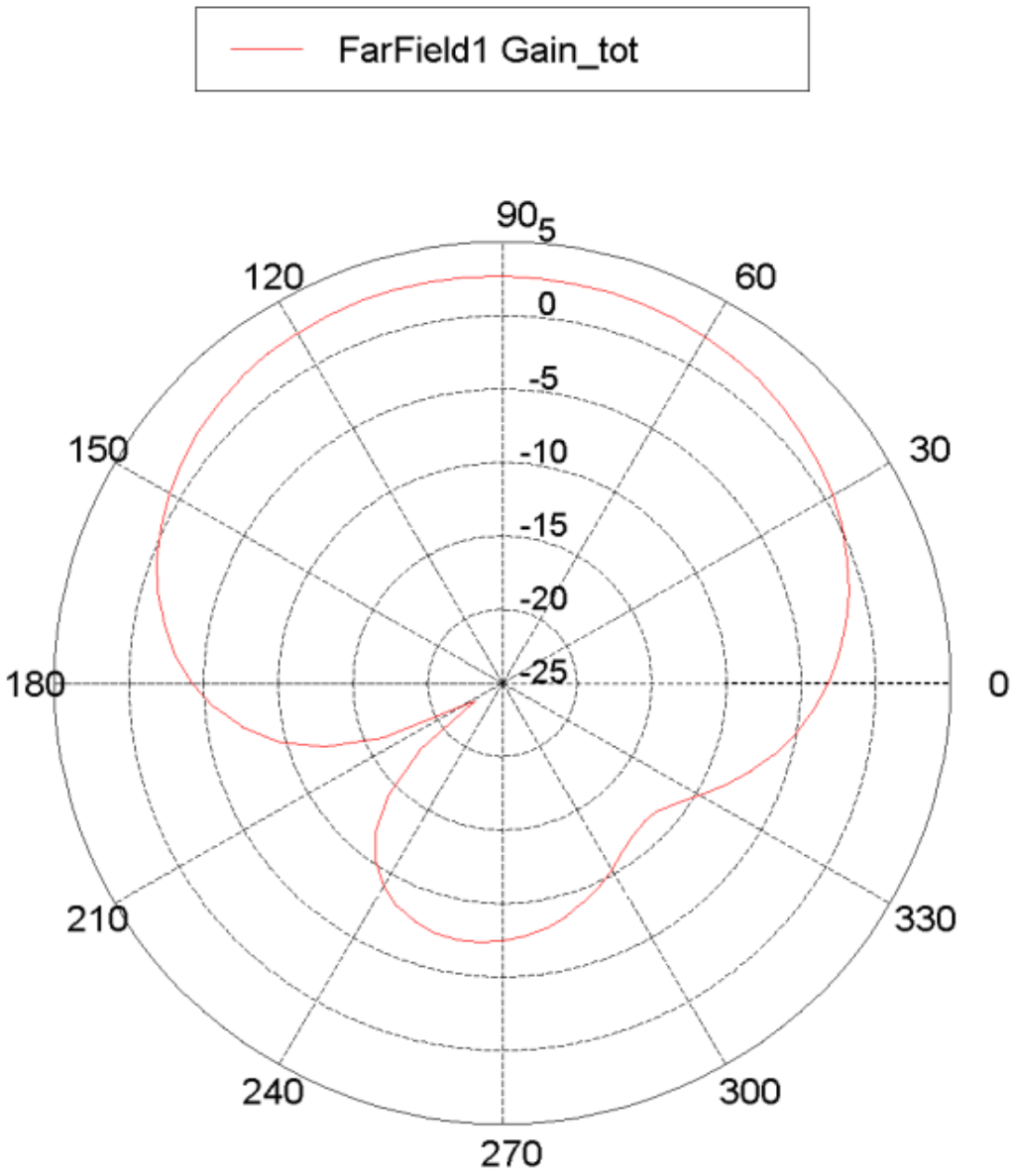

Figure 3.47: BBTA gain at θ=90^{o} along x-y plane

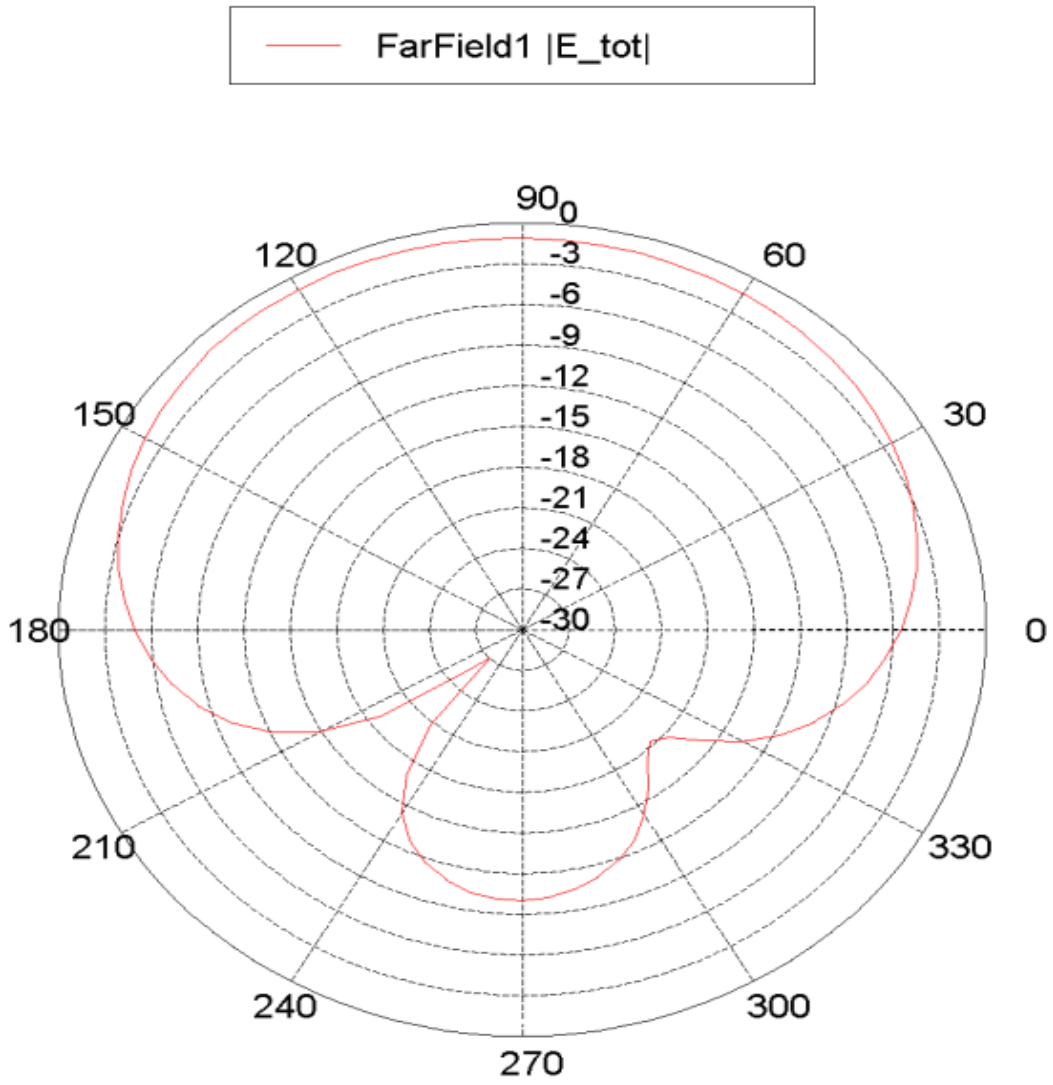

Figure 3.48: BBTA radiation pattern at θ=90^{o} along x-y plane

When we compare this antenna system with the system in [20] we can see that in this design, there are enhancements of antenna bandwidth by 200% as referred in Figure 3-44 and for other antenna parameters are listed in Table 3.7. In next chapter, we will extend the antenna arms to get better bandwidth and the tapper technique will be applied on the balun to decrease discontinuity in power flow and improve antenna gain and the radiation pattern.

Table 3.6: Results of Bow-Tie and Yagi [20]

Antenna Parameter	**BTA (FEKO result)**	**Yagi Antenna**[20]
Voltage standing wave ratio (VSWR)	1.01	1.01
Bandwidth(GHz)	(1.98-2.6)	(2.35-2.55)
Resonant frequency (GHz)	2.45	2.45
Return loss(dB)	-15	-30

Chapter 4

BROADBAND BTA WITH TAPERED BALUN

4.1 Exponential Taper

In the preceding chapter, we discussed how to use multi-sections for impedance matching. But here, multi-section transformations are replaced with a new exponential tapering technique [21] in order to reduce the reflected signals by 53% compared with the previous technique. This will be achieved by reducing the discontinuity in the power flow as suggested in Figure 4.1.

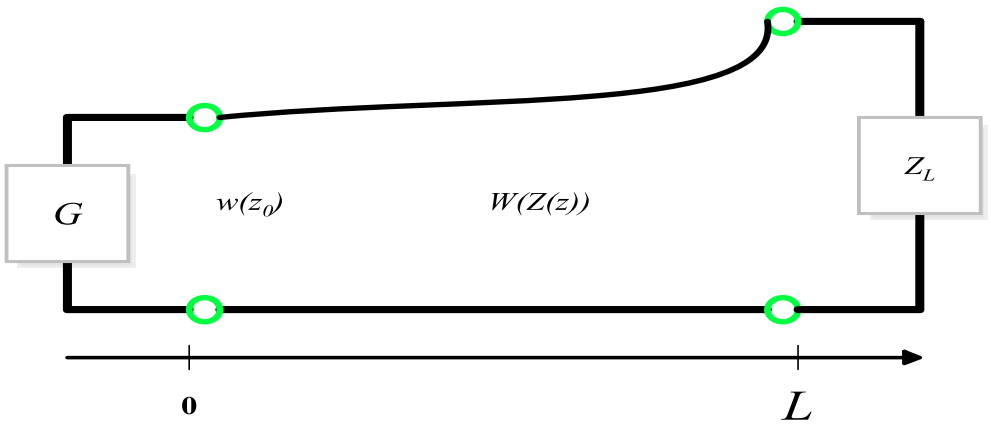

Figure 4.1: Equivalent circuit taper variance width of TL

The width of an exponential taper can be calculated by Equation 4.1.

$$W(\mathrm{Z}(\mathit{Z})) = W(\mathrm{Z}_0)\,\mathrm{e}^{aZ} \tag{4.1}$$

Where (a) is:

$$a = \frac{1}{l}\ln\left(\frac{\mathrm{W}(\mathrm{Z}_L)}{W(\mathrm{Z}_0)}\right) \tag{4.2}$$

For z=0, $W\left(Z\left(0\right)\right) = W\left(Z_0\right)$ and for z=l wish to have $W(\mathrm{Z}(\mathrm{z})) = \mathrm{W}(\mathrm{Z}_0)\,\mathrm{e}^{al}$ as indicated in Figure 4.2.

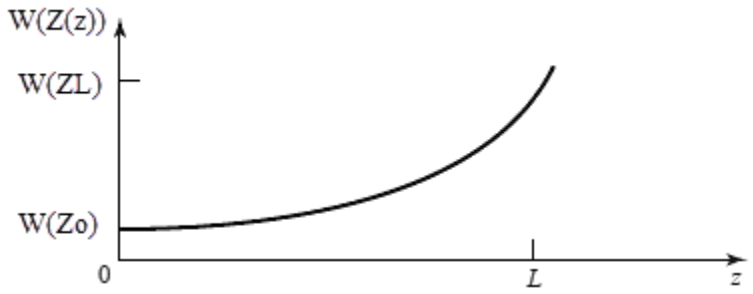

Figure 4.2: Exponential curve variation of width

The reflection coefficient after adding the taper can be calculated by using Equation (4.3) [21].

$$\Gamma = \frac{\ln\dfrac{W(Z_L)}{W(\mathrm{Z}_0)}}{2} e^{-j\beta l}\,\frac{\sin\beta l}{\beta l} \tag{4.3}$$

Now, exponential taper technique will be applied in two cases: firstly both sides of the exponential taper will be applied to the balun as suggested in Figure 4.3 and then single side exponential technique will be used on the balun as shown in Figure 4.4.

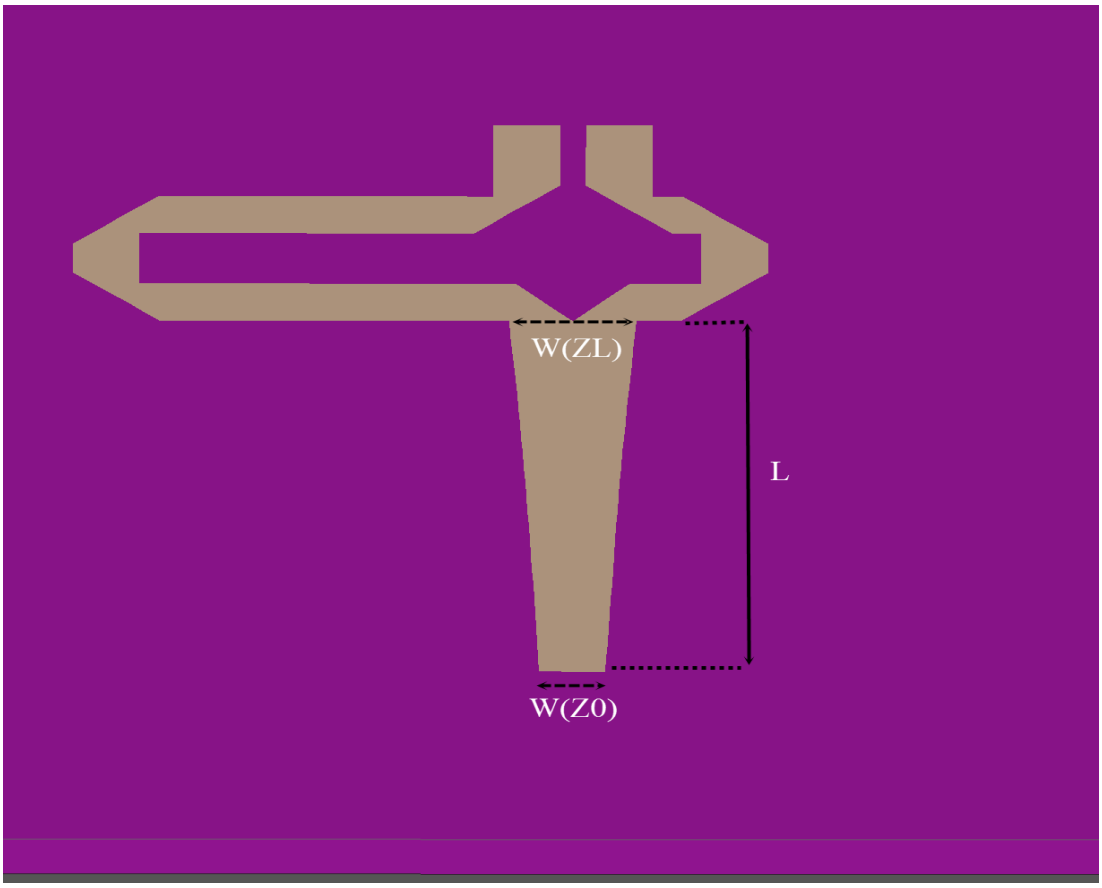

Figure 4.3: Double side exponential taper

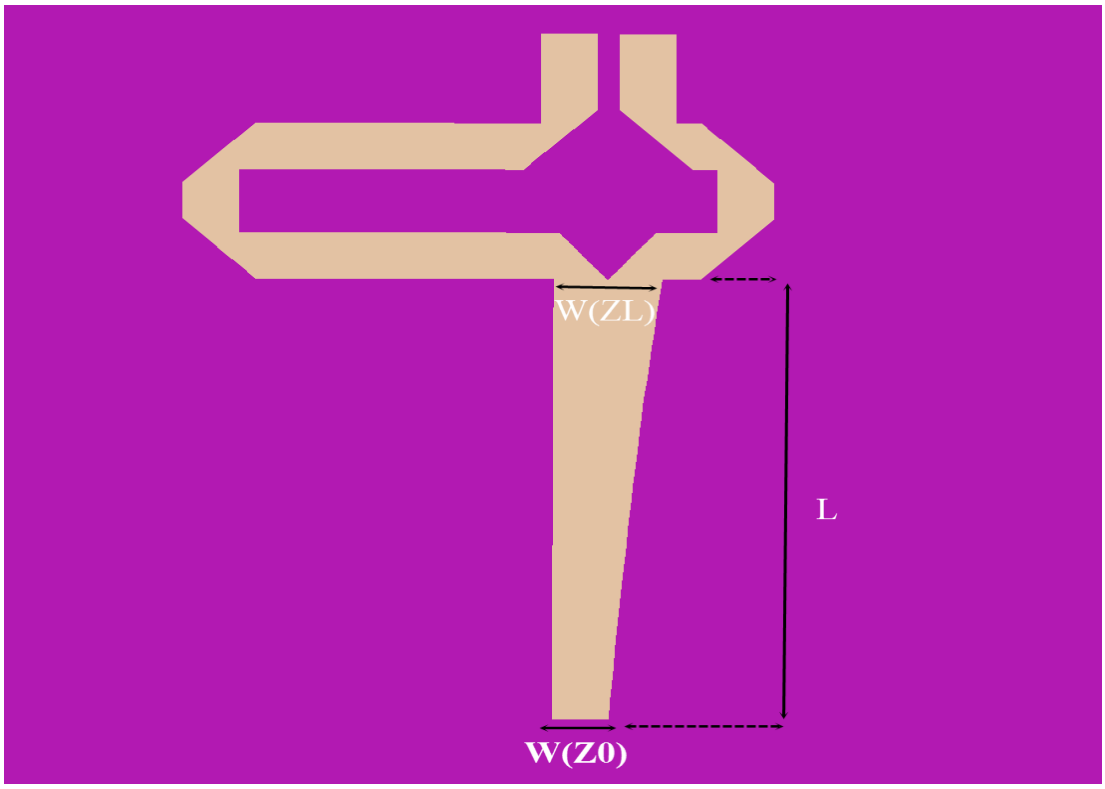

Figure 4.4: Single side exponential taper

Both types of tapers that were suggested to be used for the balun above, have width of feed port equal to 2.33 mm to satisfy 50 Ω matched impedance. The load impedance is 25 Ω which is achieved by making the line width equal to 4.48 mm. Figure 4.5 shows the return loss at resonant frequency 2.44 GHz and insertion loss of the balun with double side exponential taper. Figure 4.6 indicates that both the return and insertion losses of balun with single side exponential taper have the same resonant frequency of 2.44 GHz.

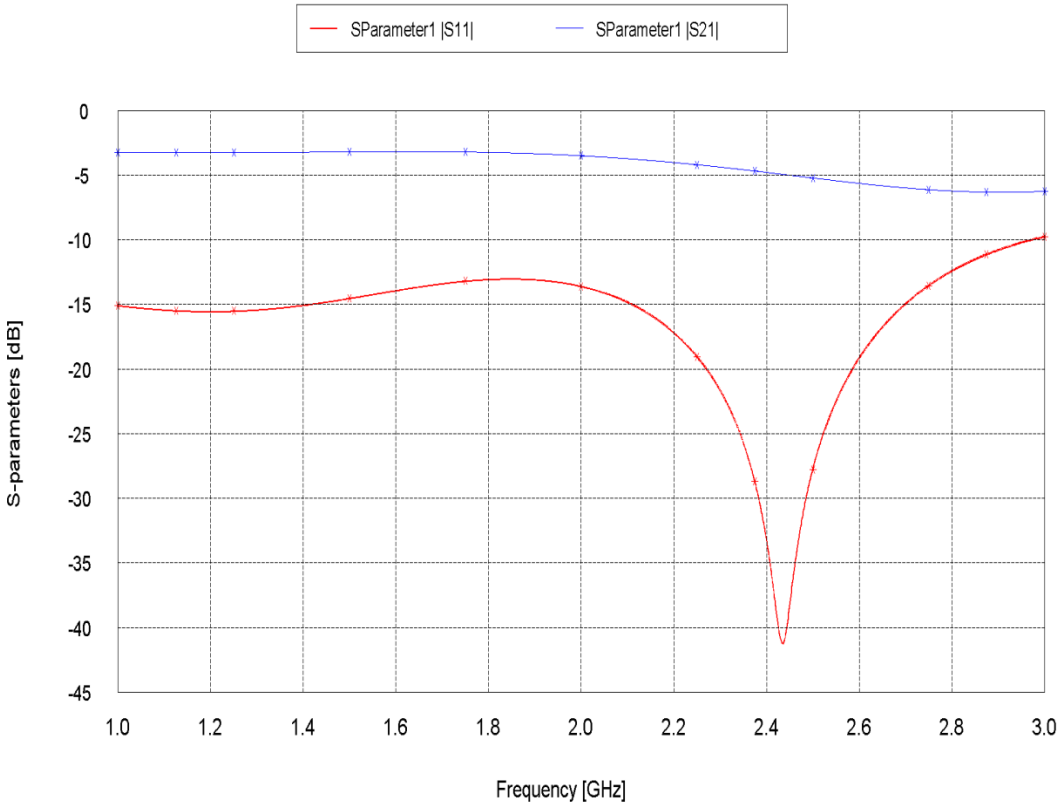

Figure 4.5: Return and insertion losses of the double side exponential taper

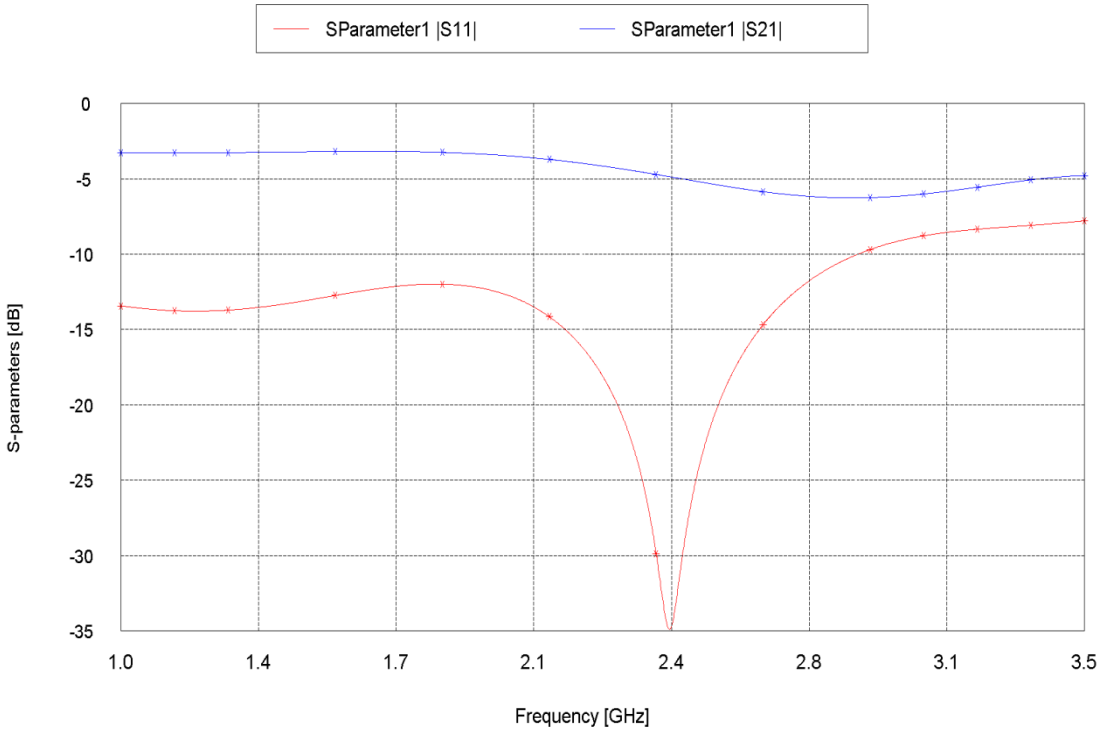

Figure 4.6: Return and insertion losses of the single side exponential taper

VSWR is less than 2 and the minimum value at resonant frequency which is equal to 1.1. Figures 4.7 and 4.8 show the propose balun for both kinds of taper have broad bandwidth with the range of frequency from 1-3 GHz.

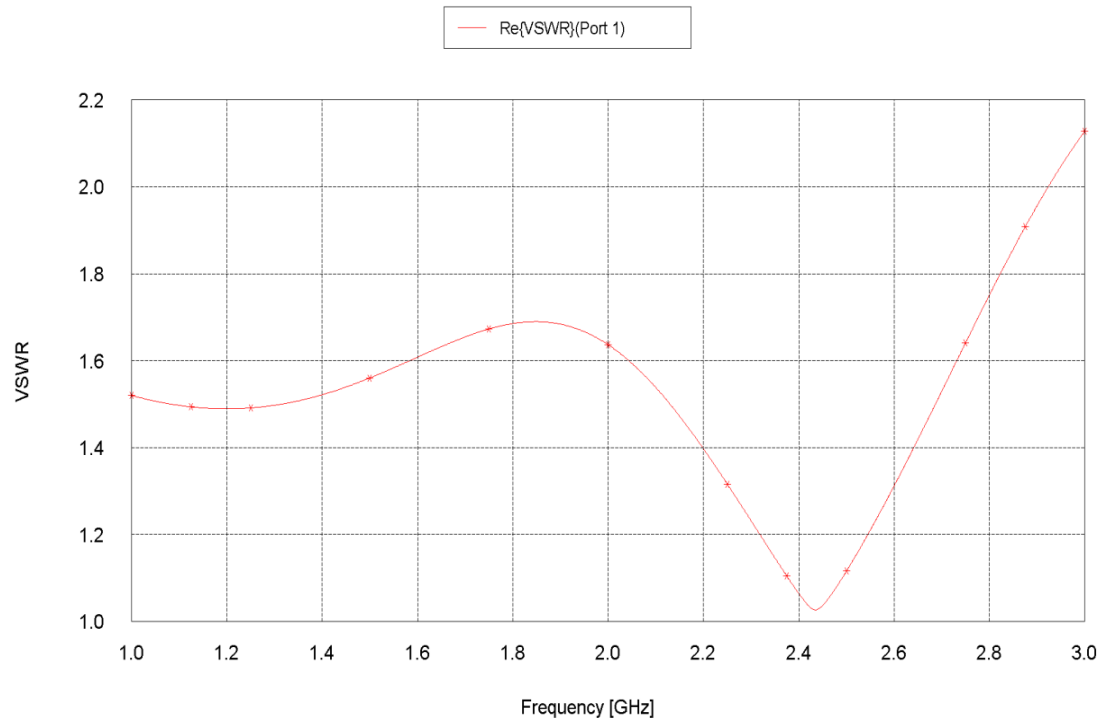

Figure 4.7: VSWR of the double side exponential taper

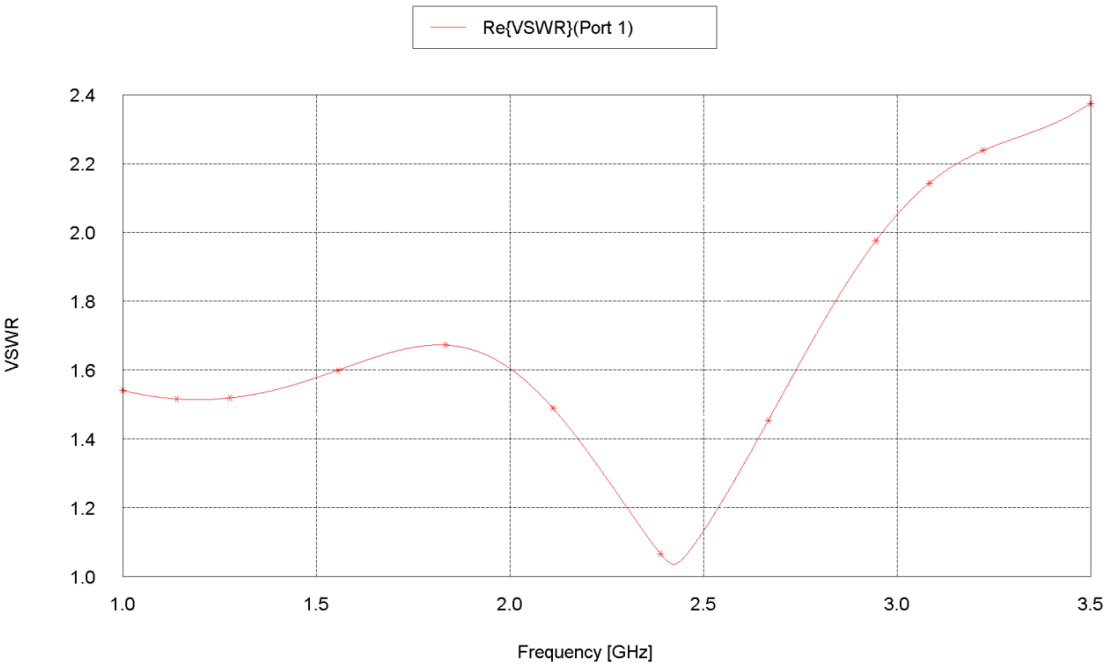

Figure 4.8: VSWR of the single side exponential taper

The real parts at the resonant frequency of the characteristics impedance of baluns with double and single side's exponential tapers are equal to 50 Ω. The imaginary parts are approximately 0 Ω as depicted in Figures 4.9 and 4.10.

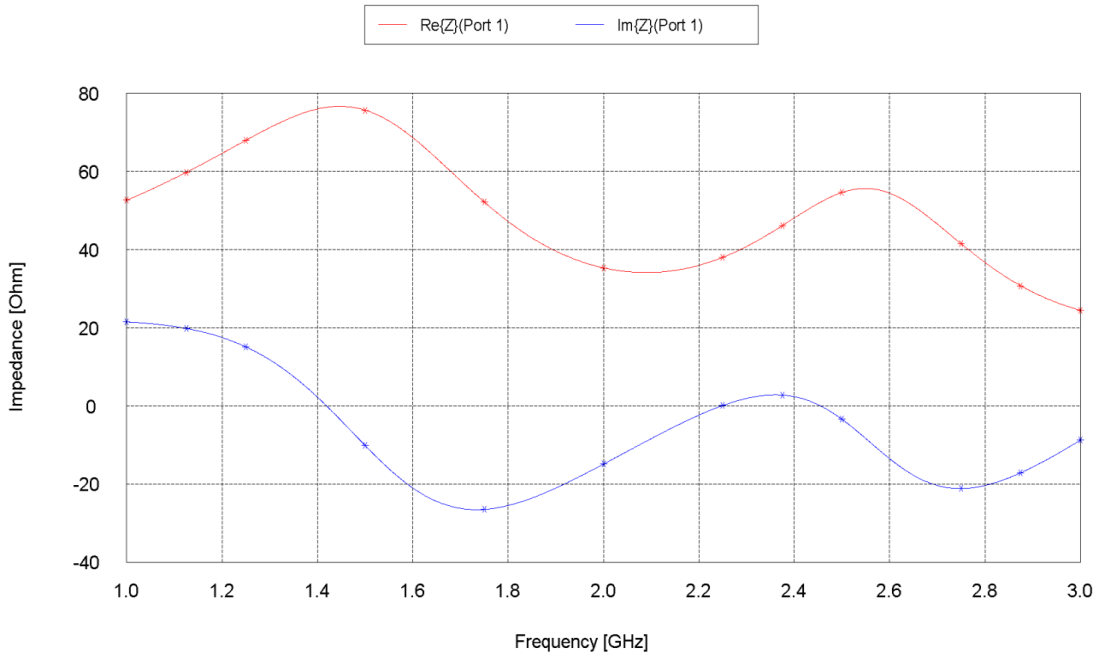

Figure 4.9: Real and imaginary parts of the input impedance for a double side exponential taper

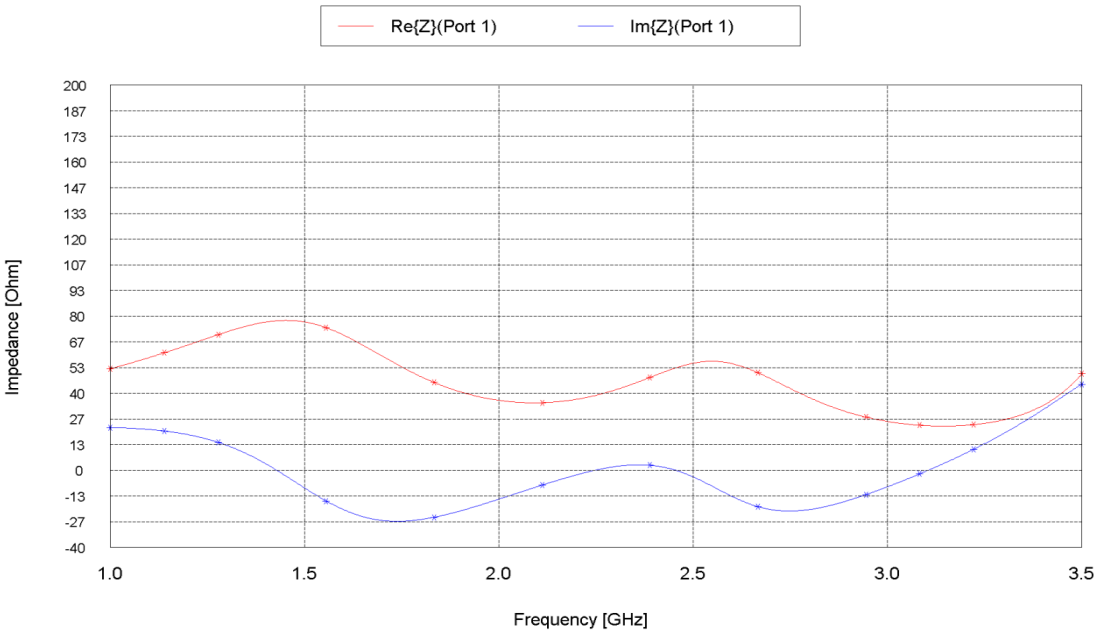

Figure 4.10: Real and imaginary parts of the input impedance for the single side exponential taper

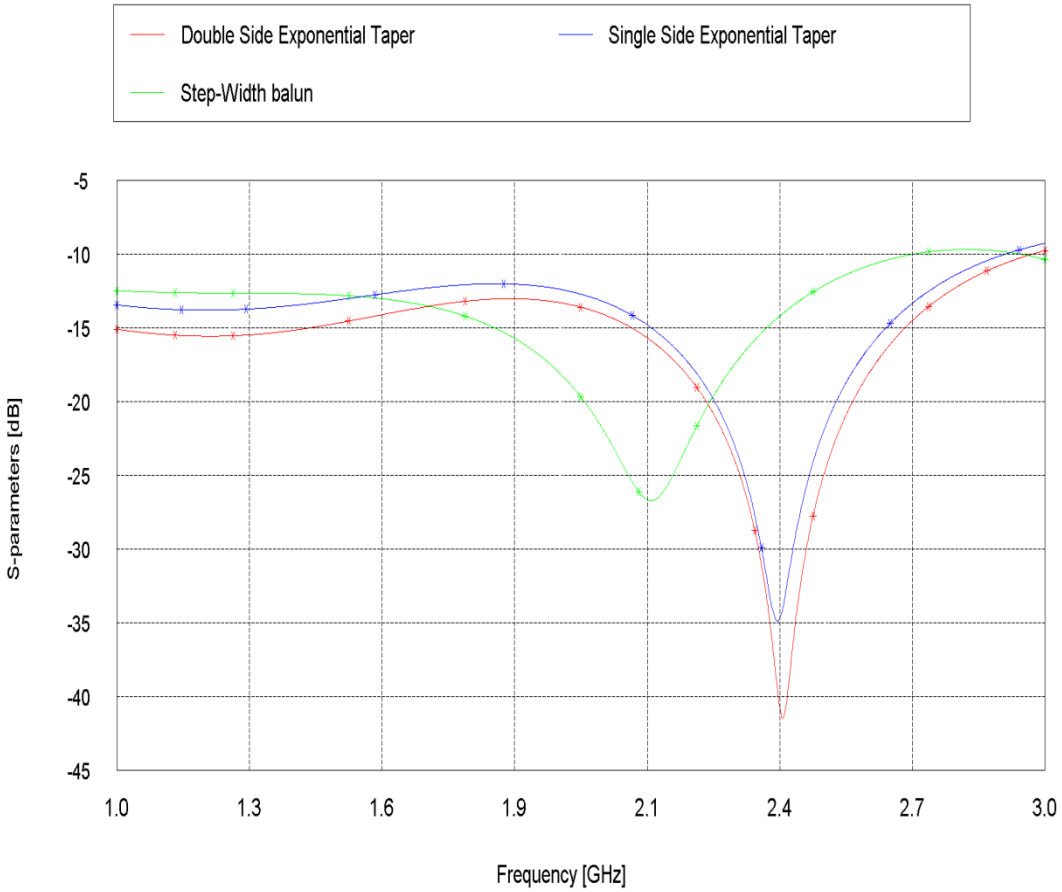

Figure 4.11: Comparison of the S-parameter of single, double side exponential taper and step-width taper

From the previous section, we conclude that the double side exponential taper had good performance such as the return losses are enhanced by 23% compared with single side exponential taper and by 80% compared with [22] as shown in Figure 4.11.

4.2 BTA Design with Double Side Exponential Taper

In this section, printed bow tie antenna with both side exponential taper as shown in Figure 4.12 is considered and simulated by FEKO 5.5. Dimensions of the antenna and the balun are the same in Table 3.5. It is necessary to mention that the taper was designed based on Equation (4.1), $W(Z_0)$ = 2.33 mm, $W(Z_L)$ = 4.48 mm, and L=22.1mm.

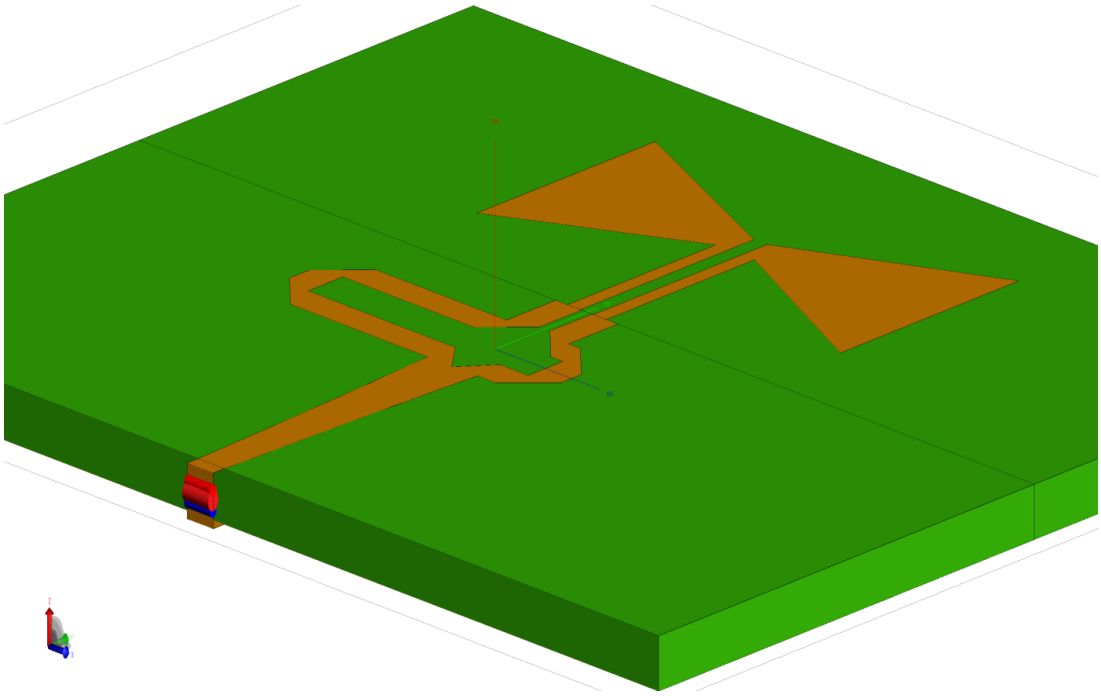

Figure 4.12: Antenna geometry with exponential taper balun

Figure 4.13 demonstrates the antenna return loss which is equal to 23 dB at 2.3 GHz and 12 dB at 3.5 GHz. The 3-D radiation pattern is shown in Figure 4.14.

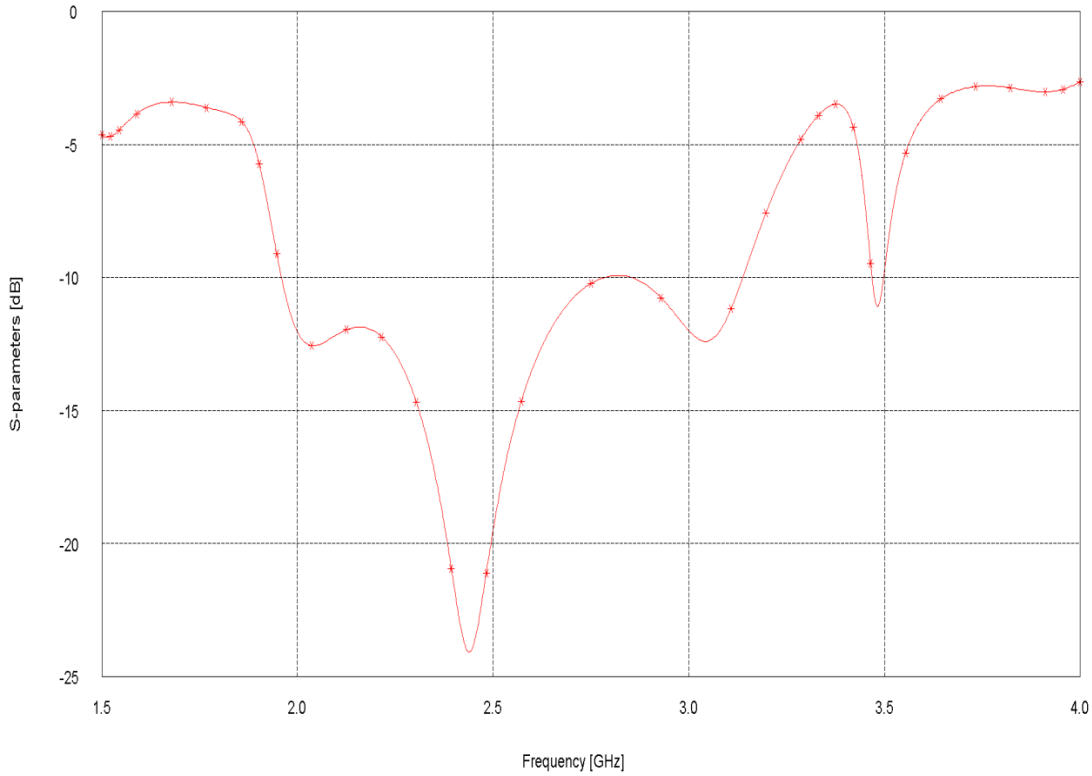

Figure 4.13: The return loss of the BTA with exponential taper

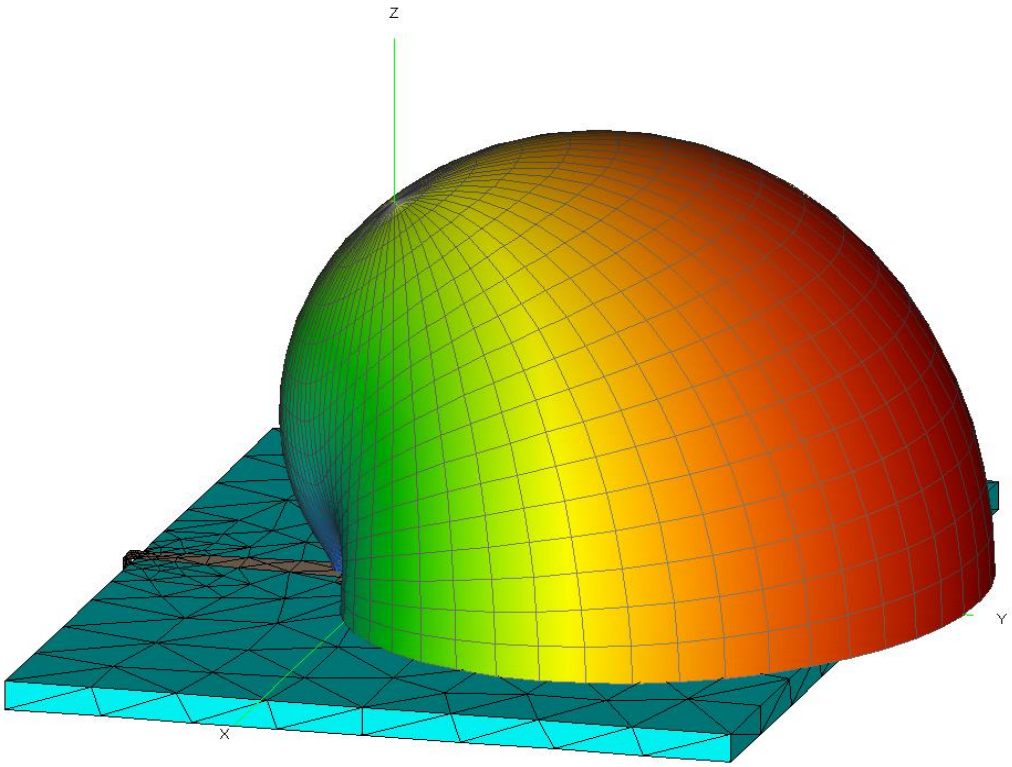

Figure 4.14: 3-D radiation pattern of the BTA simulated by FEKO

The radiation pattern shows that the antenna have maximum radiation at the 90^{o} for the resonant frequencies 2.45GHz, 3GHz and 3.5GHz as can be seen from Figure 4.15. The antenna gain at 90^{o} is 2.5 dB for 2.44 GHz, 3.1 dB for 3 GHz, and 1.5 dB at 3.5 GHz as indicated in Figure 4.16.

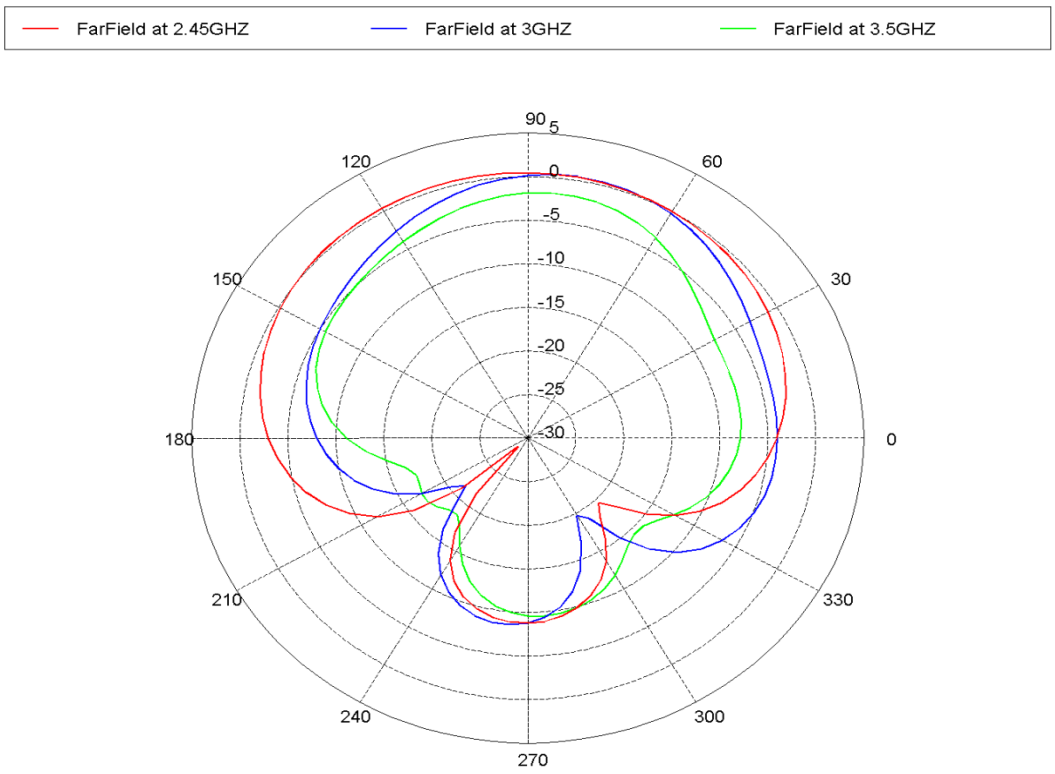

Figure 4.15: 2-D radiation pattern of BTA with exponential taper, in the a y-z plane

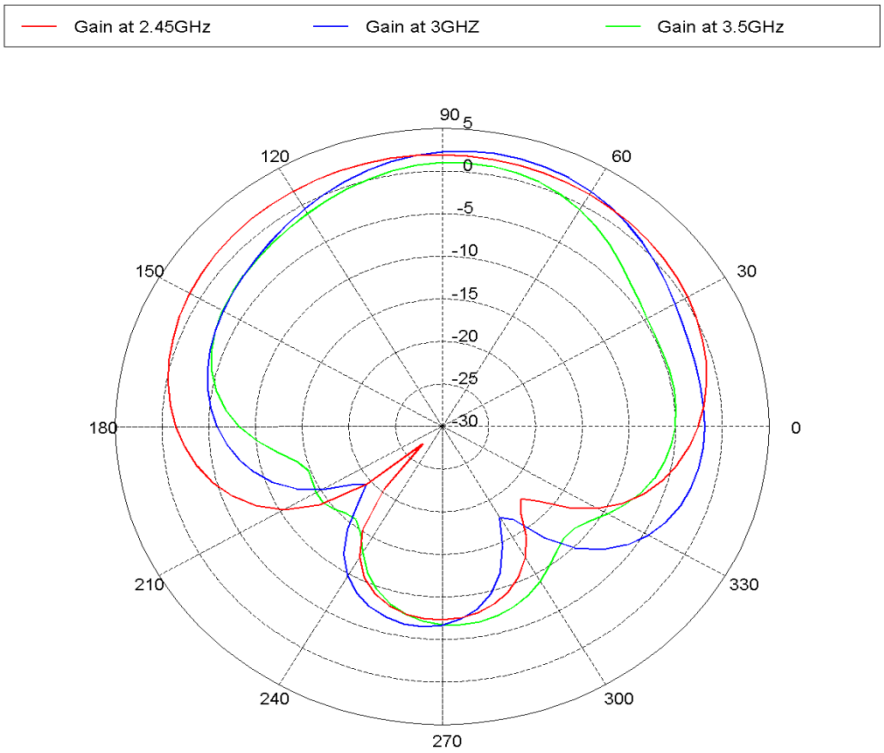

Figure 4.16: Gain of the antenna at resonant frequencies in the y-z plane

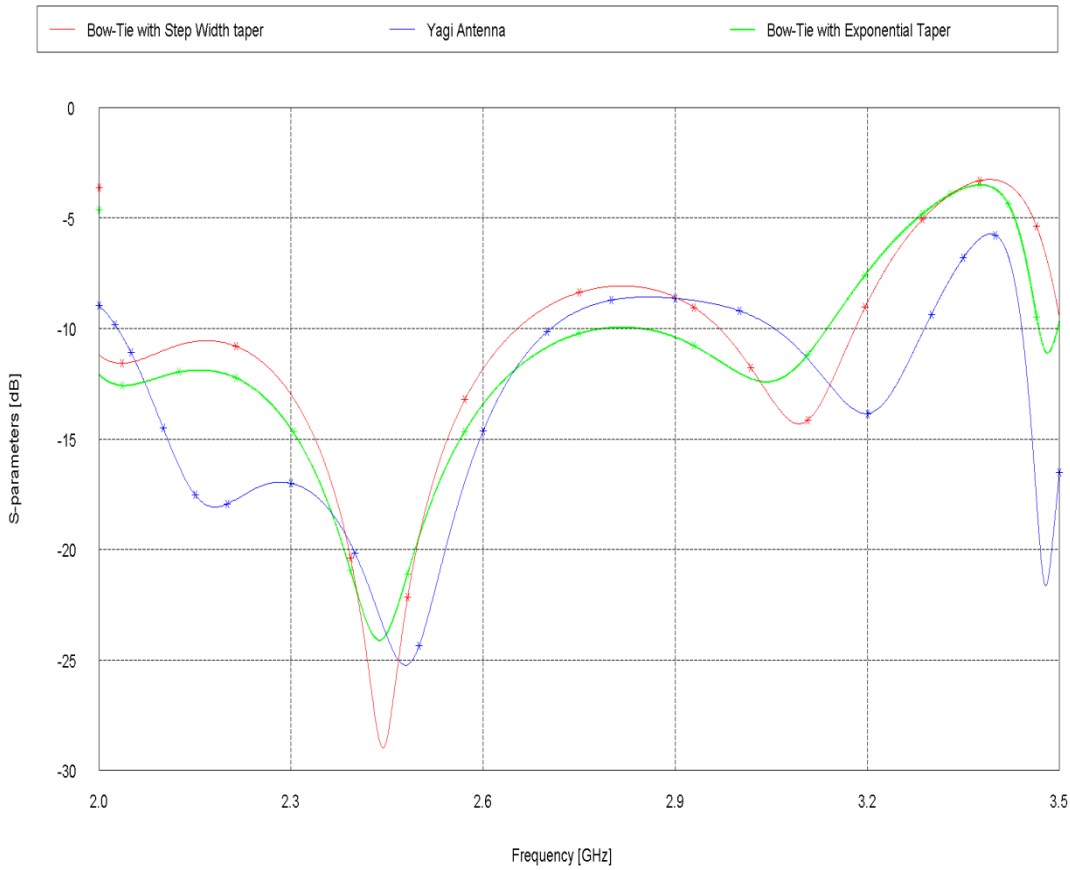

Figure 4.17: Comparison of the return loss of the BTA with Exponential taper, BTA and Step-width Taper and Yagi antenna

From Figure 4.17, we can conclude that the BTA with exponential taper balun had a broadband characteristic with the bandwidth 2 GHz-3 GHz. Comparing with Yagi antenna bandwidth [20], it is clear that there is an enhancement in the bandwidth by 75% .

4.3 Triangular Taper

This section describes triangular in double side taper schemes as indicated in Figure 4.18 to eliminate discontinuity in the power flow in Tee-junction balun transitions. We will calculate the width of a triangular taper in terms of equations below [21].

$$W(\mathrm{Z}(z)) = \mathrm{W}(\mathrm{Z}_0)\,\mathrm{e}^{2(z/\mathrm{L})^2 \ln Z_L/Z_0} \qquad \text{For } 0 \le z \le L/2 \qquad (4.4)$$

$$W(\mathrm{Z}(z)) = \mathrm{W}(\mathrm{Z}_0)\,\mathrm{e}^{(4z/\mathrm{L}-2z^2/L^2-1)\ln Z_L/Z_0} \qquad \text{For } L/2 \le z \le L \qquad (4.5)$$

$$\Gamma = \frac{1}{2} e^{-j\beta L} \ln\left(\frac{Z_L}{Z_0}\right)\left(\frac{\sin(\beta \mathrm{L}/2)}{\beta \mathrm{L}/2}\right)^2 \qquad (4.6)$$

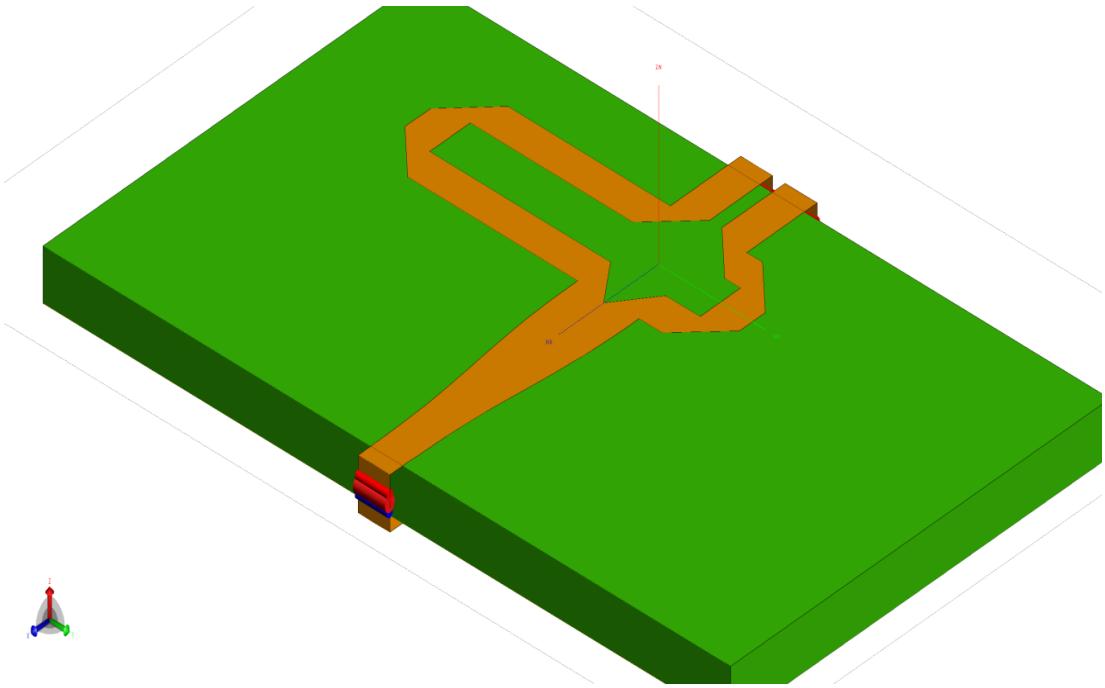

Figure 4.18: Balun geometry with triangular taper applied by using FEKO

Figure 4.19 refers to the reflection coefficient under -10 dB of broadband (1GHz-3.2GHz) taper balun transition. Figure 4.20 indicates the real and imaginary parts of input impedance of balun transition.

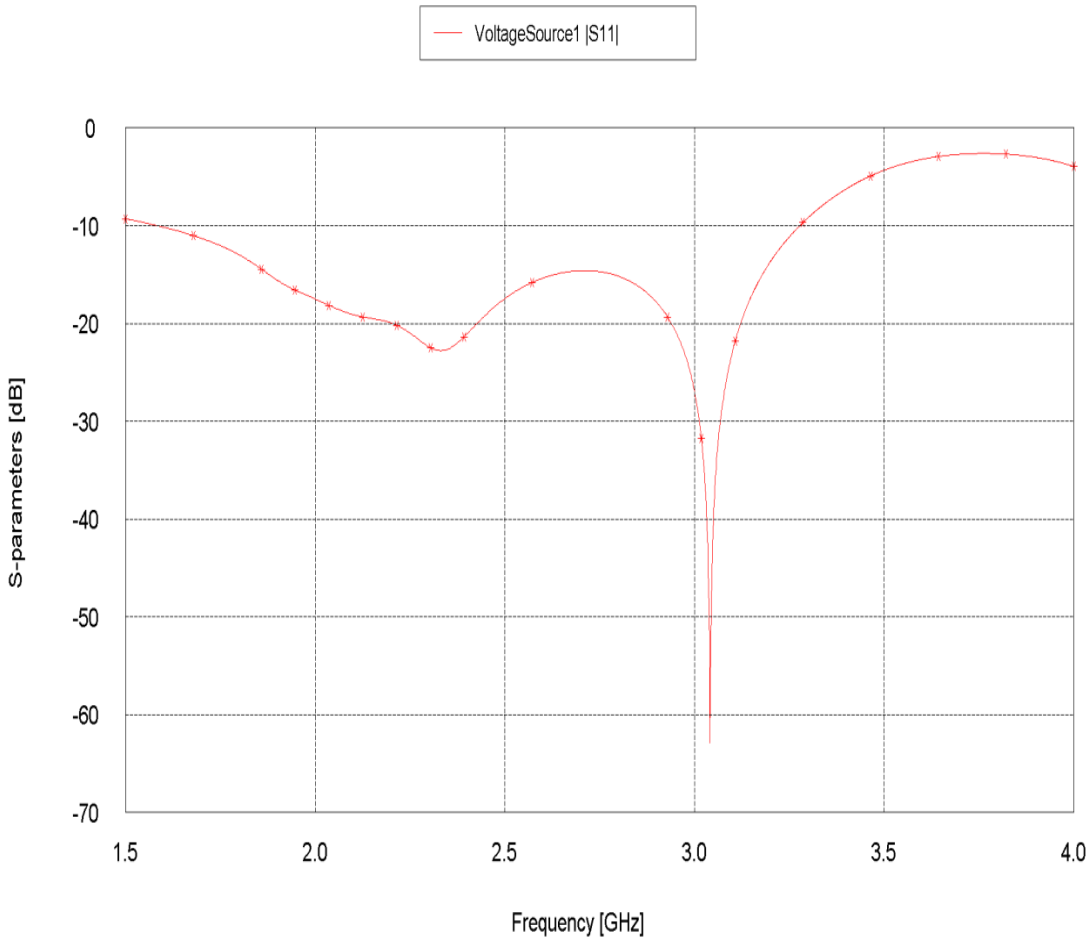

Figure 4.19: Return loss of the triangular taper balun transition

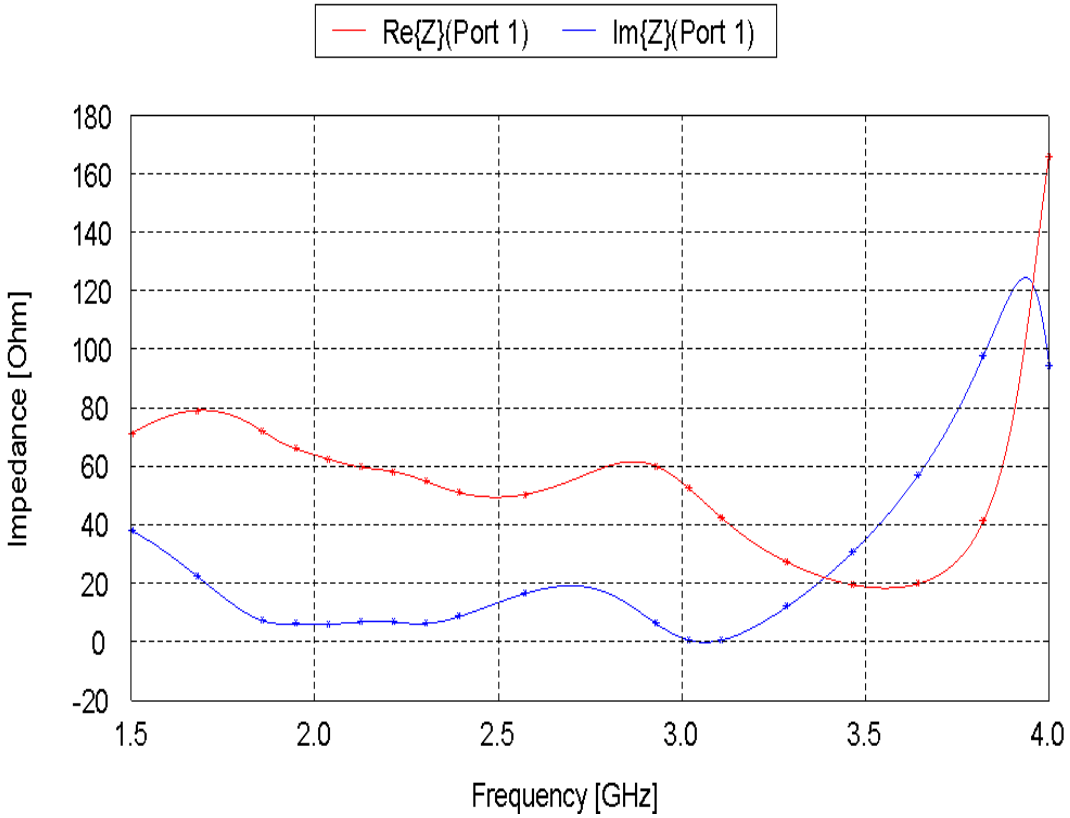

Figure 4.20: Input impedance of the triangular taper balun transition

4.4 Broadband BTA Design with Triangular Taper

New broadband BTA with double side triangular taper have been designed and simulated by FEKO 5.5 software simulator as shown in Figure 4.21. The modified BTA, antenna and balun dimensions are introduced in Table 4.1 except the dimension which is refer to the extensions in the antenna arms (E=2mm). This extension is added to increase the antenna bandwidth. The taper is designed based on Equations (4.4) and (4.5) with $W(Z_o)$ =2.33mm, $W(Z_L)$ = 4.48 and L=22.1mm. The antenna and balun were placed on the dielectric substrate RT-DROUD with ε_r=10.2 and substrate thickness of 2.5 mm.

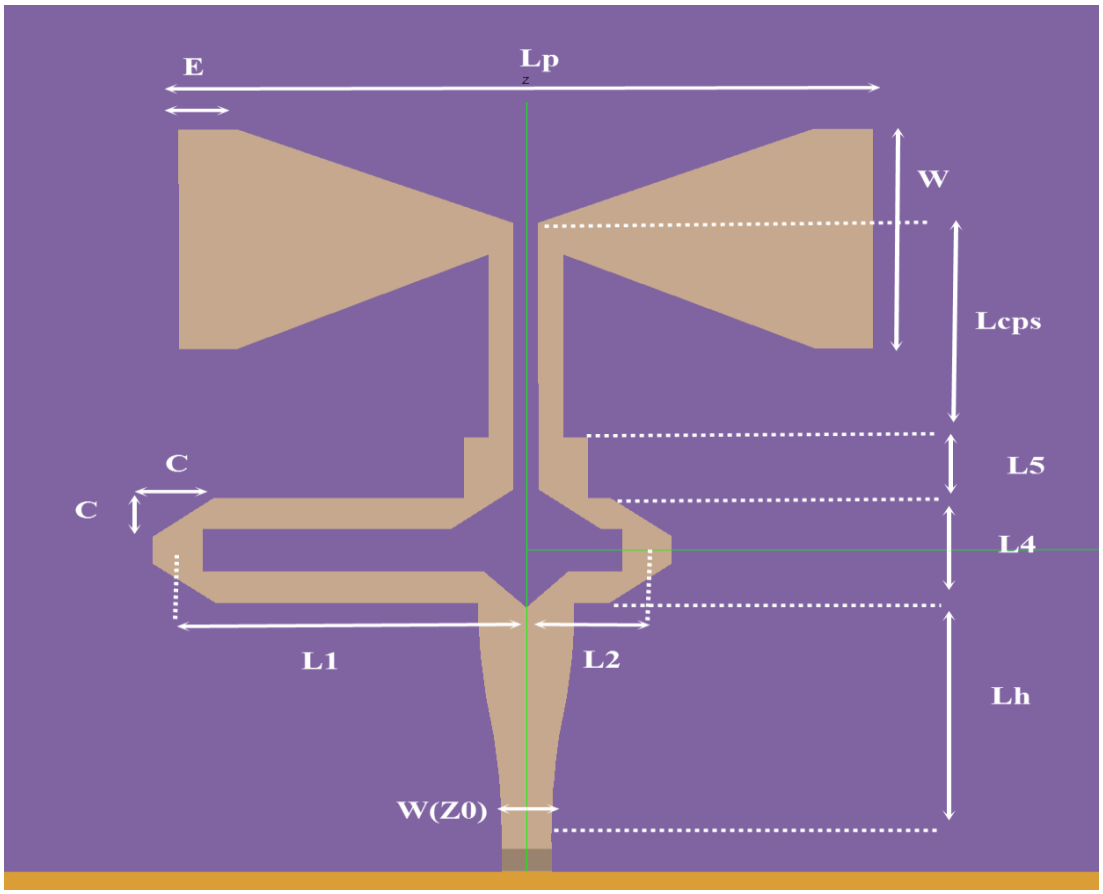

Figure 4.21: Antenna and taper balun layout

Table 4.1: Antenna gain with resonances frequencies

Frequency in (GHZ)	**2**	**2.5**	**3**	**3.5**
Gain in (dB)	6.9	5	5.1	3.8

Figure 4.22 shows a broadband antenna characteristic (1.9GHz-3.25GHz) with VSWR less than 2 as provided by Figure 4.23. The input impedance is equal to 50 Ω as shown in Figure 4.24, where red line refers to the resistive and blue line indicates the reactive part of the load.

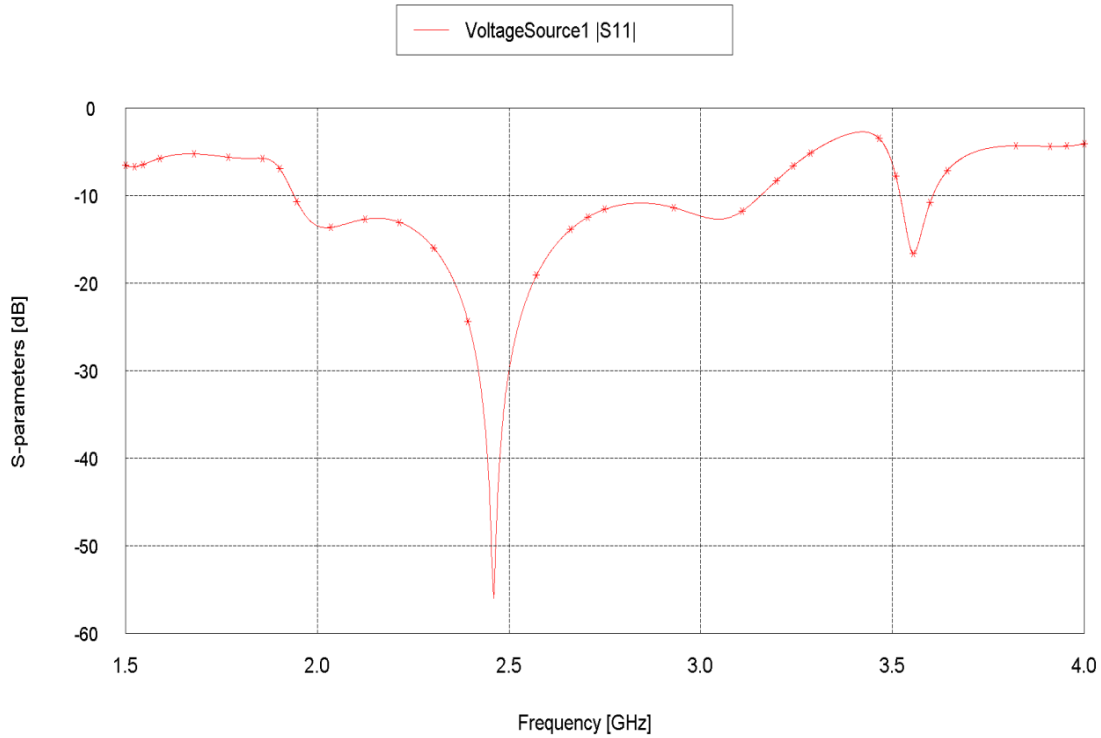

Figure 4.22: Antenna return loss

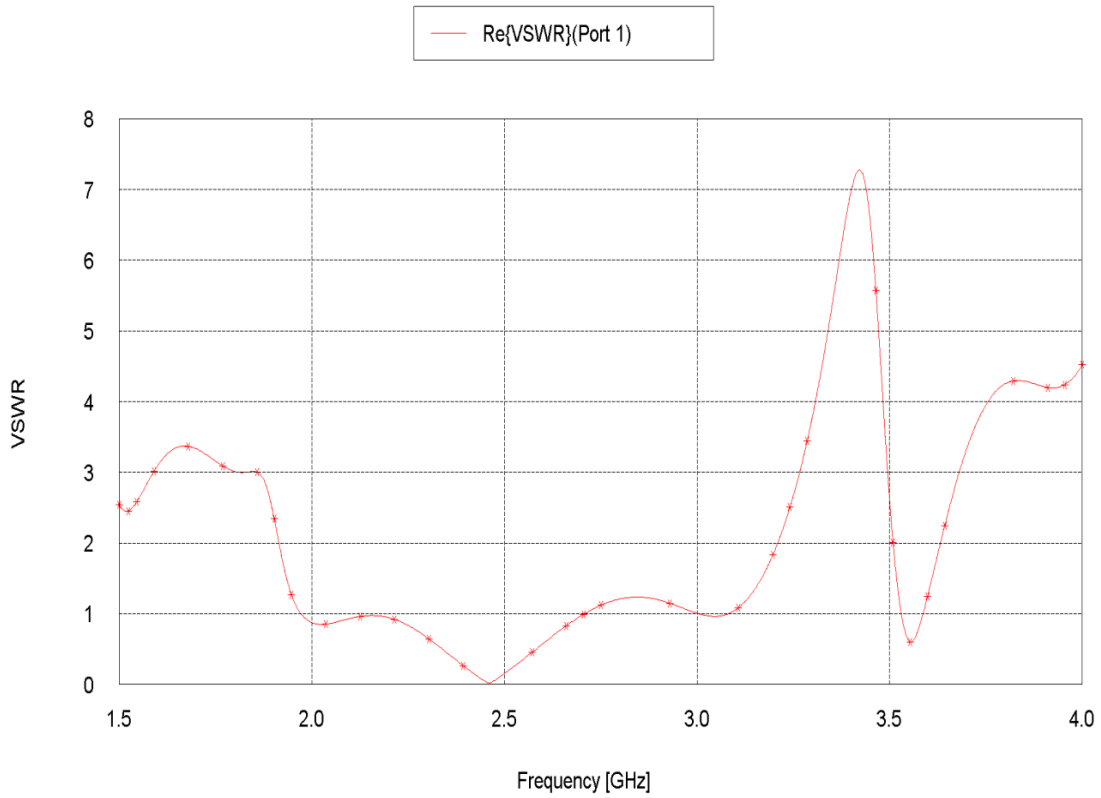

Figure 4.23: VSWR of the antenna with the balun

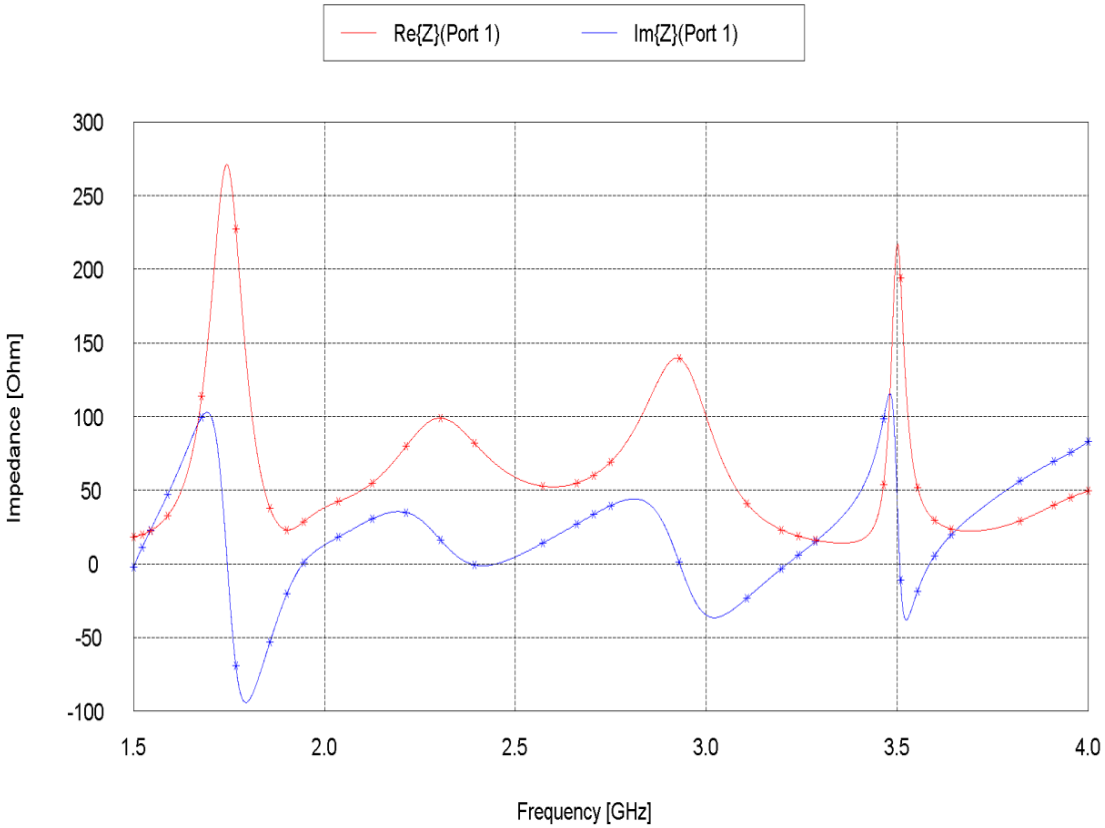

Figure 4.24: Input impedance of the BTA with the Balun

The radiation pattern in Figure 4.25 shows the maximum value at 90^{o} in both resonant frequencies at 2 GHz and 2.5 GHz and the maximum value of the radiation gain for 3GHz at 90^{o} and 3.5 GHz at 60^{o}. The antenna gain is shown in Figure 2.26 and 3-D radiation pattern is presented in Figure 4.27.

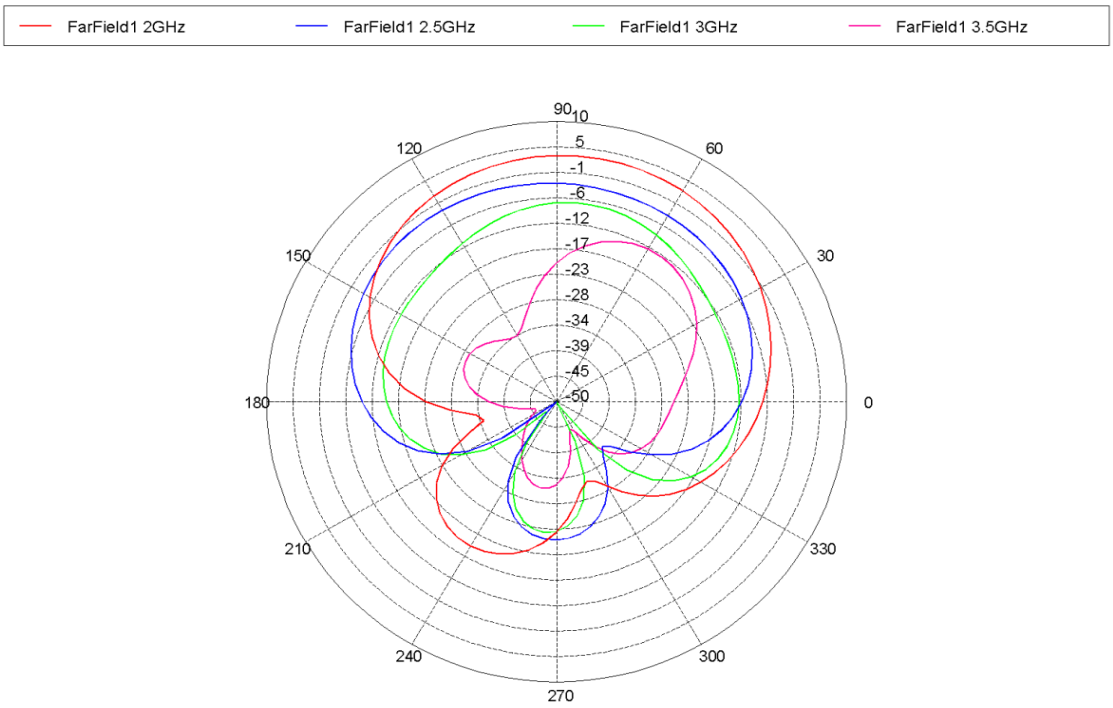

Figure 4.25: The polar electrical field of the BTA at the resonant frequencies along y-z plane

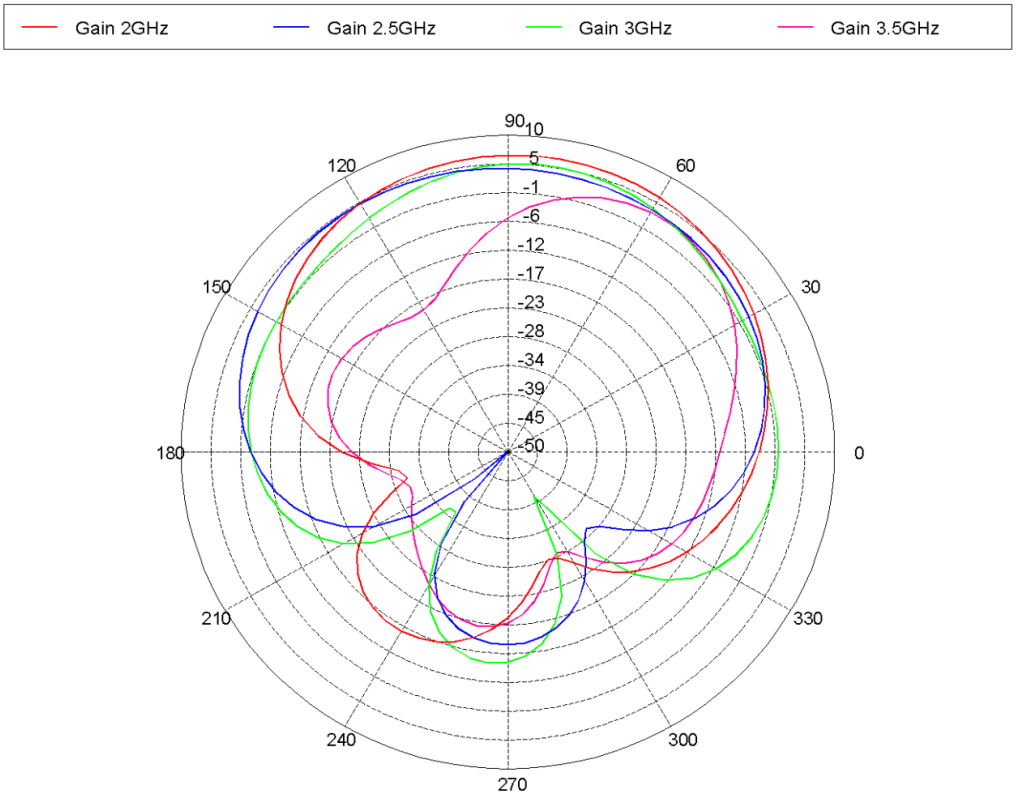

Figure 4.26: BTA gain graphic at resonance frequencies along y-z plane

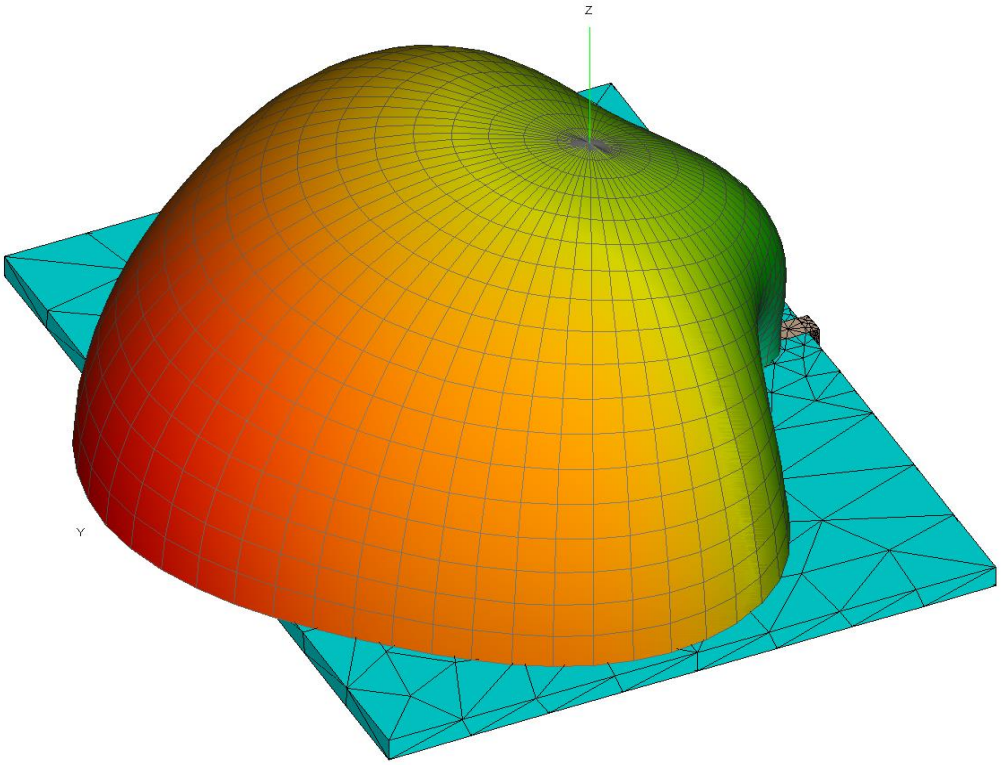

Figure 4.27: Antenna 3-D radiation pattern along y-z plane

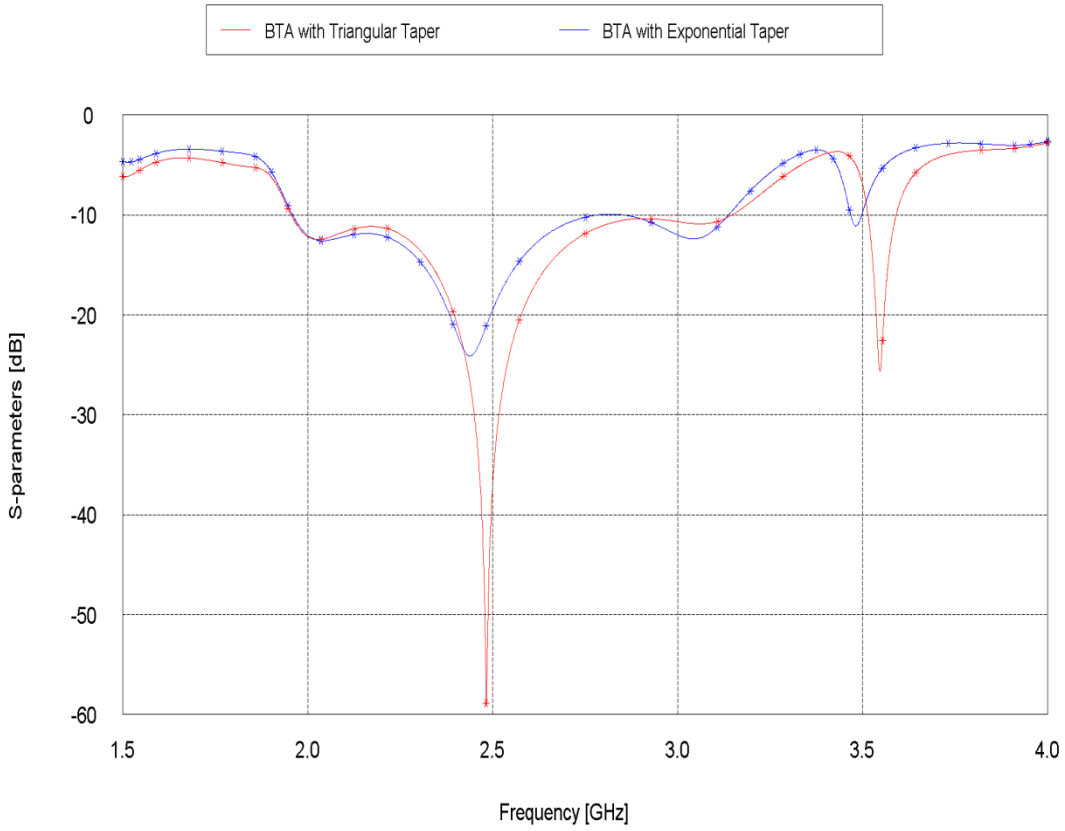

Figure 4.28: Return loss of BTA with Triangular Taper and BTA with Exponential Taper

4.5 Broadband Bow-Tie Antenna with Circular Bend

In this section the 90^{o} bending in the Tee-junction balun is replaced by a curved circular shape as shown in Figure 2.29.

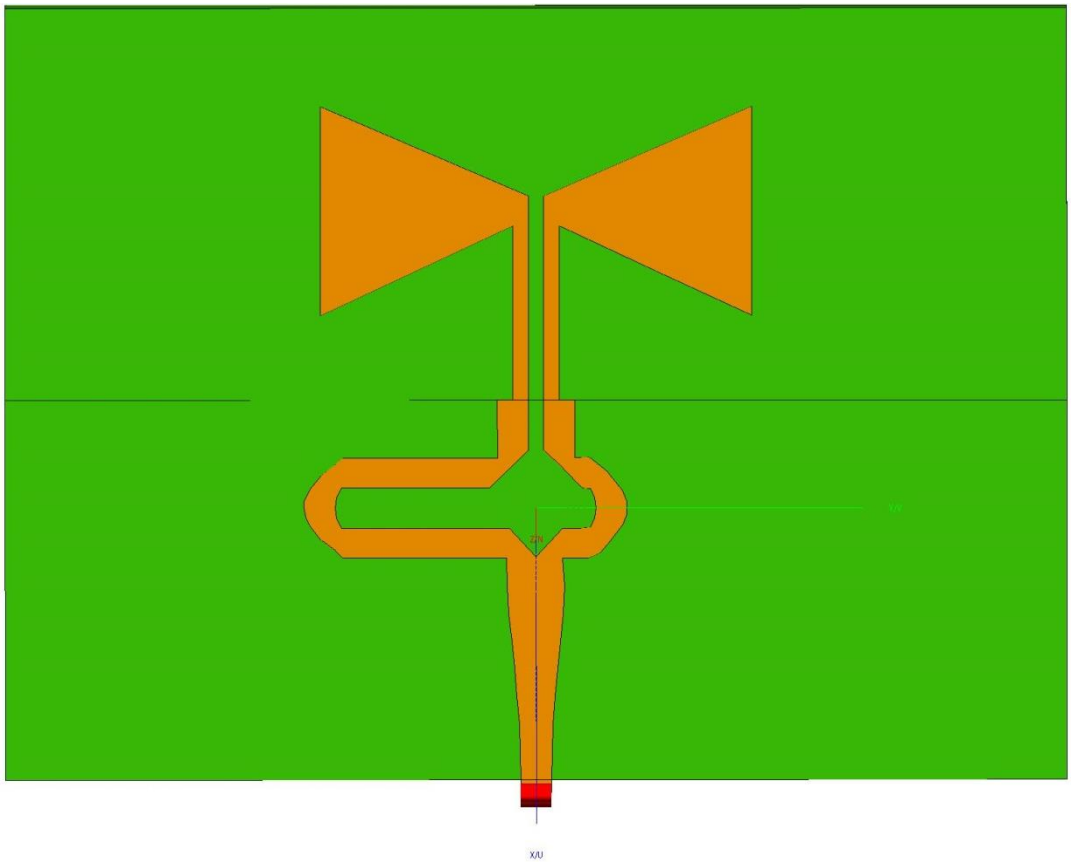

Figure 4.29: BTA with circular bending

The antenna dimensions are given in Table 4.2.

Table 4.2: Summary to the Antennas Design and their Performances

BTA Type	Operating frequency (GHz)	Return Loss (dB)	Band width(GHz)	Gain (dB)	Size (mm) L*W*H
Dipole-BTA	2.45	55	2.25-2.7	1.7	41*20.96
DS-BTA-BSF without reflector	1.5	35	1-2.6	2	110*84*15
DS-BTA-BSF with reflector	2.3	30	1-2.6	7	110*84*62
DS-BTA-MSLF	5	36	5-5.3	4.5	50*50*1.27
	2.45	12	2.35-2.46	1.8	50*50*1.27
	3.5	15	3.4-3.5	1.5	50*50*1.27
BTA-with-T.T	2	13	1.9-3.25	6.9	70*80*2.5
	2.5	60	1.9-3.25	5	70*80*2.5
	3	12	1.9-3.25	5.1	70*80*2.5
	3.5	18	3.5-3.67	3.8	70*80*2.5

The simulation results clarify that there is decrease in the return loss by 100% comparing with Bow-Tie Antenna with Triangular Taper at resonant frequency 3.6 GHz. However the return loss at 2.45 GHz is degrade up to 37 dB as shown in Figure 2.30.

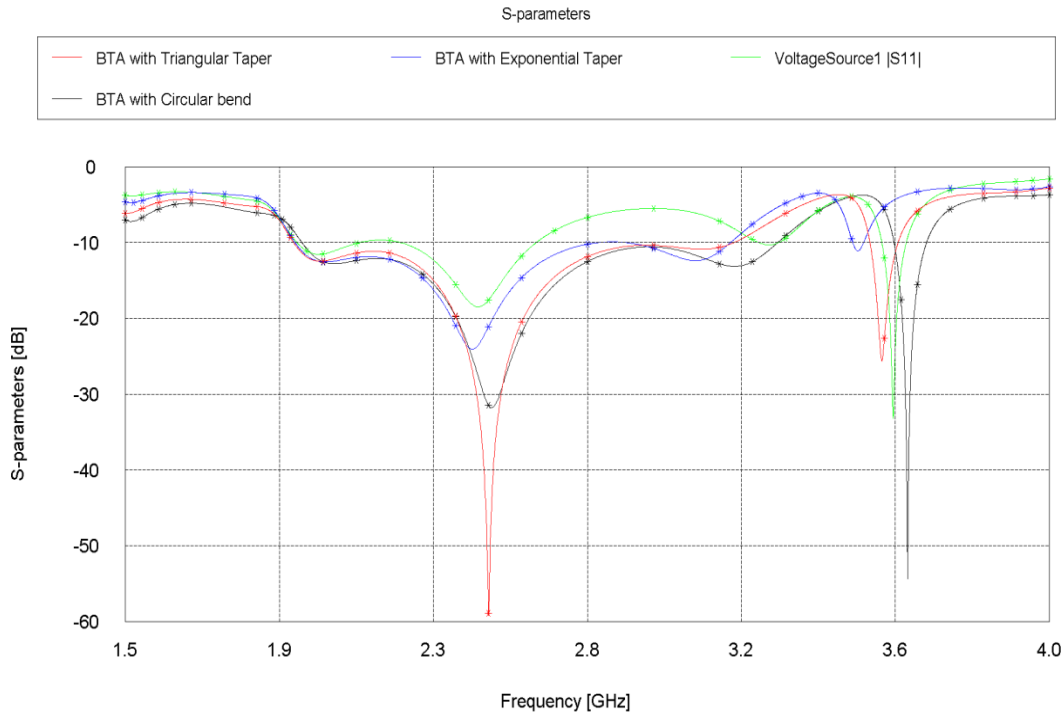

Figure 4.30: Comparison of different of the BTA's

Chapter 5

CONCLUSION AND FUTURE WORK

5.1 Conclusion

In this study, the effect of feed excitation on the antenna performance was analyzed. The feed radiation prevention by balun technique was discussed, and it reduced discontinuity in the power flow by taper technique.

A new MSL-to-CPS transitions balun for Bow-Tie Antenna has been proposed and simulated by FEKO 5.5 software, full wave simulator. The proposed antenna is in the ISM band which is especially suitable for wireless communication systems having a band from 1.89 GHz to 3.25 GHz (80%) bandwidth. The antenna radiation gain has been obtained up to 6.9 dB and 5 dB at the resonant operating frequency (2.45GHz).

5.2 Future Work

Because of the BTA configuration, it opens the way for us to apply fractal technique so as to obtain many other operating frequency bands with high gain. Therefore, we can utilize other balun shape to reduce discontinuity in power flow and enhancement for return loss at the resonant frequencies.

REFERENCES

[1] Constantine A. Balanis, *Antenna Theory*, 3rd ed. New Jersey, Canada: John Wiley, 2005.

[2] Roben. Munson, "Coformal Microstrip Phased Array," *IEEE Transactions on Antenna and Propgation*, vol. 22, no. 1, pp. 74-78, Jan. 1974.

[3] Jun-Wei Niu and Shun-Shi Z., "A CPW-Fed Broadband Slot Antenna with Line Taperd," *Microwave and Optical Technology Letters*, vol. 41, no. 3, pp. 218-221, May 2004.

[4] K.P. Ray and Y. Ranga, "Ultra-Wideband Printed Modified Triangular Monopole Antenna ," *Electronics Letters*, vol. 42, no. 19, 14th September 2006.

[5] Yu-De Lin and Syh-Nan Tsai, "Analysis and Design of Broadside-Coupled Striplines-Fed Bow-Tie Antennas," *Transactions on Antenna and Propgation*, vol. 46, no. 3, pp. 459-460, Mar. 1998.

[6] María Elena de Cos and Gomez R. C. Hadarig, "Novel Bow-tie–AMC Combination for 5.8-GHz RFID Tags Usable With Metallic Objects," *IEEE Antenna and Wirless Prop. Let.*, vol. 9, pp. 1217-1220, 2010.

[7] G.D. Boreman F.J. Gonza´lez, "Comparison of Dipole, BowTie, Spiral and Log-Periodic IR Antennas," *Infrared Physics & Technology*, vol. 46, pp. 418-428, 10 Nov. 2004.

[8] Yongxi Qian and Tatsuo Itoh, "A Broadband Uniplanar Microstrip-to-CPS Transition," in *Asia Pacific Microwave Conference*, 1997, pp. 609-612.

[9] J. Q. Howell, "Microstrip Antenna," *IEEE Trans. Antenna and Pro.*, vol. 17, no. 3, pp. 90-93, May 1969.

[10] M. K. A., Aziz, M. Z. A. A., and Goh, C. S. Rahim, "Bow-tie Microstrip Antenna Design," in *Universiti Teknologi Malaysia*, Johor, Malaysia, 2005, pp. 17-20.

[11] G.H. Brown and O.M.Woodward Jr., "Experimentally Determined Radiation Characteristics of Conical and Triangular Antenna," vol. 13, no. 4, p. 425, Dec. 1952.

[12] P. E. Mayes, D. Schaubert, and R. J. Mailloux J. T. Bernhard, "Micostrip microwave Antenna," *Antenna Applications Symposium*, vol. 1, pp. 189-209, Sep. 2003.

[13] Ross C.M., and Zorana P. Richard C.C, "Bow-Tie Antenna on a Dielectric Half-Space: Theory and Experimental," *IEEE Tran. on Antenna and Prop.*, vol. AP-35, no. 6, pp. 622-631, Jun. 1987.

[14] Michal S. M., and David B. R., "Imaging Antenna Arrays," *IEEE Tran.on Antenna and Pro.*, vol. 30, no. 4, pp. 535-540, July 1989.

[15] IPC-2141A, *Design Guide for High Speed Controlled Impedance Circuit Board*.: IPC Controlled Task Group, 1996.

[16] K. R. Mahmoud, "Design Optimization of A Bowtie Antenna for 2.45 GHz RFID Readers Using A HYBRID BSO-NM Methods," in *Progress In Electromagnetics Research*, 2010, pp. 105-117.

[17] Linyan Guo, and Minhua Li, Helin Yang Boxun Xiao, "A Broadband Bow-tie Antenna Used in UHF with Metalic Reflection Plane," in *Yangtze University*, Chaia, 2013, pp. 148-150.

[18] K. Y. Kabalan, and A. El-Hajj, C. G. Christodoulou, Y. Tawk, "A Simple Multiband Printed Bowtie Antenna," *IEEE Antenna and Wireless Prop. Let.*, vol. 7, no. 3, pp. 557-560, May 22 2008.

[19] Walt Fair. Antenna Notes. [Online]. http://www.comportco.com/~w5alt/antennas/notes/ant-notes.php?pg=6

[20] Sergio E. Melais and Thomas M. Weller, "A Quasi Yagi Antenna Backed by a Metal Reflector," *IEEE Trans. on Antenna and Prop.*, vol. 56, no. 12, pp. 3868-3872, Dec. 2008.

[21] David M. Pozar, *Microwave Engineering*, 3rd ed., Bill Zobrist, Ed. Massachusetts, United State: Wiley, 2005.

[22] Sergio E. Melais, "A quasi Yagi antenna with end fire radiation over a metal ground," University of South Florida, Florida, PhD Thesis 2009.

[23] K. B. Jakobsen and J. Appel-Hansen J. Thaysen, "A Wideband Balun — How Does It Work?," *Microwave & Wireless*, vol. 12, no. 10, pp. 40-50, 2000.

[24] Rainee N. Simons, and Nihad I. Dib, "New Uniplanar Transitions for Circuit and Antenna Applications," *IEEE Tran. on Microwave Theory and Tech.*, vol. 43, no. 12, pp. 2868-2873, Dec. 1995.